KYOTO UNIVERSITY

PHD THESIS

Theoretical and Experimental Research on Coupled Phase-Oscillator Models

---

Author:
Ryosuke Yoneda

Supervisor:
Toshio Aoyagi

CONTENTS

i

LIST OF FIGURES

LIST OF TABLES

LIST OF ALGORITHMS

CHAPTER 1

INTRODUCTION

This chapter provides an introduction to the thesis. We first discuss the importance of mathematical models, and then introduce rhythmic phenomena and coupled phase-oscillator models, which are the central topics of this thesis. Finally, the outline of this thesis is summarized.

1.1   Mathematical modeling

Humankind has undergone a remarkable development from a lifestyle based primarily on hunting and gathering, through the age of agrarian society, to the present-day industrial society. This history of human development has also been a history of human discovering the principles behind complex natural phenomena, from materials to life phenomena and sometimes economic activities. The principles have often been described by using the language of mathematics, and they are called **mathematical models**. Looking back to ancient times, it was very important for the ancient Greeks to know the exact movement of the seasons in order to know the exact time of harvest for agriculture. For this reason, it is said that a calendar was invented to determine which day of the year it was based on the phases of the moon and the position of the sun. The story of Thales, an astronomer at that time, who successfully predicted the day of the eclipse by the use of mathematics and stopped the war is well known. In recent times, our daily lives have been drastically changed by the outbreak of a new coronavirus. At a time when vaccines had not yet been developed, the use of mathematical models of infectious diseases was extremely important as a means of containing the outbreak. These models can be used to make predictions about the future course of an outbreak and this information was used to guide decision-making and prevent the spread of disease.

These examples show that mathematical models are important, but why do we use them? One advantage of using mathematical models would be that they can provide a systematic and precise way of representing and analyzing complex phenomena. These models can help to clarify the underlying principles and mechanisms at work in a system, and they can also make it possible to make predictions and test hypotheses. However, there are also some disadvantages

to using mathematical models in science. One disadvantage is that these models are often based on simplifying assumptions and idealized conditions, which may not accurately reflect the complexity and variability of real-world systems. As a result, the predictions and conclusions based on these models may not be completely reliable.

This thesis focuses on a natural phenomenon called **synchronization** and presents research on **coupled phase-oscillator models**, a mathematical model of such phenomena. An overview is given in the next section.

1.2 Synchronization and coupled phase-oscillator model

Synchronization is the coordination of events to operate together in a consistent, orderly manner. This can occur in various systems, including biological, chemical, and physical processes [Str03]. One example of synchronization in nature is the flashing patterns of fireflies [Smi35; BB68]. These insects emit light in a synchronized manner, allowing them to communicate and attract mates. This synchronization is achieved through the coordination of their neural activity, which is controlled by chemical signaling within the fireflies' brains. Another example of synchronization can be found in the activity of neurons in the human brain [CAY03; Win67; Lu+16]. Neurons communicate with each other through the release of chemical signals, known as neurotransmitters. When multiple neurons are activated at the same time, they can synchronize their firing patterns, allowing for the coordination of complex behaviors and cognitive processes. This synchronization is essential for the proper functioning of the brain and the ability to process information.

The coupled phase-oscillator model is a mathematical framework that describes the dynamics of oscillators that are coupled together [Str00; Kur75; KM11]. In this model, each oscillator has its own phase, which is the relative position in its own periodic cycle. The coupling between oscillators is typically represented by a coupling function that describes how the phase of one oscillator affects the phase of another, and the function is only dependent on the phase difference. The coupled phase-oscillator model is typically described by a set of differential equations:

$$\frac{\mathrm{d}\theta_i}{\mathrm{d}t} = \omega_i + \sum_{j=1}^{N} \Gamma_{ij}(\theta_j - \theta_i), \tag{1.1}$$

where θ_i is the phase of the ith oscillator, ω_i is its natural frequency. $\Gamma_{ij} \colon \mathbb{S}^1 \to \mathbb{R}$ is the coupling function between ith and jth oscillators, and its input is the phase difference $\theta_j - \theta_i$. Without the coupling, each oscillator moves on a circle independently with the velocity ω_i[1]. These equations describe how the phases of the oscillators evolve over time, and can be used to analyze the synchronization behavior of coupled phase-oscillators.

---

[1]In this sense, the natural frequency ω_i is not a frequency but a velocity, but it is referred to as such by convention since ω_i originally represents the frequency of the limit cycle oscillator.

1.3 Questions

Once coupled phase oscillator systems began to be considered useful as a model for describing synchronous phenomena, researchers began to investigate the theoretical properties of the model. *Why does this model synchronize? Under what conditions does it synchronize? Under what conditions is synchronization likely to occur? Conversely, under what conditions would it fail to synchronize?* If we can answer these questions, we will be able to investigate the properties of systems that exhibit synchronization all at once. This is an advantage of mathematical models, including coupled phase-oscillator models.

While understanding the theoretical properties of the coupled phase-oscillator model allows us to reduce its properties to a real system, deriving the equations that the system follows is also an important problem. *Given data that represent a rhythmic phenomenon, what is the coupled phase oscillator system that it follows?* This is also a question that continues to be studied to this day.

Thus, research on coupled phase-oscillator models has both a *theoretical aspect* regarding conditions that exhibit synchronization and an *experimental aspect* regarding derivations of the model from real data. This thesis attempts to answer both aspects of this challenge. See Fig. 1.1 for a schematic drawing of this thesis.

Synchronization

Fireflies

Metronomes

Neurons

The Model

$$\frac{\mathrm{d}\theta_i}{\mathrm{d}t} = \omega_i + \sum_{j=1}^{N} \Gamma_{ij}(\theta_j - \theta_i)$$

Coupled phase-oscillator model

θ_i

Chap. 5

Chap. 3, 4

Theory

$r \propto (K - K_c)^{1/2}$

$f^{0}(\omega)$: stable $f^{0}(\omega)$: unstable

Bifurcation theory
Phase transition

Network structure
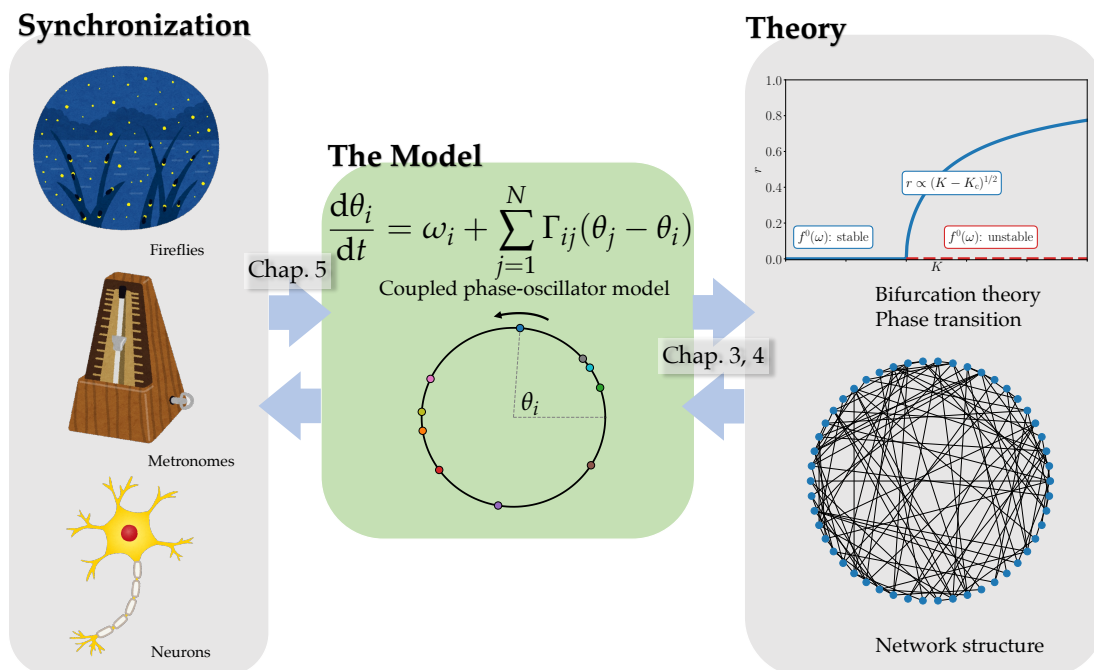
Figure 1.1: Schematic representation on our study.

1.4 Thesis Outline

We conclude this chapter with an outline of this thesis.

In Chapter 2, we give a brief review of coupled phase-oscillator models. Using the Kuramoto model, a representative example of a coupled phase oscillator

system, we will review our past research on the conditions for synchronization and the transition phenomena from an asynchronous state to a synchronous state. The critical exponents obtained near the transition point when this transition phenomenon is regarded as a critical phenomenon in statistical mechanics will also be summarized.

Chapter 3 is constructed based on our paper [YHY20] entitled "Critical exponents in coupled phase-oscillator models on small-world networks". As in the previous chapter, the synchronization transition is characterized by several critical exponents, and we focus on the critical exponent defined by coupling strength dependence of the order parameter for revealing universality classes. In a typical interaction represented by the perfect graph, an infinite number of universality classes is yielded by dependency on the natural frequency distribution and the coupling function. Since the synchronization transition is also observed in a model on a small-world network, whose number of links is proportional to the number of oscillators, a natural question is whether the infinite number of universality classes remains in small-world networks irrespective of the order of links. Our numerical results suggest that the number of universality classes is reduced to one and the critical exponent is shared in the considered models having coupling functions up to second harmonics with unimodal and symmetric natural frequency distributions.

Chapter 4 is constructed based on our paper [YTT21] entitled "The lower bound of the network connectivity guaranteeing in-phase synchronization". In-phase synchronization is a stable state of identical Kuramoto oscillators coupled on a network with identical positive connections, regardless of network topology. However, this fact does not mean that the networks always synchronize in-phase because other attractors besides the stable state may exist. The critical connectivity μ_c is defined as the network connectivity above which only the in-phase state is stable for all the networks. In other words, below μ_c, one can find at least one network that has a stable state besides the in-phase sync. The best known evaluation of the value so far is $0.6828 \cdots \leq \mu_c \leq 0.7889 \ldots$. In this paper, focusing on the twisted states of the circulant networks, we provide a method to systematically analyze the linear stability of all possible twisted states on all possible circulant networks. This method using integer programming enables us to find the densest circulant network having a stable twisted state besides the in-phase sync, which breaks a record of the lower bound of the μ_c from $0.6828 \ldots$ to $0.6838 \ldots$. We confirm the validity of the theory by numerical simulations of the networks not converging to the in-phase state.

Chapter 5 is constructed based on our paper [Yon+22] entitled "Gaussian process regression approach to estimating phase dynamics from rhythmic data". The problem of estimating from data the mathematical model behind natural phenomena has long been studied. Since it has been theoretically shown that rhythmic phenomena, including synchronous phenomena, can be modeled by coupled phase-oscillator models, methods have been proposed to estimate models from real data that show these phenomena. A method in which the coupling function is approximated by a Fourier series expansion of finite order and the Fourier coefficients are estimated by Bayesian linear regression has been used so far, but problems of order determination and the Gibbs phenomenon have sometimes been encountered. In this study, we propose a method to estimate the coupling

function using Gaussian process regression. By setting the covariance function to a periodic kernel, we expect to estimate a smooth periodic function. We report the successful application of Gaussian process regression to a network model of van der Pol oscillators and spiking neurons to accurately estimate the coupling function.

Finally we conclude this thesis in Chapter 6 and discuss some future works.

References

[BB68]   John Buck and Elisabeth Buck. "Mechanism of Rhythmic Synchronous Flashing of Fireflies". In: *Science* 159.3821 (1968), pp. 1319–1327. ISSN: 0036-8075. DOI: 10.1126/science.159.3821.1319. URL: https://science.sciencemag.org/content/159/3821/1319.

[CAY03]   Rosa Cossart, Dmitriy Aronov, and Rafael Yuste. "Attractor dynamics of network UP states in the neocortex". In: *Nature* 423.6937 (May 2003), pp. 283–288. DOI: 10.1038/nature01614. URL: https://doi.org/10.1038/nature01614.

[KM11]   Hiroshi Kori and Yoshihisa Morita. *Dynamical System Approach to Biological Rhythms*. Kyoritshu Shuppan, 2011.

[Kur75]   Yoshiki Kuramoto. "Self-entrainment of a population of coupled nonlinear oscillators". In: *International Symposium on Mathematical Problems in Theoretical Physics*. Springer-Verlag, 1975, pp. 420–422. DOI: 10.1007/bfb0013365. URL: https://doi.org/10.1007/bfb0013365.

[Lu+16]   Zhixin Lu, Kevin Klein-Cardeña, Steven Lee, Thomas M. Antonsen, Michelle Girvan, and Edward Ott. "Resynchronization of circadian oscillators and the east-west asymmetry of jet-lag". In: *Chaos: An Interdisciplinary Journal of Nonlinear Science* 26.9 (Sept. 2016), p. 094811. DOI: 10.1063/1.4954275. URL: https://doi.org/10.1063/1.4954275.

[Smi35]   Hugh M. Smith. "SYNCHRONOUS FLASHING OF FIREFLIES". In: *Science* 82.2120 (1935), pp. 151–152. ISSN: 0036-8075. DOI: 10.1126/science.82.2120.151. URL: https://science.sciencemag.org/content/82/2120/151.

[Str00]   Steven H. Strogatz. "From Kuramoto to Crawford: exploring the onset of synchronization in populations of coupled oscillators". In: *Physica D: Nonlinear Phenomena* 143.1-4 (Sept. 2000), pp. 1–20. DOI: 10.1016/s0167-2789(00)00094-4. URL: https://doi.org/10.1016/s0167-2789(00)00094-4.

[Str03]   Steven H. Strogatz. *Sync: The Emerging Science of Spontaneous Order*. Penguin, 2003.

[Win67]   Arthur T. Winfree. "Biological rhythms and the behavior of populations of coupled oscillators". In: *Journal of Theoretical Biology* 16.1 (1967), pp. 15–42. ISSN: 0022-5193. DOI: https://doi.org/10.1016/0022-5193(67)90051-3. URL: https://www.sciencedirect.com/science/article/pii/0022519367900513.

[YHY20]   Ryosuke Yoneda, Kenji Harada, and Yoshiyuki Y. Yamaguchi. "Critical exponents in coupled phase-oscillator models on small-world networks". In: *Physical Review E* 102.6 (Dec. 2020). DOI: 10.1103/physreve.102.062212. URL: https://doi.org/10.1103/physreve.102.062212.

[Yon+22]   Ryosuke Yoneda, Haruma Furukawa, Daigo Fujiwara, and Toshio Aoyagi. "Gaussian process regression approach to estimating phase dynamics from rhythmic data". In: *preparation* (2022).

[YTT21]   Ryosuke Yoneda, Tsuyoshi Tatsukawa, and Jun-nosuke Teramae. "The lower bound of the network connectivity guaranteeing in-phase synchronization". In: *Chaos: An Interdisciplinary Journal of Nonlinear Science* 31.6 (June 2021), p. 063124. DOI: 10.1063/5.0054271. URL: https://doi.org/10.1063/5.0054271.

CHAPTER 2

REVIEW OF COUPLED PHASE-OSCILLATOR MODEL

2.1 Phase reduction theory

We first review the phase reduction theory for ordinary differential equations (ODEs) in this section. The approach is basically composed of three steps: (i) We first define the phase of an ODE having a stable periodic orbit, (ii) then we derive the phase equation of a perturbed ODE, and (iii) finally we make a simplification of the phase equation by using the method of averaging. In the following, we briefly review these three steps, which follow the analysis procedure presented in [KM11].

2.1.1 Definition of phases

We begin by considering an ordinary differential equation (ODE) of the form,

$$\frac{\mathrm{d}x}{\mathrm{d}t} = f(x), \tag{2.1}$$

where $x \in \mathbb{R}^d$ is a d-dimensional vector representing a state and $f \colon \mathbb{R}^d \to \mathbb{R}^d$ is a smooth vector field. We assume that this ODE has a stable periodic orbit $p(t)$ with a period T.

After sufficiently long time, the state $x(t)$ of the ODE (2.1) approaches the periodic orbit. We can define a **phase** on such a periodic orbit $p(t)$ as follows,

$$\phi(p(t)) = \omega t, \tag{2.2}$$

where $\omega = 2\pi/T$ is the angular velocity of the periodic orbit. This phase can be seen as a filed over the input space $\mathbb{R}^d$, but it is now only defined over the periodic orbit $p(t) \subset \mathbb{R}^d$. We extend the definition of the phase to the whole input space $\mathbb{R}^d$. It is mathematically proved that for an initial point x_0 with the

7

orbit $x(t; x_0)$[1], we can find a phase ϕ_0 with

$$\lim_{t \to \infty} \| x(t; x_0) - p(\phi_0/\omega + t) \| = 0, \tag{2.3}$$

as long as x_0 resides in a basin of the periodic orbit $p(t)$. Then we define the phase $\phi(x_0)$ as ϕ_0. We note that the phase ϕ_0 is uniquely determined up to a 2π modulus for every point x_0 in a basin. A set $\{x \in \text{basin} \mid \phi(x) = \phi_0\}$ is called an **isochron** for the phase ϕ_0. We demonstrate phase fields for several ODEs having a stable periodic orbit in Figure 2.1.
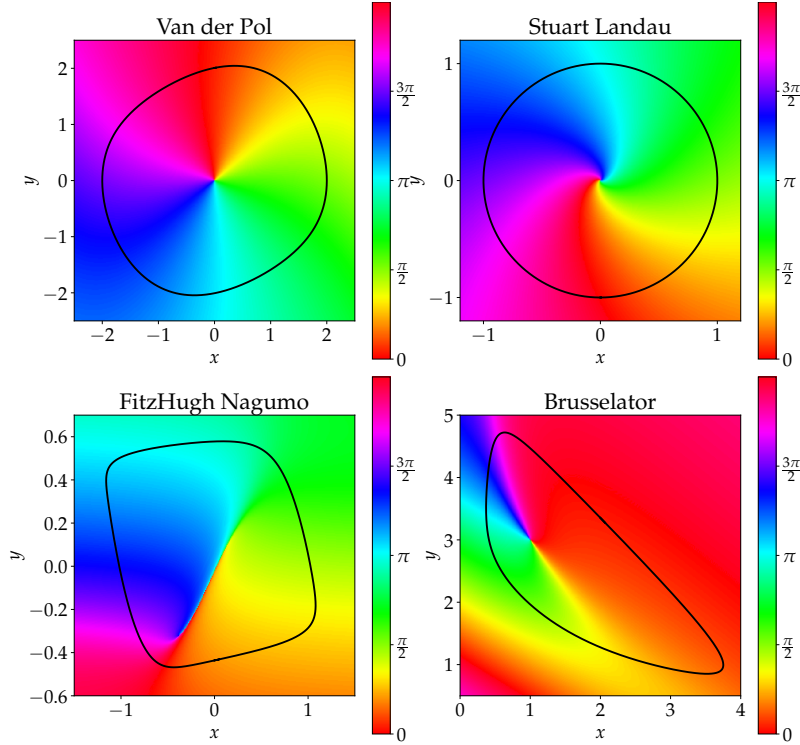
Figure 2.1: The phase fields for the Van der Pol oscillator, the Stuart-Landau oscillator, the FitzHugh-Nagumo oscillator, and the Brusselator oscillator. The black lines denote periodic solutions.

We note some properties of the phase field. If $\phi(x_0) = \phi_0$ for $x_0 \in \mathbb{R}^d$, then for a time shift $\phi(x(\Delta t; x_0)) = \phi_0 + \omega \Delta t$. This can be seen from the property of the orbit $x(t; x(\Delta t; x_0)) = x(t + \Delta t; x_0)$ and the following calculation:

$$\left\| x(t; x(\Delta t; x_0)) - p\left(\frac{\phi_0 + \omega \Delta t}{\omega} + t \right) \right\| = \| x(t + \Delta t; x_0) - p(\phi_0/\omega + (t + \Delta t)) \| \to 0, \tag{2.4}$$

as $t \to \infty$. Therefore the differentiation of the phase on the orbit over time is ω, that is,

$$\frac{d\phi(x(t))}{dt} = \lim_{\Delta t \to 0} \frac{\phi(x(t + \Delta t)) - \phi(x(t))}{\Delta t} = \omega. \tag{2.5}$$

---

[1] In the following, we denote $x(t; x_0)$ by the solution of the ODE (2.1) with the initial condition $x(0) = x_0$.

Or, we can also write this as

$$\frac{\partial \phi}{\partial x}\frac{\mathrm{d}x}{\mathrm{d}t} = \frac{\partial \phi}{\partial x}f(x) = \omega, \tag{2.6}$$

by the use of the chain rule. We can view this as a **phase equation** for an unperturbed ODE system (2.1) (as opposed to the phase equation for a perturbed system, which we will discuss later). In the following, we may simply write $\frac{\mathrm{d}\phi}{\mathrm{d}t} = \omega$ as if the phase itself is developing in time along the ODE (2.1). Also, by taking $\Delta t = mT$ for integer m, we have

$$\phi(x(mT)) \equiv \phi(x(0)) \bmod 2\pi. \tag{2.7}$$

Therefore $x(mT)$ resides in the same isochron as $x(0)$ for any $m \in \mathbb{Z}$.

2.1.2 Phases for perturbed systems

In the previous subsection, we have defined a phase field for a system with a stable periodic orbit, and obtained the phase equation (2.5). Our next challenge is to find a perturbed version of the phase equation.

We set a perturbed ODE as follows,

$$\frac{\mathrm{d}x}{\mathrm{d}t} = f(x) + \varepsilon g(t, x), \tag{2.8}$$

where $g\colon \mathbb{R} \times \mathbb{R}^d \to \mathbb{R}^d$ is a perturbation function and ε denotes its strength. We assume that the perturbation function g is sufficiently smooth as we need. By substituting (2.6) and (2.8), we have the phase equation for the perturbed system as

$$\frac{\mathrm{d}\phi}{\mathrm{d}t} = \frac{\partial \phi}{\partial x}\frac{\mathrm{d}x}{\mathrm{d}t} = \omega + \varepsilon \frac{\partial \phi}{\partial x}g(t, x). \tag{2.9}$$

This is the exact equation for the phases, but we need the information of the original state $x(t)$ for the analysis of the phase $\phi(t)$ since the right hand side of (2.9) depends on $x(t)$. In the following, we see that for a small perturbation, we have a closed form of the phase $\phi(t)$.

When $\varepsilon = 0$, the unperturbed case, the orbit $x(t)$ gets close to the periodic orbit $p(t)$ after a long time. If the perturbation is sufficiently small $\varepsilon \ll 1$, we can assume that the orbit $x(t)$ is close to the periodic orbit $p(t)$ for a long time. Then, we can write the orbit $x(t)$ as

$$x(t) = p(\phi(x(t))/\omega) + \mathcal{O}(\varepsilon), \tag{2.10}$$

or we can directly write $x(t) = p(\phi(t)/\omega) + \mathcal{O}(\varepsilon)$. By substituting this into the right hand side of (2.9) and expand it with respect to ε, we have

$$\frac{\mathrm{d}\phi}{\mathrm{d}t} = \omega + \varepsilon \frac{\partial \phi}{\partial x}\bigg|_{x=p(\phi/\omega)} g(t, p(\phi)/\omega) + \mathcal{O}(\varepsilon^2). \tag{2.11}$$

For simplicity, let us define the following functions:

$$Z(\phi) := \left.\frac{\partial \phi}{\partial x}\right|_{x=p(\phi/\omega)}, \tag{2.12}$$

$$G(t,\phi) := g(t, p(\phi/\omega)), \tag{2.13}$$

and discarding the higher order terms of ε, we have

$$\frac{\mathrm{d}\phi}{\mathrm{d}t} = \omega + \varepsilon Z(\phi) G(t,\phi). \tag{2.14}$$

This is the closed form of the phase equation for the perturbed system. We note that $Z(\phi)$ is a d-dimensional row vector, or an element of the adjoint space of $\mathbb{R}^d$, and $G(t,\phi)$ is a d-dimensional column vector, or an element of $\mathbb{R}^d$. Therefore $Z(\phi)G(t,\phi)$ is calculated by inner product. $Z(\phi)$ is often called the **phase response curve** (PRC) of the system, and is known to be numerically calculated by solving the adjoint equation[2]. We demonstrate the phase response curve for several ODEs having a stable periodic orbit in Fig. 2.2.
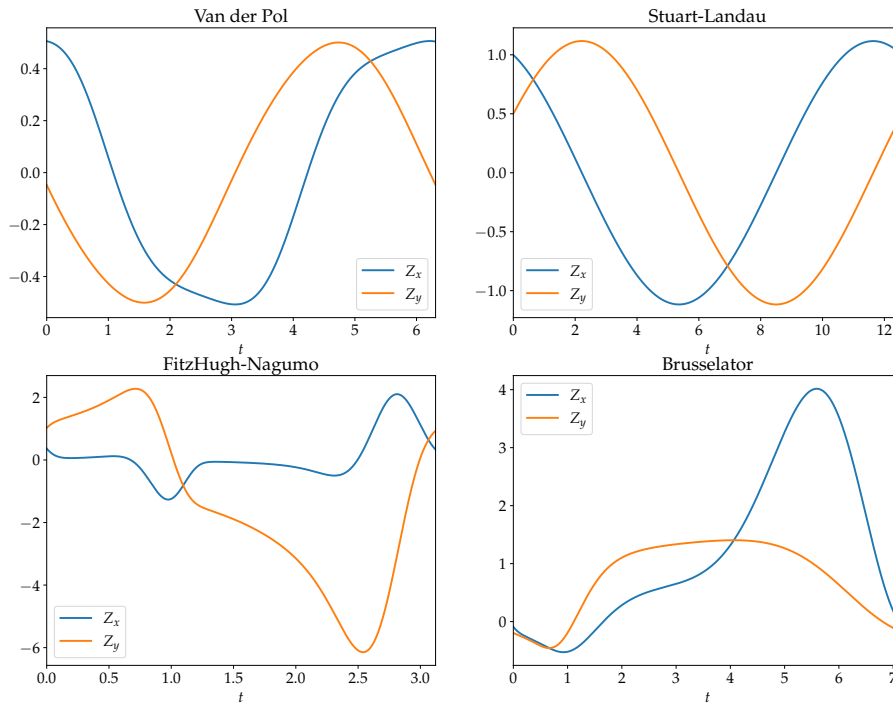
Figure 2.2: Phase response curves for several ODEs having a stable periodic orbit.

The same procedure can be applied to the case of coupled systems. For example, let us consider the following N-body system:

$$\frac{\mathrm{d}x_i}{\mathrm{d}t} = f(x_i) + \varepsilon f_i(x) + \varepsilon \sum_{j=1}^{N} g_{ij}(x_i, x_j), \quad i = 1, 2, \ldots, N, \tag{2.15}$$

---

[2]We made a Python package `prax` for solving a phase response curve of a limit cycle oscillator using the automatic differentitation. See the source code on GitHub: https://github.com/yonesuke/prax.

where $f_i \colon \mathbb{R}^d \to \mathbb{R}^d$ and $g_{ij} \colon \mathbb{R}^d \times \mathbb{R}^d \to \mathbb{R}^d$ are perturbation functions. The unperturbed version of this equation $\dot{x}_i = f(x_i)$ has a stable periodic orbit homeomorphic to N-dimensional torus $\mathbb{T}^d$. Applying the same procedure as the previous subsection, we have the phase equation of (2.15) as

$$\frac{\mathrm{d}\phi_i}{\mathrm{d}t} = \omega_i + \varepsilon Z(\phi_i) \left(F_i(\phi_i) + \sum_{j=1}^{N} G_{ij}(\phi_i, \phi_j) \right), \quad i = 1, 2, \ldots, N, \tag{2.16}$$

where $F_i(\phi_i) = f_i(p(\phi_i/\omega))$ and $G_{ij}(\phi_i, \phi_j) = g_{ij}(p(\phi_i/\omega), p(\phi_j/\omega))$.

2.1.3 Method of averaging

Basically the phase equatuion is derived in the previous subsection, but we can further make the equation simpler by the **method of averaging**.

We first consider the equation (2.14) with $G(t, \phi) = G(\phi)$. By denoting $S(\phi) = Z(\phi)G(\phi)$, we have the following equation:

$$\dot{\phi} = \omega + \varepsilon S(\phi). \tag{2.17}$$

By integrating both sides with respect to time, we have

$$\phi(t + \tau) - \phi(t) = \omega\tau + \varepsilon \int_{t}^{t+\tau} S(\phi(t + t'))\mathrm{d}t' = \omega\tau + \mathcal{O}(\varepsilon T). \tag{2.18}$$

Here we make a bold assumption that we can rewrite $\dot{\phi}$ with a averaged velocity $\langle \dot{\phi} \rangle := (1/T) \int_{t}^{t+T} \dot{\phi}(\tau)\mathrm{d}\tau$[3]. Then we can expand the equation (2.17) with respect to ε:

$$\dot{\phi} \approx \omega + \frac{\varepsilon}{T} \int_{0}^{T} S(\phi(t) + \omega t' + \mathcal{O}(\varepsilon T))\mathrm{d}t' = \omega + \varepsilon\omega_1 + \mathcal{O}(\varepsilon^2 T), \tag{2.19}$$

where

$$\omega_1 := \frac{1}{2\pi} \int_{0}^{2\pi} S(\eta)\mathrm{d}\eta. \tag{2.20}$$

This is the phase equation and the angle velocity becomes $\omega + \varepsilon\omega_1$.

For the case of coupled systems, we obtained the phase equation (2.16) in the previous subsection. By averaging the equation with respect to time similar to the above paragraph, we have the following equation:

$$\dot{\phi}_i = \omega + \varepsilon\omega_i + \varepsilon \sum_{j=1}^{N} \Gamma_{ij}(\phi_i - \phi_j), \tag{2.21}$$

where the coupling function $\Gamma_{ij}(\phi)$ is calculated by

$$\Gamma_{ij}(\phi) := \frac{1}{2\pi} \int_{0}^{2\pi} Z(\phi + \eta)G_{ij}(\phi + \eta, \phi)\mathrm{d}\eta. \tag{2.22}$$

By the method of averaging, the phase equation (2.21) now becomes shift-invariant, that is the vector field is invariant under the shift $\phi_i \mapsto \phi_i + c$ for all i, which makes the analysis much easier than the original equation (2.15).

---

[3]It turns out that this assumption is justified via the **near-identity transformation**, but we do not discuss it here.

2.2 Coupled phase-oscillator models

In the previous section, we have derived the phase equation of the coupled ODEs in the form of (2.21). We can rewirte the equation in the general form as follows:

$$\frac{\mathrm{d}\theta_i}{\mathrm{d}t} = \omega_i + \sum_{j=1}^{N} \Gamma_{ij}(\phi_i - \phi_j), \tag{2.23}$$

and we call this equation the **coupled phase-oscillator model**. In this section, we review the theoretical results of the coupled phase-oscillator models, especially focusing on the **Kuramoto model**.

2.2.1 The Kuramoto model

The Kuramoto model consists of N phase-oscillators where N is a large integer, and evolutes in time with the following equations,

$$\frac{\mathrm{d}\theta_i}{\mathrm{d}t} = \omega_i + \frac{K}{N} \sum_{j=1}^{N} \sin(\theta_j - \theta_i), \tag{2.24}$$

for $i = 1, \ldots, N$. θ_i, ω_i are the phase and the natural frequency of the ith oscillator, and each ω_i is drawn from a distribution $g(\omega)$, which we call the natural frequency distribution. In this thesis, we assume that $g(\omega)$ is symmetric and unimodal, or more precisely, $g(-\omega) = g(\omega)$ and $g'(\omega) < 0$ for $\omega > 0$. Each oscillator is coupled through the sine function of the phase difference with a homogeneous coupling strength $K \geq 0$. When we take $K = 0$, there are no interactions among oscillators, and they move with their own frequencies ω_i, On the other hand, when $K > 0$ is sufficiently large, oscillators tend to attract each other, as we discuss later.

To visualize the extent of synchronization of oscillators, the complex order parameter z is introduced,

$$z = re^{i\phi} = \frac{1}{N} \sum_{j=1}^{N} e^{i\theta_j}, \tag{2.25}$$

where $r, \phi \in \mathbb{R}$. This order parameter z represents the centroid of the oscillators moving on the complex unit circle $\mathbb{S}^1$. As shown in Fig. 2.3, when the oscillators are uniformly distributed on $\mathbb{S}^1$, which corresponds to the nonsynchronized state, r gets close to 0. On the other hand, when the oscillators gather at a point on $\mathbb{S}^1$, which corresponds to the synchronized state, r equals 1. Calculating r is therefore useful for monitoring synchronization of the Kuramoto model. We will look into the relation between the order parameter r and the coupling strength K.

We give a brief explanation why the Kuramoto model describes synchronization. Using the order parameter, the equations of the Kuramoto model are written as

$$\frac{\mathrm{d}\theta_i}{\mathrm{d}t} = \omega_i + Kr \sin(\phi - \theta_i). \tag{2.26}$$
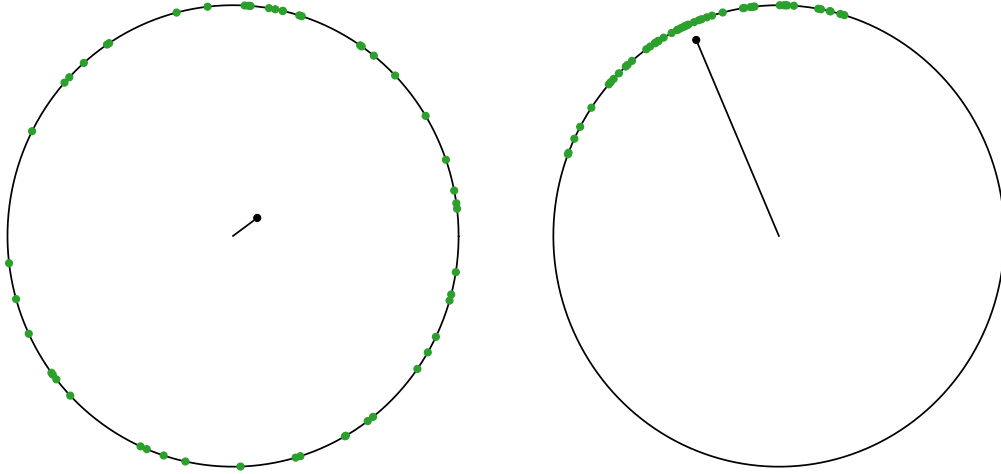
Figure 2.3: Oscillators moving on $\mathbb{S}^1$. When the oscillators are uniformly distributed on $\mathbb{S}^1$, the centroid is close to 0 (left). When the oscillators gather around a point on $\mathbb{S}^1$, r gets close to 1 (right).

In the previous equations (2.24), each oscillator couples with the other oscillators, but this modification allows us to treat each oscillator as it couples only with the order parameter. We will see what happens when K is sufficiently large. Let us assume that the phase of the ith oscillator is going ahead of the phase of the order parameter. In this case $\sin(\phi - \theta_i)$ is negative and this makes the ith phase θ_i slow down. We can interpret this deceleration of the ith phase as the ith oscillator being attracted to the order parameter. When the order parameter is going ahead of the ith oscillator, the deceleration changes to the acceleration and the ith oscillator gets attracted to the order parameter.

2.2.2 The synchronization transition

The Kuramoto model is known to exhibit the synchronization transition from the nonsynchronized state to (partially) synchronized states, and the order parameter r shows a continuous transition

$$r \propto (K - K_c)^\beta \tag{2.27}$$

around the critical point $K \gtrsim K_c$, where β is the critical exponent. We will look back to the original Kuramoto's analysis and derive the self-consistent equation of r. Also, we will review a discussion on the stability of the solution to the Kuramoto model.

In the large population limit $N \to \infty$, by the conservation of the number of oscillators, (2.24) can be written in the equation of continuity [Lan05],

$$\frac{\partial F}{\partial t} + \frac{\partial}{\partial \theta}(v[F]F) = 0, \tag{2.28}$$

$$v[F] = \omega + K \int_{\mathbb{S}^1} d\theta' \int_{\mathbb{R}} d\omega' \sin(\theta' - \theta) F(\theta', \omega', t), \tag{2.29}$$

where $F(\theta, \omega, t)$ is the probability distribution function of θ and ω at the time t. In other words, $F(\theta, \omega, t)\mathrm{d}\theta\mathrm{d}\omega$ represents the fraction of oscillators having phases between θ and $\theta + \mathrm{d}\theta$ and natural frequencies between ω and $\omega + \mathrm{d}\omega$ at the time t. From the normalization condition $\int_{S^1} \mathrm{d}\theta \int_{\mathbb{R}} \mathrm{d}\omega F(\theta, \omega, t) = 1$,

$$\int_{S^1} \mathrm{d}\theta F(\theta, \omega, t) = g(\omega). \tag{2.30}$$

In this limit the order parameter is expressed by

$$z = re^{i\phi} = \int_{S^1} \mathrm{d}\theta \int_{\mathbb{R}} \mathrm{d}\omega F(\theta, \omega, t)e^{i\theta}. \tag{2.31}$$

We first seek for a solution to (2.28) where oscillators distributed uniformly on S^1. In this case the distribution function has to be constant with respect to θ. From the normalization condition (2.30), the flat distribution is expressed by

$$f^0(\omega) = \frac{g(\omega)}{2\pi}. \tag{2.32}$$

Since this uniform solution $f^0(\omega)$ is independent of K,

$$z = \int_{S^1} \mathrm{d}\theta \int_{\mathbb{R}} \mathrm{d}\omega f^0(\omega)e^{i\theta} = 0 \tag{2.33}$$

is valid for all K. This fact induces $v[f^0] = \omega$ and f^0 is a stationary solution of (2.28) as $\frac{\partial}{\partial\theta}(v[f^0]f^0) = 0$.

The stability analysis of $f^0(\omega)$ is studied through the linearized equation around $f^0(\omega)$ by expanding (2.28) with $F = f^0 + f$, which reads

$$\frac{\partial f}{\partial t} = \mathcal{L}f := -\omega\frac{\partial f}{\partial\theta} - Kf^0\Im(ze^{-i\theta}). \tag{2.34}$$

Here, z reads

$$z = \int_{S^1} \mathrm{d}\theta \int_{\mathbb{R}} \mathrm{d}\omega(f^0 + f)e^{i\theta} = \int_{S^1} \mathrm{d}\theta \int_{\mathbb{R}} \mathrm{d}\omega f e^{i\theta}. \tag{2.35}$$

$\mathcal{L}$ has a continuous spectrum on the imaginary axis. This continuous spectrum was a huge obstacle to study the asymptotic behavior of the solution to the Kuramoto model, but the generalized spectrum theory introduced by Chiba [Chi15] solved this difficulty, and the stability of $f^0(\omega)$ is solved; for $K < K_c := 2/(\pi g(0))$, $f^0(\omega)$ is asymptotically stable, whereas unstable for $K > K_c$.

To obtain the bifurcation diagram of the stationary solutions, we derivate the stationary solution of (2.28) for a given K. The stationary solution $F^{\mathrm{st}}(\theta, \omega)$ is defined so as to satisfy

$$\frac{\partial}{\partial\theta}(v[F^{\mathrm{st}}]F^{\mathrm{st}}) = 0, \tag{2.36}$$

which implies $\frac{\partial}{\partial t}F^{\mathrm{st}} = 0$. This stationary solution $F^{\mathrm{st}}(\theta, \omega)$ gives a constant order parameter, hence r and ϕ are constant. By shifting the frame with the phase ϕ, we can set ϕ to zero without loss of generality. Then the velocity field becomes

$v[F^{st}] = \omega - Kr \sin \theta$. The value of r is unknown because it is determined by F^{st}, which we will compute in the following, as

$$r = \int_{\mathbb{S}^1} d\theta \int_{\mathbb{R}} d\omega \cos \theta F^{st}(\theta, \omega). \tag{2.37}$$

We will determine the value of r self-consistently.

The solution of (2.36) is separately written in two parts of the ω-axis. An oscillator with $|\omega| < Kr$ has two fixed points of θ solving

$$v[F^{st}] = \omega - Kr \sin \theta = 0. \tag{2.38}$$

One solution is in the interval $|\theta| < \pi/2$ and the other is in $\pi/2 < |\theta| < \pi$. Looking back (2.26), we observe that the derivation of v is negative (positive) at the former (latter) fixed point, and hence it is stable (unstable). All the oscillators having the natural frequency ω converge to the above stable fixed point, therefore $F^{st} \propto \delta(\omega - Kr \sin \theta)$. From the normalization condition

$$\int_{-\pi/2}^{\pi/2} d\theta F^{st}(\theta, \omega) = g(\omega), \tag{2.39}$$

the stationary solution is

$$F_{lock}^{st}(\theta, \omega) = \begin{cases} \sqrt{(Kr)^2 - \omega^2} \delta(\omega - Kr \sin \theta) g(\omega), & |\theta| < \frac{\pi}{2}, \\ 0, & \frac{\pi}{2} < |\theta| < \pi. \end{cases} \tag{2.40}$$

We refer to these oscillators as the locked oscillators. In contrast, a oscillator with $|\omega| > Kr$ does not have fixed points, and they drift on $\mathbb{S}^1$. From the stationarity condition (2.36) and the normalization condition (2.30),

$$F_{drift}^{st}(\theta, \omega) = \frac{g(\omega)}{2\pi} \frac{\sqrt{\omega^2 - (Kr)^2}}{|\omega - Kr \sin \theta|}. \tag{2.41}$$

We check the validity of (2.40) and (2.41) by numerical simulation. We consider the Kuramoto model with $K = 5.0$ and $N = 50000$ oscillators and see the scattering plot with theoretical line $\omega = Kr \sin \theta$ in Fig. 2.4.

(2.40) and (2.41) depend on unknown variable r, and putting these two types of oscillators together, we have the self-consistent equation for r as

$$r = \int_{\mathbb{S}^1} d\theta \int_{|\omega| < Kr} d\omega \cos \theta F_{lock}^{st}(\theta, \omega) + \int_{\mathbb{S}^1} d\theta \int_{|\omega| > Kr} d\omega \cos \theta F_{drift}^{st}(\theta, \omega). \tag{2.42}$$

Since $F_{drift}^{st}(\theta + \pi, -\omega) = F_{drift}^{st}(\theta, \omega)$, the contribution from the drifting oscillators cancels out, and (2.42) is reduced to

$$r = Kr \int_{-\pi/2}^{\pi/2} d\theta \cos^2 \theta g(Kr \sin \theta). \tag{2.43}$$

This equation has the trivial nonsynchronized solution $r = 0$ for any K. The (partially) synchronized solution $r \neq 0$ satisfies

$$1 = K \int_{-\pi/2}^{\pi/2} d\theta \cos^2 \theta g(Kr \sin \theta). \tag{2.44}$$

15
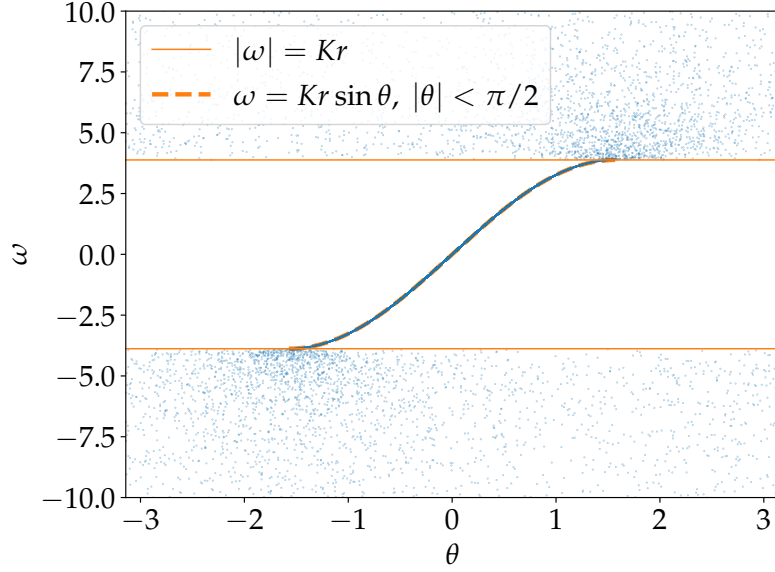
Figure 2.4: (θ, ω) distribution of the Kuramoto model at $K = 5.0$ with total number of oscillators $N = 50000$. Numerical results are shown by scatter points and we see that the lock state is consisten with theoretical line $\omega = Kr \sin \theta$.

Assuming that a partially synchronized branch bifurcates from $K = K_c$, we take the limit $K \to K_c + 0$ together with $r \to +0$ and we have the critical point

$$K_c = \frac{2}{\pi g(0)}, \tag{2.45}$$

which is consistent with the value obtained from the stability analysis of $f^0(\omega)$.

When we set the natural frequency distribution $g(\omega)$ to Lorentzian distribution,

$$g(\omega) = \frac{\Delta}{\pi} \frac{1}{\omega^2 + \Delta^2}, \tag{2.46}$$

we can perform the integration in (2.43) and have

$$r = \sqrt{1 - \frac{K_c}{K}} \tag{2.47}$$

for $K \geq K_c = 2\Delta$. See Fig. 2.5. Therefore, the partially synchronized branch bifurcates with $r \propto (K - K_c)^{1/2}$, and the critical exponent is $\beta = 1/2$. We will discuss the critical exponent for a general $g(\omega)$ in the next subsection.

We note on the unimodality and symmetry of the natural frequency distribution $g(\omega)$. The above proof does not hold for $g(\omega)$ with bimodality or asymmetry, which may yield different synchronization transitions [Mar+09; Ter+17; YY20].

2.2.3 Critical exponents

To calculate the critical exponent β for general natural frequency distribution $g(\omega)$, we expand (2.44) around $r = 0$, and we have

$$1 = \frac{K}{K_c} + \frac{K^3 g''(0)}{16} r^2 + \cdots. \tag{2.48}$$
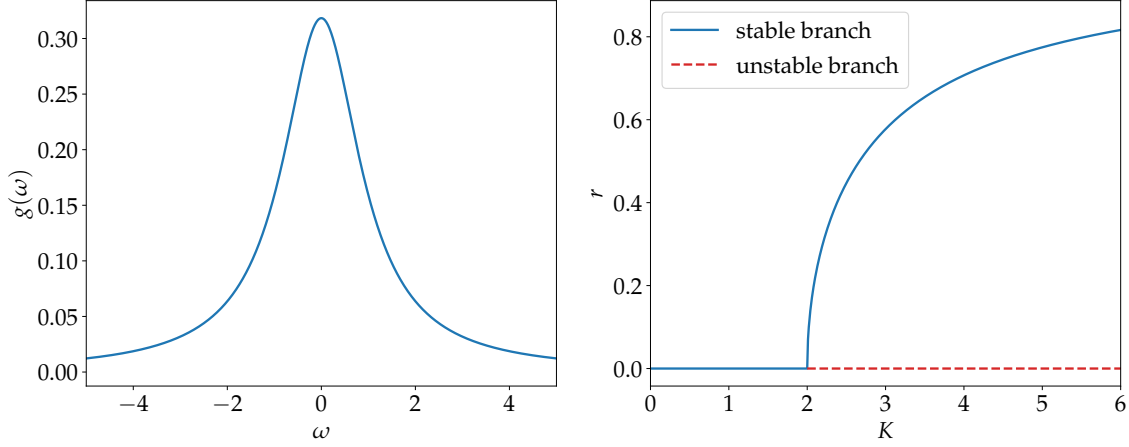
Figure 2.5: Lorentzian distribution (left) and the corresponding bifurcation diagram (right). We set $\Delta = 1$. The stable/unstable branches are drawn in a solid/dashed line, respectively.

Here, we used the critical point formula (2.45). However, this expansion is not enough when $g''(0) = 0$, and in this case we have to expand $g(\omega)$ up to higher degrees. Therefore we assume that $g(\omega)$ has the following expansion around $\omega = 0$,

$$g(\omega) = g_n(\omega) = g(0) - C_n \omega^{2n} + \cdots, \tag{2.49}$$

for $n \in \mathbb{N}$ where $C_n > 0$, coming from the unimodality. We set the second lower order of $g_n(\omega)$ to $2n$, which is even because of the symmetry $g(-\omega) = g(\omega)$. We note that the Lorentzian distribution and Gaussian distribution are in the $n = 1$ case. We give two families of natural frequency distribution as examples of $g_n(\omega)$,

$$g_n^{(L)}(\omega) = \frac{n \sin(\frac{\pi}{2n})}{\pi} \frac{\Delta^{2n-1}}{\omega^{2n} + \Delta^{2n}}, \tag{2.50}$$

$$g_n^{(G)}(\omega) = \frac{n\Delta}{\Gamma(\frac{1}{2n})} e^{-\Delta^{2n} \omega^{2n}}, \tag{2.51}$$

where $g_n^{(L)}(\omega)$ and $g_n^{(G)}(\omega)$ are generalizations of the Lorentzian distribution and the Gaussian distribution, respectively [PDD18]. In the limit $n \to \infty$, $g_n^{(L)}(\omega)$ and $g_n^{(G)}(\omega)$ converge to

$$g_\infty(\omega) := \begin{cases} \frac{1}{2\Delta}, & \omega \in [-\Delta, \Delta], \\ 0, & \text{otherwise.} \end{cases} \tag{2.52}$$

This distribution is a uniform distribution on a compact support. See Fig. 2.6.

Let us observe the value of β takes for the distribution $g_n(\omega)$ (2.49). We again expand (2.44) around $r = 0$,

$$1 = \frac{K}{K_c} - D_n r^{2n} + \cdots, \tag{2.53}$$

$$D_n = C_n K_c^{2n+1} B \left(n + \frac{1}{2}, \frac{3}{2} \right), \tag{2.54}$$
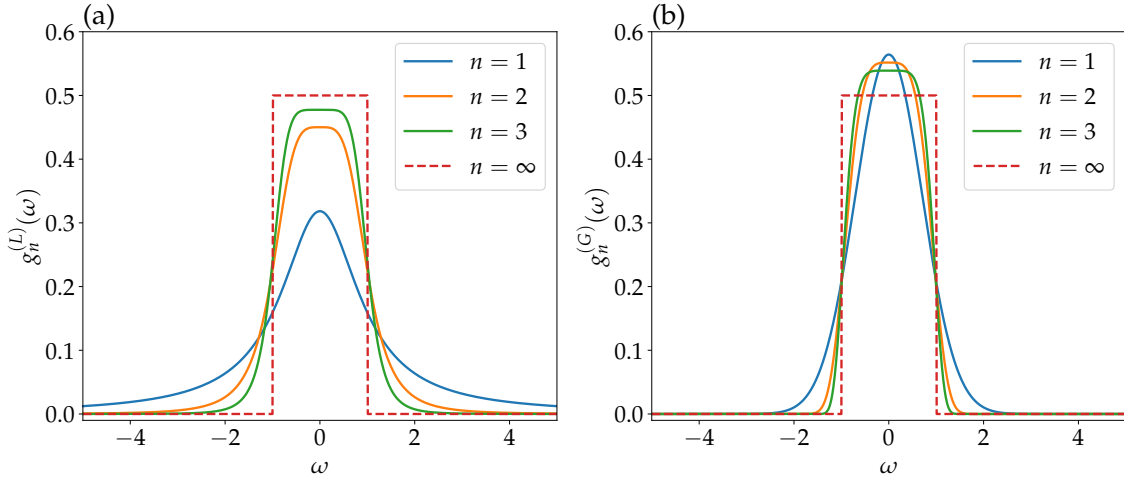
Figure 2.6: Graphs of natural frequency distributions (a) $g_n^{(L)}(\omega)$ and (b) $g_n^{(G)}(\omega)$ for $n = 1, 2, 3$, and ∞ for $\Delta = 1$. $g_n^{(L)}(\omega)$ and $g_n^{(G)}(\omega)$ converge to $g_\infty(\omega)$ (2.52).

where $B(x, y)$ is the beta function[4]. Therefore r bifurcates from $K = K_c$ with

$$r \sim \left(\frac{K - K_c}{D_n K_c} \right)^{\frac{1}{2n}} \propto (K - K_c)^{\frac{1}{2n}}, \tag{2.55}$$

and the critical exponent is $\beta = 1/(2n)$. For the Lorentzian distribution, (2.55) is consistent with (2.47) since $n = 1$.

What left to calculate is the critical exponent β for $g_\infty(\omega)$ (2.49). In this case, $g_\infty(\omega)$ is no longer an analytic function, hence we have to solve this case separately. $g_\infty(\omega)$ is an uniform distribution, and the discontinuity at the boundary of the support leads to the jump in the order parameter at the critical point. Reference [BU07] has showed that the critical point $K = K_c$ and the jump point r_c at $K = K_c$ read

$$K_c = \frac{4\Delta}{\pi}, \quad r_c = \frac{\pi}{4}, \tag{2.56}$$

and the K-dependency of the order parameter r reads

$$r - r_c \propto (K - K_c)^{\frac{2}{3}}. \tag{2.57}$$

We note that this jump is different from the one we see when $g(\omega)$ is bimodal [Mar+09; Ter+17; YY20] in the sense that the jump with the uniform distribution exhibits no hysteresis, whereas the jump with the bimodal distribution exhibits hysteresis.

2.2.4 General coupling functions

The Kuramoto model with a general coupled function is defined by

$$\frac{\mathrm{d}\theta_i}{\mathrm{d}t} = \omega_i + \frac{K}{N} \sum_{j=1}^{N} \Gamma(\theta_j - \theta_i), \tag{2.58}$$

---

[4]The beta function is defined by $B(x, y) = \int_0^1 t^{x-1}(1 - t)^{y-1}\mathrm{d}t$ for $\Re(x) > 0$ and $\Re(y) > 0$.
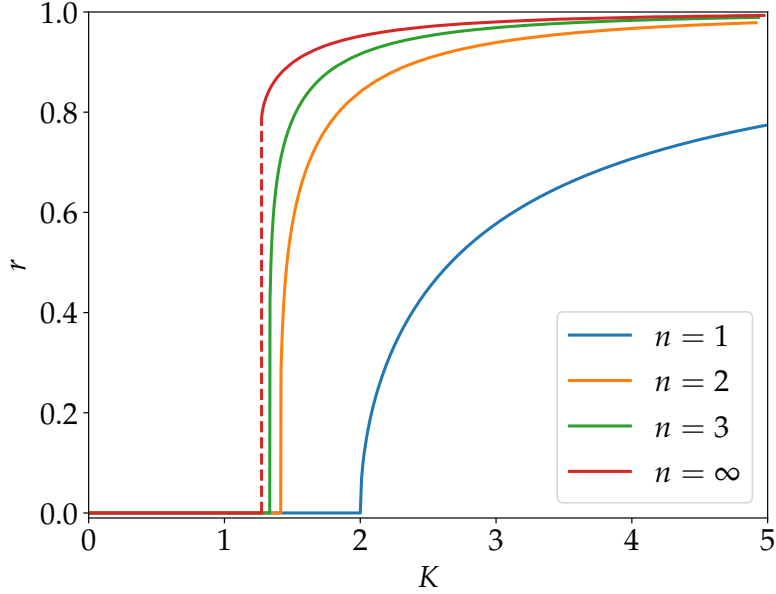
Figure 2.7: Stable branches of the Kuramoto model for natural frequency distributions $g_n^{(L)}(\omega)$ with $n = 1, 2, 3, \infty$ for $\Delta = 1$.

where $\Gamma(\theta)$ is a 2π-periodic function, and the interactions depend on the phase difference $\theta_j - \theta_i$, from the phase reduction theory [KN19].

A natural and simple extension of the Kuramoto model is to add a bi-harmonic function [KP14]:

$$\Gamma(\theta) = \sin\theta + a\sin 2\theta, \quad a < 1. \tag{2.59}$$

When $a = 0$, this model falls back to the original Kuramoto model (2.24). Reference [CN11] has proved that the order parameter exhibits a transcritical bifurcation at the critical point $K = K_c$ with

$$r \sim \frac{2(1-a)}{K_c^3 Ca}(K - K_c) \propto K - K_c, \tag{2.60}$$

where

$$C = \mathcal{PV} \int_{\mathbb{R}} d\omega \frac{g'(\omega)}{\omega}. \tag{2.61}$$

Here, $\mathcal{PV}$ represents the principal value of an integral. C takes a negative value for unimodal and symmetric $g(\omega)$. Therefore, the critical exponent β becomes unity when $a < 0$ for unimodal and symmetric $g(\omega)$, which is different from $\beta = 1/(2n)$ in the Kuramoto model. We note that this model exhibits a first-order phase transition when $0 < a < 1$ since $r < 0$ is forbidden. In Fig. 2.8, we show the numerical results of the Kuramoto model with (2.59). We can see the hysteresis in the order parameter r for $a = 0.5$, indicating the first-order phase transition.

2.2.5 Coupled phase-oscillator models on networks

There exist many types of networks in the real-world, such as human relationships, World Wide Web, citations of scientific papers, and so on. We refer to these
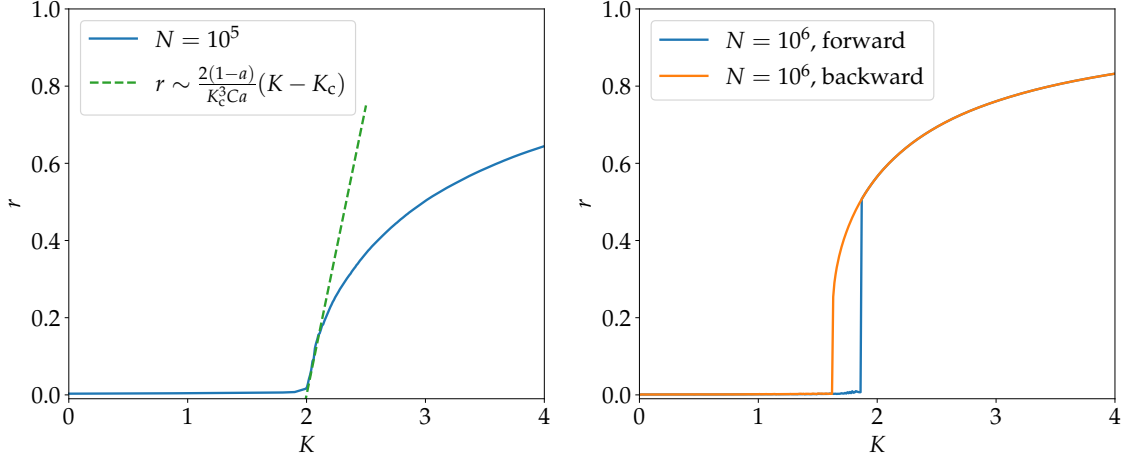
Figure 2.8: Numerical results of the Kuramoto model with a bi-harmonic coupling function (2.59) for $a = -0.2$ (left) and $a = 0.5$ (right).

networks as complex networks, and dynamical systems on the complex networks attract widespread interest. See [DGM08] for a review of dynamical systems on complex networks, especially on their critical phenomena. The coupled phase-oscillator models are no exceptions, and there are extensive researches on the coupled phase-oscillator models on complex networks. One extended Kuramoto model on a complex network is

$$\frac{\mathrm{d}\theta_i}{\mathrm{d}t} = \omega_i + \frac{K}{\langle k \rangle} \sum_{j \in \Lambda_i} \sin(\theta_j - \theta_i), \tag{2.62}$$

for $i = 1, \cdots, N$. Here $\langle k \rangle$ is the average degree of the network, and Λ_i is the index set of the oscillators connecting to the ith oscillator. If the network is all-to-all, $\langle k \rangle = N$ and $\Lambda_i = \{1, \cdots, N\}$, therefore (2.62) falls back to the original Kuramoto model (2.24). One of the most successful studies to tackle the model (2.62) is to use a graphon [CMM18], defined by a symmetric measurable function $W : [0,1]^2 \to [0,1]$, which can be seen as, in some sense, a "limit" of the adjacency matrix of the network. For an all-to-all network, the continuum limit graphon is $W(x,y) = 1$ for all $x,y \in [0,1]$. Another example is the Erdős–Rényi graph, in which existence of an edge is probablistically determined with probability p, and its graphon in the continuum limit is

$$W(x,y) = p, \quad \forall x,y \in [0,1]. \tag{2.63}$$

There is only a constant difference between the all-to-all graph and the Erdős–Rényi graph, therefore we can easily know the critical point and critical exponents of the Erdős–Rényi graph from an analogy of previous discussions.

In [CMM18], extended Kuramoto models on many other networks are discussed, and their results suggest that the critical exponent are the same as the ones in the all-to-all Kuramoto model. Thus, we can see that graphons are a powerful tool to analyze the extended Kuramoto model on networks, but we have to note that graphons can be defined only for a graph with $O(N^2)$ edges with N nodes. Whereas real-world networks are often very sparse, say $O(N)$ edges, analyzing

by graphons cannot be adopted to an extended Kuramoto model on a sparse network. One of the most important networks with $O(N)$ edges is the small-world network. In [HCK02], the critical exponent of the extended Kuramoto model on small-world networks for the Gaussian distribution $g(\omega)$ is numerically calculated, and it is claimed that $\beta = 1/2$. This value is the same as the one from the Kuramoto model with the Gaussian distribution, but we do not know the dependency on natural frequency distributions $g(\omega)$ or coupling functions $\Gamma(\theta)$. Moreover, in [JKÓ19], the critical exponent of the Kuramoto model on a sparse Erdős–Rényi network for the Gaussian distribution is numerically calculated, and it is claimed that $\beta = 0.66$, which is different from $1/2$. This result suggests that extended Kuramoto models on $O(N^2)$ networks take the same critical exponent as the Kuramoto model, whereas extended Kuramoto models on $O(N)$ networks take different values.

In the next section, we numerically calculate the critical exponent β for coupled phase-oscillator models on small-world networks, and observe dependence on n of $g_n(\omega)$ or the coupling function $\Gamma(\theta)$ to reveal difference between the all-to-all network and the small-world network.

References

[BU07]   Lasko Basnarkov and Viktor Urumov. "Phase transitions in the Kuramoto model". In: *Physical Review E* 76.5 (2007), p. 057201.

[Chi15]   Hayato Chiba. "A proof of the Kuramoto conjecture for a bifurcation structure of the infinite-dimensional Kuramoto model". In: *Ergodic Theory and Dynamical Systems* 35.3 (2015), pp. 762–834.

[CMM18]   Hayato Chiba, Georgi S Medvedev, and Matthew S Mizuhara. "Bifurcations in the Kuramoto model on graphs". In: *Chaos: An Interdisciplinary Journal of Nonlinear Science* 28.7 (2018), p. 073109.

[CN11]   Hayato Chiba and Isao Nishikawa. "Center manifold reduction for large populations of globally coupled phase oscillators". In: *Chaos: An Interdisciplinary Journal of Nonlinear Science* 21.4 (2011), p. 043103.

[DGM08]   S. N. Dorogovtsev, A. V. Goltsev, and J. F. F. Mendes. "Critical phenomena in complex networks". In: *Reviews of Modern Physics* 80.4 (Oct. 2008), pp. 1275–1335. DOI: 10.1103/revmodphys.80.1275. URL: https://doi.org/10.1103/revmodphys.80.1275.

[HCK02]   Hyunsuk Hong, Moo-Young Choi, and Beom Jun Kim. "Synchronization on small-world networks". In: *Physical Review E* 65.2 (2002), p. 026139.

[JKÓ19]   Róbert Juhász, Jeffrey Kelling, and Géza Ódor. "Critical dynamics of the Kuramoto model on sparse random networks". In: *Journal of Statistical Mechanics: Theory and Experiment* 2019.5 (2019), p. 053403.

[KM11]   Hiroshi Kori and Yoshihisa Morita. *Dynamical System Approach to Biological Rhythms*. Kyoritshu Shuppan, 2011.

[KN19]   Yoshiki Kuramoto and Hiroya Nakao. "On the concept of dynamical reduction: the case of coupled oscillators". In: *Philosophical Transactions of the Royal Society A* 377.2160 (2019), p. 20190041.

[KP14]   M Komarov and A Pikovsky. "The Kuramoto model of coupled oscillators with a bi-harmonic coupling function". In: *Physica D: Nonlinear Phenomena* 289 (2014), pp. 18–31.

[Lan05]   Carlo Lancellotti. "On the Vlasov Limit for Systems of Nonlinearly Coupled Oscillators without Noise". In: *Transport Theory and Statistical Physics* 34.7 (2005), pp. 523–535. DOI: 10.1080/00411450508951152.

[Mar+09] E. A. Martens, E. Barreto, S. H. Strogatz, E. Ott, P. So, and T. M. Antonsen. "Exact results for the Kuramoto model with a bimodal frequency distribution". In: *Physical Review E* 79.2 (Feb. 2009). DOI: 10.1103/physreve.79.026204. URL: https://doi.org/10.1103/physreve.79.026204.

[PDD18]   Bastian Pietras, Nicolás Deschle, and Andreas Daffertshofer. "First-order phase transitions in the Kuramoto model with compact bimodal frequency distributions". In: *Physical Review E* 98.6 (2018), p. 062219.

[Ter+17] Yu Terada, Keigo Ito, Toshio Aoyagi, and Yoshiyuki Y Yamaguchi. "Nonstandard transitions in the Kuramoto model: a role of asymmetry in natural frequency distributions". In: *Journal of Statistical Mechanics: Theory and Experiment* 2017.1 (Jan. 2017), p. 013403. DOI: 10.1088/1742-5468/aa53f6. URL: https://doi.org/10.1088/1742-5468/aa53f6.

[YY20]   Ryosuke Yoneda and Yoshiyuki Y Yamaguchi. "Classification of bifurcation diagrams in coupled phase-oscillator models with asymmetric natural frequency distributions". In: *Journal of Statistical Mechanics: Theory and Experiment* 2020.3 (Mar. 2020), p. 033403. DOI: 10.1088/1742-5468/ab6f5f. URL: https://doi.org/10.1088/1742-5468/ab6f5f.

CHAPTER 3

CRITICAL EXPONENTS IN COUPLED PHASE-OSCILLATOR MODELS ON SMALL-WORLD NETWORKS

This chapter is constructed based on the published paper [YHY20].

3.1 Introduction

Ever since Huygens found that two pendulum clocks hanging on a wall swung in the opposite direction from each other, many illustrations of synchronization have been established in various fields of nature, such as frog choruses [Aih+14], flashing of fireflies [Smi35; BB68], metronomes [Pan02], and circadian rhythms [Win67]. It is natural to try to understand synchronization theoretically, and a coupled phase-oscillator model is one of successful models to describe synchronization [KN19]. This model consists of many coupled oscillators, and the coupling is expressed by a periodic coupling function. Each oscillator has the so-called natural frequency, randomly drawn from a natural frequency distribution. When the coupling strength K increases, the oscillators exhibit the synchronization transition from the non-synchronized state to (partially) synchronized states. The synchronization transition is continuous or discontinuous, depending on the natural frequency distribution and the coupling function [Kur75; Str00; Chi15; Dai15; BU07; Paz05; Dai90; Cra95; CN11; KP13; KP14].

The critical phenomena have been extensively studied in statistical mechanics. One of their remarkable features is the existence of universality classes; the systems in a universality class share the critical exponents defined around the critical point $K = K_c$ of a continuous transition. One of the critical exponents is β, defined by $r \sim (K - K_c)^\beta$, where r is the order parameter. Thus, it is natural to ask the universality classes in the coupled phase-oscillator models through values of the critical exponent β.

For the all-to-all and uniform coupling, extended researches have revealed

that the value of β depends on the coupling function and the natural frequency
distribution [Kur75; Str00; Chi15; Dai15; BU07; Paz05; Dai90; Cra95; CN11; KP13;
KP14]. For simplicity, we focus on coupling functions which have two harmonics at most, and review values of the critical exponent β for the following three
cases: (i) the second harmonics is absent, (ii) the second harmonics has the opposite sign with the leading harmonics, and (iii) the second harmonics has the
same sign with the leading harmonics. We assume that the natural frequency
distribution is unimodal and symmetric, and that the second-leading term of its
Maclaurin expansion is of the order $2n$, where $n \in \mathbb{N}$. A Gaussian distribution
and a Lorentzian distribution have $n = 1$ for instance.

In the case (i) and (ii), the model shows a continuous transition, whereas
in the case (iii), a discontinuous transition occurs [CN11], hence we cannot define the critical exponent β. In the case (i), the model becomes the Kuramoto
model [Kur75], a paradigmatic coupled phase-oscillator model. Several researches
have pointed out that the critical exponent $\beta = 1/(2n)$ [Kur75; Str00; Chi15;
Dai15]. This n dependence is a strong feature of the Kuramoto model and gives a
sharp contrast with the case (ii). In the case (ii), the critical exponent β becomes 1
for $n = 1$ [Cra95; CN11; KP13; KP14], and this value is suggested to be universal
irrespective of $n \in \mathbb{N}$ [CN11].

Apart from the all-to-all coupling, couplings represented by complex networks are of interests like random graphs, scale-free networks, and small-world
networks [DGM08]. In particular, we focus on the small-world network because
it is ubiquitous in the real world [WS98], and it is a notable network for the
synchronization. The synchronization transition appears with the critical exponent $\beta = 1/2$ in small-world networks even if they are very close to the one-dimensional lattice [HCK02], while the one-dimensional lattice hardly shows the
synchronization [SSK87; Dai88; HCK02]. The previous research [HCK02] however lacks to consider universality since it has treated only the case (i) with $n = 1$,
whereas other universality classes might be hidden in other cases as mentioned
above. In this chapter, we numerically study the synchronization transitions on
small-world networks in all the cases (i), (ii), and (iii) with varying the value of
n. Our results suggest that the critical exponent is universally $\beta = 1/2$ for any
$n \in \mathbb{N}$ in the cases (i) and (ii), where the transition is continuous, while discontinuity in the case (iii) is inherited.

This chapter is organized as follows. In Sec. 3.2, we briefly introduce the small-world network and coupled phase-oscillator models on it. We also introduce a
family of the natural frequency distributions, whose second-leading term is of
the order $2n$. In Sec. 3.3, we show the finite-size scaling to calculate the critical
exponent β. A similarity between systems on the small-world network and noisy
systems is discussed in Sec. 3.4. Finally, in Sec. 3.5, we summarize this chapter
and note some future works.

3.2 Coupled phase-oscillator models on small-world networks

A coupled phase-oscillator model is defined by

$$\frac{d\theta_i}{dt} = \omega_i + \frac{K}{2k} \sum_{j \in \Lambda_i} f_a(\theta_j - \theta_i),$$

$$f_a(\theta) = \sin\theta + a\sin 2\theta, \qquad (3.1)$$

for $i = 1, \cdots, N$. θ_i and ω_i are the phase and the natural frequency of the ith oscillator respectively, and ω_i is randomly drawn from a natural frequency distribution $g(\omega)$. $K > 0$ is a coupling constant, describing how strong the coupling between oscillators are. The index set Λ_i contains the indexes of oscillators connecting to the ith oscillator, and it determines the network of couplings. For instance, the all-to-all coupling gives $\Lambda_i = \{1, \cdots, N\}$, and the nearest neighbor coupling on the one-dimensional lattice gives $\Lambda_i = \{i-1, i+1\}$.

The coupling network represented by $\{\Lambda_i\}_{i=1}^N$ is arbitrarily chosen. In this chapter, we are interested in the small-world network, which possesses the property of a small diameter and a large clustering coefficient despite its sparsity. The small-world network can be seen in various fields of the real world, such as human relationships, World Wide Web, citations of scientific papers, and so on. In 1998, Watts and Strogatz proposed a breakthrough network model showing the property of small-world network, which is created in the following algorithm [WS98]. We first make a periodic k-nearest neighbor network with N nodes, which results in kN links. Then we rewire each link with probability p, keeping in mind that we do not allow self-loops or link duplications. Moreover, we use only connected small-world networks: if a generated network is disconnected, we discard it and generate another one until connected one is created. See Fig. 3.1 for a comparison between the all-to-all network and a small-world network. In this chapter, we use the Watts–Strogatz small-world network with $k = 3$ and $p = 0.2$, following the previous research [HCK02] which shows emergence of the synchronization transition on a small-world network.

As the natural frequency distribution $g(\omega)$, we introduce a family of distributions parametrized by a natural number $n \in \mathbb{N}$,

$$g_n(\omega) = \frac{n}{\Gamma(1/(2n))\Delta} e^{-(\omega/\Delta)^{2n}}, \qquad (3.2)$$

where $\Gamma(z) = \int_0^\infty t^{z-1} e^{-t} dt$ is the Gamma function defined on $\Re(z) > 0$. Here, $\Delta > 0$ is a parameter describing the width of the distribution. We note that $n = 1$ gives the Gaussian distribution. The distribution $g_n(\omega)$ is unimodal and symmetric with respect to $\omega = 0$, and its Maclaurin expansion has the following form,

$$g_n(\omega) = g_n(0) - C_n \omega^{2n} + \cdots, \qquad (3.3)$$

where $C_n = n/(\Gamma(1/(2n))\Delta^{2n+1})$ is positive. We remark that the generalized Lorentzian distribution introduced in [PDD18] also has the same expansion form up to the second leading term. In the limit $n \to \infty$, $g_n(\omega)$ converges to $g_\infty(\omega)$ in
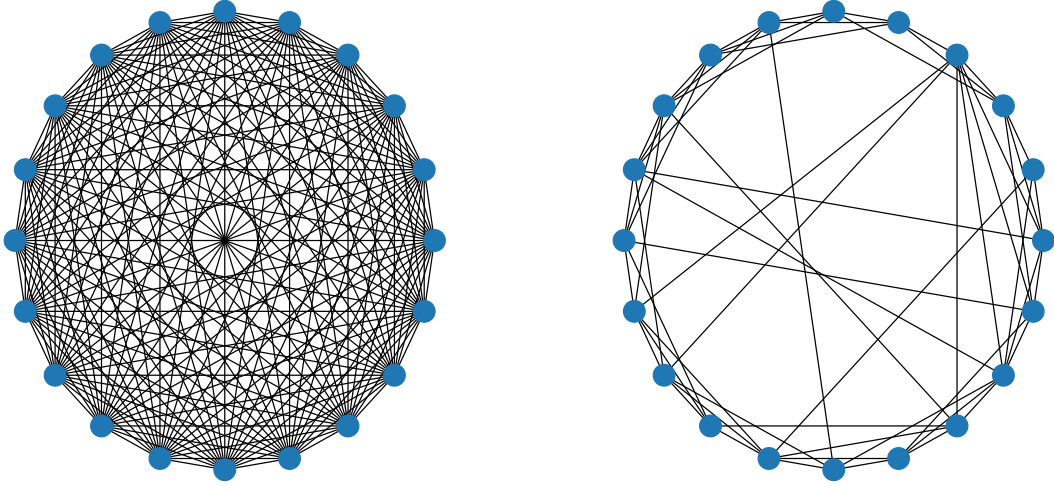
Figure 3.1: Comparison between the all-to-all network (left) and a small-world network (right) with 20 nodes. The small-world network is constructed from the k-nearest neighbour lattice ($k = 3$) with the rewriting probability $p = 0.2$.

the L^1-norm,

$$g_\infty(\omega) = \begin{cases} 1/(2\Delta), & \omega \in (-\Delta, \Delta), \\ 0, & \text{otherwise.} \end{cases} \tag{3.4}$$

This distribution is a uniform distribution on a compact support.

To visualize the extent of synchronization of oscillators, we introduce the order parameter r_N defined by

$$r_N = \left| \frac{1}{N} \sum_{j=1}^{N} e^{i\theta_j} \right|. \tag{3.5}$$

The order parameter represents the centroid of the oscillators moving on the complex unit circle $\mathbb{S}^1$. When the oscillators are uniformly distributed on $\mathbb{S}^1$, which corresponds to the non-synchronized state, r_N gets close to 0. On the other hand, when the oscillators gather at a point on $\mathbb{S}^1$, which corresponds to the synchronized state, r_N equals to 1. The order parameter r_N is therefore useful for monitoring synchronization of the coupled phase-oscillator models. In the next section, we will look into the dependency of the order parameter r_N on the coupling strength K.

The coupled phase-oscillator model on the small-world network represented by Eq. (3.1) has been considered previously [CMM18; Med14], but we stress that the numbers of links are completely different from ours. From the construction algorithm, a small-world network has kN links and $k = 3$ in our networks while $k = O(N)$ in the literature. An advantage of networks with $k = O(N)$ is that they can be analyzed through the equation of continuity [Lov12]. Nevertheless, this advantage implies at the same time that such a small-world network in the

literature is essentially the same with the all-to-all coupling, and is not suitable for detecting new universality classes.

3.3 Numerical simulations

In the large population limit $N \to \infty$, the coupled phase-oscillator model, Eq. (3.1), is expected to show a synchronization transition around a critical point K_c. For $K < K_c$, the order parameter $r(K) := \lim_{N \to \infty} r_N(K)$ is zero, which corresponds to the non-synchronized state. On the other hand, for $K > K_c$, the model shows partially synchronized states, in which $r(K)$ exhibits power law behavior close to the critical point in the form of

$$r(K) \sim (K - K_c)^\beta, \tag{3.6}$$

where β is one of the critical exponents. The critical exponents are crucial to describe critical phenomena, and models are classified into universality classes, each of which shares the same critical exponents. Calculating the critical exponents, including β, is therefore an important topic from theoretical and numerical perspectives.

3.3.1 Finite-size scaling

The critical exponent β is defined in the large population limit $N \to \infty$, but the limit cannot be achieved through the numerical simulations. To overcome this difficulty, we use the finite-size scaling theory, which provides us the limit from observations in finite-size systems. The first assumption of our finite-size scaling theory is existence of the coherent number $N_c(K)$ [BJP82] diverging at the critical point $K = K_c$ as

$$N_c(K) \propto (K - K_c)^{-\bar{\nu}}, \tag{3.7}$$

where $\bar{\nu}$ is another unknown positive critical exponent. The coherent number corresponds to the correlation length in a simple lattice model. The second assumption is that the order parameter $r_N(K)$ depends on K only through the ratio

$$\frac{N}{N_c(K)} \propto \left[(K - K_c) N^{1/\bar{\nu}} \right]^{\bar{\nu}}. \tag{3.8}$$

These assumptions imply that $r_N(K)$ can be represented by

$$r_N(K) = N^{-\beta/\bar{\nu}} F((K - K_c) N^{1/\bar{\nu}}), \tag{3.9}$$

where the function F, which is called the scaling function, must be

$$F(x) \propto x^\beta \quad \text{for large } x \tag{3.10}$$

to reproduce the critical exponent β in the limit $N \to \infty$. We remark that the exponent $\beta/\bar{\nu}$ expresses the finite-size fluctuation of $r_N(K)$ at the critical point $K = K_c$.

The finite-size scaling is widely used for numerical studies of critical phenomena in continuous phase transitions, including coupled phase-oscillator models

[HCK02; PV02; Has10; PR15; Hon+15; CDJ17; JKÓ19]. An important remark on
Eq. (3.9) is that, on the $((K - K_c)N^{1/\bar{v}}, N^{\beta/\bar{v}}r_N)$ plane, observed values of $r_N(K)$
must collapse on a single graph of F for any values of N and K. The unknown
values of K_c, β, and $\bar{v}$ are determined by detecting the best fit values. The de-
tection will be performed by using the Bayesian scaling analysis [Har11; Har15],
whose brief introduction is given in Appendix 3.A.

3.3.2   Computation of the order parameter

We determine the value of the order parameter $r_N(K)$ for a given set of (N, K)
through temporal evolution of the system and two steps of averaging. The model
equation, Eq. (3.1), is numerically integrated by using the fourth-order Runge–
Kutta algorithm with the time step $\delta t = 0.1$. Initial values of the phases $\{\theta_i\}$
are randomly drawn from the uniform distribution on the interval $[0, 2\pi)$, and
the natural frequencies $\{\omega_i\}$ are randomly drawn from the distribution function
$g_n(\omega)$. The order parameter r_N defined by Eq. (3.5) depends on time t, and we
take the time average in the time interval $t \in [300, 500]$. This is the first averaging.

Further, we perform 400 realizations by changing small-world networks, the
initial values of $\{\theta_i\}$, and $\{\omega_i\}$ for a given set of (N, K). To compute the con-
fidence interval of the order parameter, the resampling technique is in use. We
choose 200 samples out of 400 realizations, and calculate the mean of the time-
averaged order parameter in the chosen 200 samples. The mean of the ith resam-
pling is denoted by $r_N^{(i)}(K)$, and we perform the resampling for $S = 1000$ times.
The value $r_N(K)$ is determined by taking the second averaging over S samples
$\{r_N^{(i)}(K)\}_{i=1}^{S}$, which also provide the confidence interval of $r_N(K)$.

See Fig. 3.2 for the obtained $r_N(K)$ for $a = 0$ and -0.2 with $n = 1$, where
the condition $a \leq 0$ is expected to give a continuous transition. In the following
two sections, we compute the critical exponents for $a = 0$ and $a = -0.2$, and
show discontinuity for $a = 0.5$, respectively. We remark that $a = -0.2$ and 0.5
are not special values. They are arbitrarily chosen from a neighborhood of $a = 0$
to demonstrate differences among the three cases of (i) $a = 0$, (ii) $a < 0$, and (iii)
$a > 0$.

3.3.3   Critical exponents for continuous transition

The finite-size scaling, Eq. (3.9), is a powerful tool to compute the unknown val-
ues of K_c, β, and $\bar{v}$, but it is not perfect if N is not sufficiently large. We thus
compute the unknown variables for three values of $N \in \{N_{\min}, 2N_{\min}, 4N_{\min}\}$,
and observe convergence by varying $N_{\min}$. Moreover, we use the resampling
technique again to estimate the unknown values with their confidence intervals.
Consequently, we have $S = 1000$ sets of the three values for a given $N_{\min}$ as re-
ported in Fig. 3.3 because each resampling set $r_N^{(i)}(K)$ determines them. Finally,
the values and the confidence intervals of K_c, β, and $\bar{v}$ are computed as the av-
erages and the standard deviations over $S = 1000$ sets. The estimated values
are verified in Fig. 3.4, where all the points lie on a single curve representing the
scaling function F for $N_{\min} = 6400$.

The estimated values of K_c, β and $\bar{v}$ are summarized in Table 3.1. The row
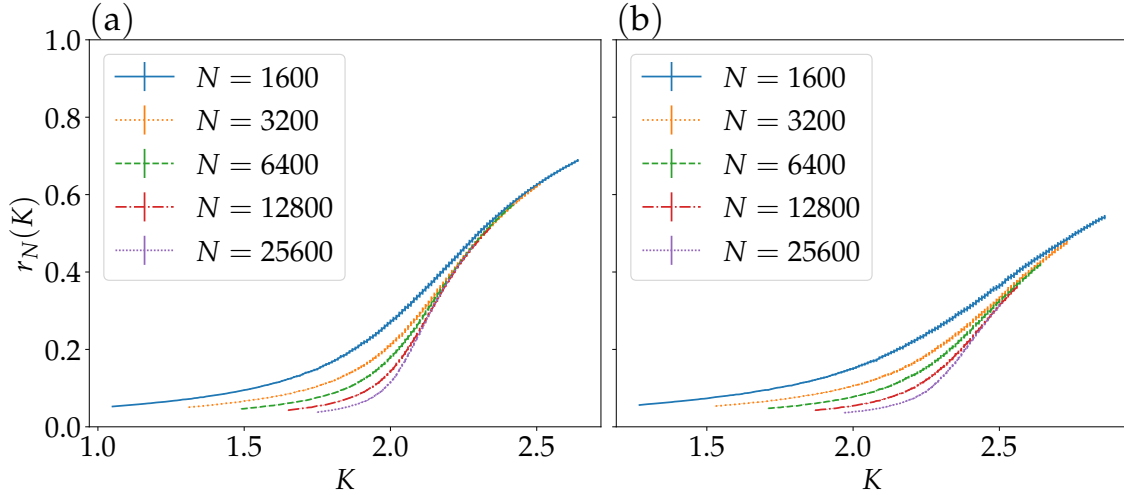
Figure 3.2: Graphs of order parameter $r_N(K)$ with its confidence interval for the model (3.1), where we take the coupling function $f_a(\theta)$ with (a) $a = 0$ and (b) $a = -0.2$. As a natural frequency distribution, we use $g_1(\omega)$ with $\Delta = 1$, and $N = 1600, 3200, 6400, 12800$, and 25600 from top to bottom. $r_N(K)$ and its confidence interval are evaluated by the resampling technique. Errorbars are so small that they may not be visible.

of $N_{\min} = \infty$ is obtained by extrapolation from $N_{\min} = 1600, 3200$, and 6400 as demonstrated in Fig. 3.5. We note that the extrapolated values of β are close to $1/2$ and ones of $\bar{\nu}$ are close to $5/2$ irrespective of the values of a and n. The universality is completely unlike the all-to-all interaction case. Here we note that this result shares the same critical exponent $\bar{\nu} = 5/2$ as the all-to-all interaction case for $(a, n) = (0, 1)$ calculated in [Hon+07].

The value $\bar{\nu} \simeq 5/2$ is not in agreement with the value $\bar{\nu} \simeq 2$ previously reported for $(a, n) = (0, 1)$ [HCK02]. We suppose that the discrepancy comes from the method to compute the critical exponents. In the literature, the authors used the fact that $r_N(K)N^{\beta/\bar{\nu}}$ takes a constant value irrespective of N at the critical point $K = K_c$ (See Eq. (3.9)). Using this fact, they first find the best fit values of $\beta/\bar{\nu}$ and K_c by varying the system size N. One more equation is obtained by derivating the finite-size scaling, Eq. (3.9), which produces

$$\log\left[\frac{\mathrm{d}r_N}{\mathrm{d}K}(K_c)\right] = \frac{1-\beta}{\bar{\nu}}\log N + \text{const.} \tag{3.11}$$

Plotting the left-hand side as a function of $\log N$, one has the slope $(1 - \beta)/\bar{\nu}$. A remarkable disadvantage of this method is that the estimation relies on high precision of $r_N(K)$ around the critical point $K = K_c$, while the Bayesian scaling analysis uses $r_N(K)$ in a wider interval of $(K - K_c)N^{1/\bar{\nu}}$ and provides persistence against fluctuation. We, therefore, believe that $\bar{\nu} \simeq 5/2$ obtained by the Bayesian scaling analysis is more reliable.
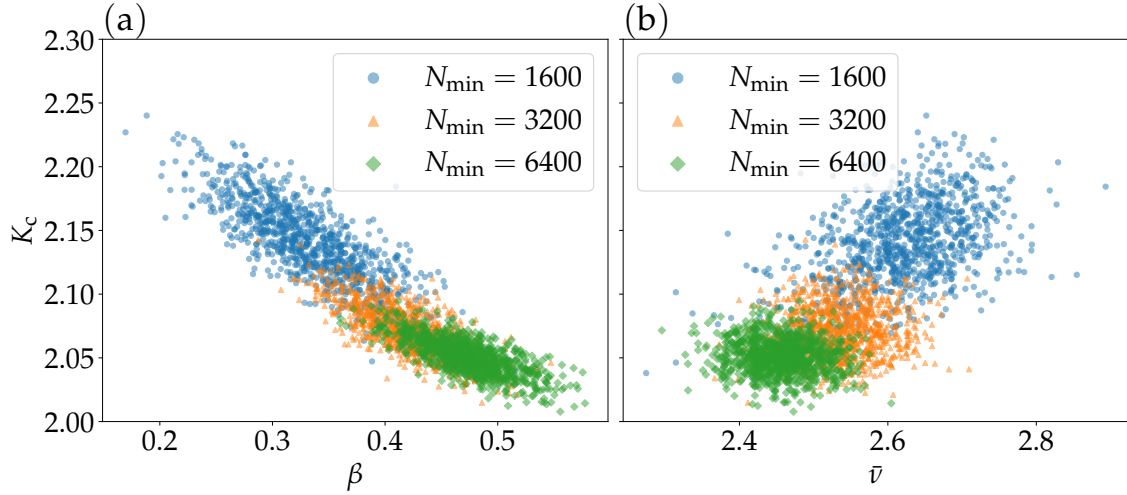
Figure 3.3:   Scattering plots of computed parameters (a)(β, K_c) and (b)$(\bar{v}, K_c)$, evaluated by the Bayesian scaling analysis. Here, we use $(a, n) = (0, 1)$, and we set $N_{\min}$ to $1600, 3200$ and 6400.

3.3.4 Discontinuity of transition

In the all-to-all interaction a positive a induces discontinuity of the synchronization transition [CN11]. We reveal that the transition is discontinuous also in a small-world network. The discontinuity appears as a result of a subcritical transition, and a subcritical transition has metastability: A partially synchronized state is stable in addition to a stable nonsynchronized state for a fixed K close to the critical point. The metastability implies that the final state depends on choice of the initial state, and the dependency is extracted by observing hysteresis.

Fixing $a = 0.5$, we check existence of the hysteresis by preparing two sets of the initial phases $\{\theta_i\}_{i=1}^N$ for each K: (i) We start from $K = K_{\text{start}}$, where K_{start} is sufficiently smaller than the critical value K_c, and the initial phases $\{\theta_i\}_{i=1}^N$ are randomly drawn from the interval $[0, 2\pi)$. At a certain value of K, the final phases at $t = 500$ is used as the initial phases at the successive value $K + \Delta K$ in the increasing direction. The increase of K is continued up to $K = K_{\text{end}}$, where K_{end} is sufficiently larger than the critical value K_c. We call the process (i) the "forward" process, and $r_N^{(\text{forward})}(K)$ denotes its order parameter. (ii) Contrary to the "forward" process, we start with the random initial phases $\{\theta_i\}_{i=1}^N$ at $K = K_{\text{end}}$ and decrease K up to $K = K_{\text{start}}$ following the same procedure with the "forward" process. We call this process the "backward" process, and $r_N^{(\text{backward})}(K)$ denotes its order parameter. We have executed the numerical simulations of Eq. (3.1) for $a = 0, -0.2$, and 0.5, and $n = 1, 2, 3$, and ∞. For the system size $N = 25600$, the hysteresis appears only for $a = 0.5$ regardless of n as exampled in Fig. 3.6 for $n = 1$. We have checked that $t = 500$ is sufficiently long to pass the transient period, and simulations up to $t = 800$ do not affect the hysteresis. We therefore conclude that the system represented by Eq. (3.1) shows a discontinuous transition for $a = 0.5$ as the all-to-all interaction case.
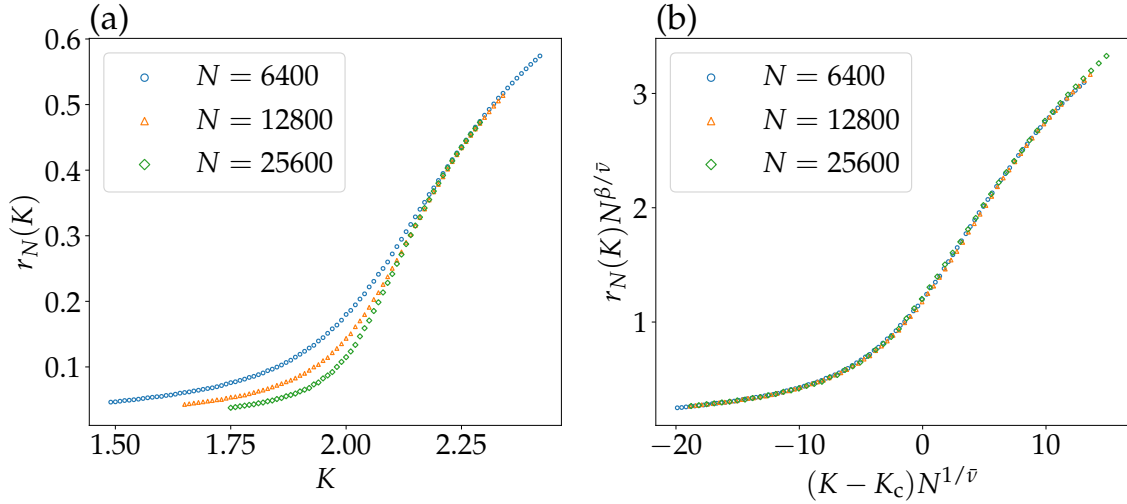
Figure 3.4: Graph of scaled order parameter $r_N(K)N^{\beta/\bar{\nu}}$ versus scaled coupling constant $(K - K_c)N^{1/\bar{\nu}}$ for $(a, n) = (0, 1)$, where we use $\beta, \bar{\nu}$ and K_c, obtained by the Bayesian scaling analysis for $N_{\min} = 6400$. The values of β, $\bar{\nu}$, and K_c are shown in Table 3.1. We see that the scaled data are well collapsed to the scaling function F.

3.4 Small-world network and noise

We discuss similarity between systems on small-world networks and noise systems. For simplicity, we consider the Kuramoto model $(a = 0)$ for a while. The steady state in the Kuramoto model is proportional to $\delta(\omega - Kr\sin\theta)$ in the synchronized regime of ω [Str00; DA18], where δ is the Dirac's delta function. The δ function with the integration over ω and symmetry of the natural frequency distribution yield the self-consistent equation of the order parameter r as

$$r = Kr \int_{-\pi/2}^{\pi/2} g_n(Kr\sin\theta)\cos^2\theta d\theta. \tag{3.12}$$

The order parameter r is sufficiently small around the critical point and we perform the Maclaurin expansion of g_n. The leading order of the expansion, which is of $O(r)$, determines the celebrated critical point $K_c = 2/[\pi g_n(0)]$. The partially synchronized branch is obtained by balancing the second leading order of $O(r^{2n+1})$ with the first leading order of $O(r(K - K_c))$, and the balance results to $r \propto (K - K_c)^{1/(2n)}$. We then obtain the critical exponent $\beta = 1/(2n)$.

To the contrary, on a small-world network, a steady state is not written in the form of the δ function and the synchronized oscillators are still "noisy" as shown in Fig. 3.7. The synchronized oscillators no longer capture the flatness of $g_n(\omega)$ around $\omega = 0$, and the critical exponent β falls into the classical value $1/2$ regardless of natural frequency distribution $g_n(\omega)$ as a noisy system [Sak88].

Moreover, in the model having the nonvanishing second harmonics of the coupling function with $a < 0$, the noise recovers $\beta = 1/2$ [Cra95] whereas no noise system gives $\beta = 1$ [Dai94]. The universality of $\beta = 1/2$ observed in systems on small-world networks is therefore very similar to the one in noisy systems.
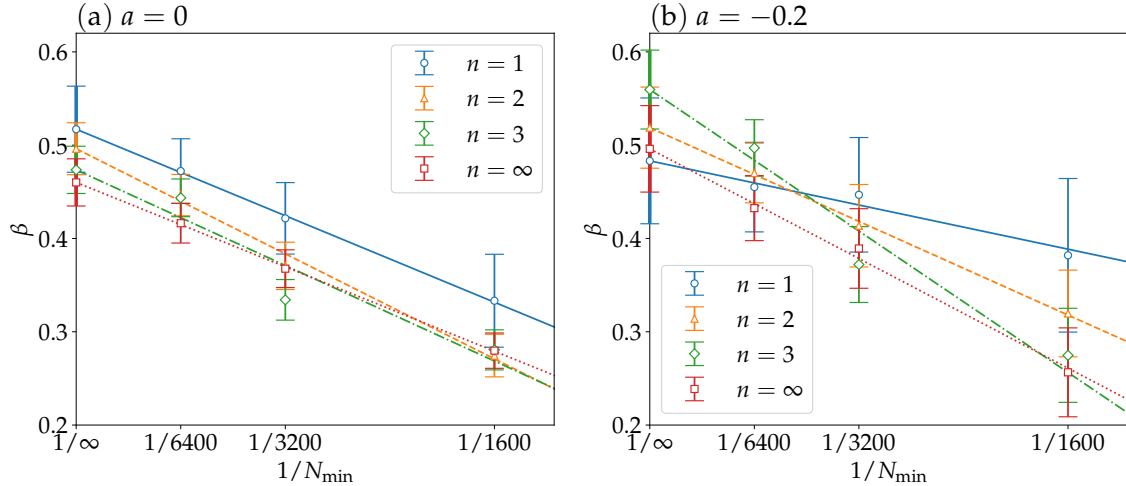
Figure 3.5: Graphs of β as a function of $1/N_{\min}$ for (a) $a = 0$ and (b) $a = -0.2$ in Eq. (3.1). Critical exponents obtained by the finite-size scaling are shown with errorbars, and the least square method gives the extrapolations at the left boundary of the panels. For each a, the resulting linear regression lines are drawn with the solid line for $n = 1$, the dashed line for $n = 2$, the dot-dashed line for $n = 3$, and the dotted line for $n = \infty$.

3.5 Summary and Discussions

We calculated the critical exponents β and $\bar{\nu}$ for coupled phase-oscillator models on small-world networks by using the finite-size scaling method. We set the coupling function as $f_a(\theta) = \sin\theta + a\sin 2\theta$, and the natural frequency distribution as $g_n(\omega)$ defined in Eq. (3.2), and we studied the (a, n)-dependency of the critical exponents. Our numerical results suggest $\beta = 1/2$ and $\bar{\nu} = 5/2$ for all $g_n(\omega)$ and coupling function $f_a(\theta)$ with $a = 0$ and -0.2. This universality shows a sharp contrast with the all-to-all interaction case, which has various values of β depending on the coupling function and the natural frequency distribution. A possible explanation of the source of contrast can be found in the number of links of considering networks: our small-world networks has $O(N)$ links, while the all-to-all interaction have $O(N^2)$ links. We have also found that the model, Eq. (3.1), shows a discontinuous transition for $a = 0.5$. The (dis)continuity is a weaker property than the values of the critical exponents, and it is shared between the two types of networks: networks with $O(N)$ links and $O(N^2)$ links.

We end this chapter commenting on two future works. Firstly, we picked up two representative points of a from a neighborhood of $a = 0$ to investigate universality of the critical exponents. Studying a global phase diagram on the (K, a)-plane is a subject for future researches. Secondly, we note universal value $\beta = 1/2$ in the Kuramoto model which is recovered by adding noise regardless of the natural frequency distribution [Sak88]. A small-world network may play a role of noise due to inhomogeneous couplings, and another work to do is to make a bridge between a noisy Kuramoto model and a model on a small-world network.
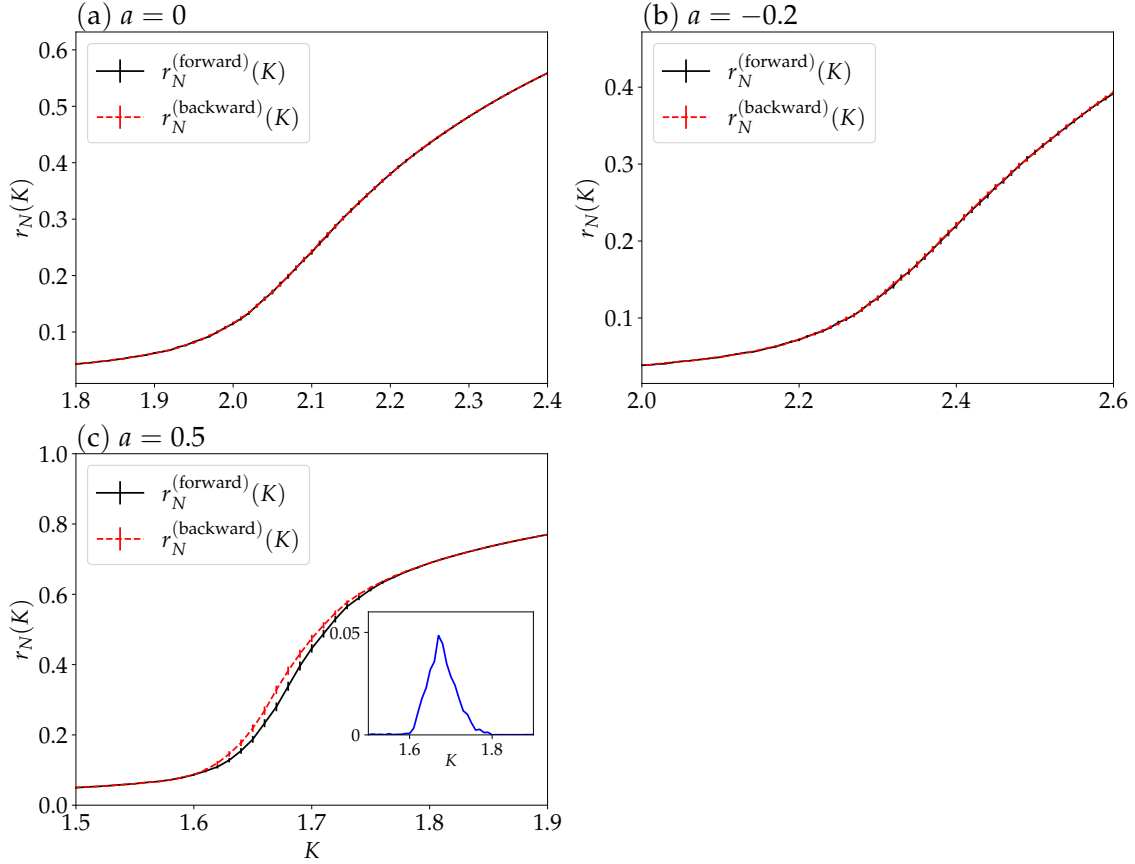
Figure 3.6: Graphs of $r_N(K)$ and its errorbar of (3.1) for (a) $(a, n) = (0, 1)$, (b) $(a, n) = (-0.2, 1)$, and (c) $(a, n) = (0.5, 1)$ with two different types of initial phases, where we set the number of oscillators $N = 25600$. We see that, only in (c), $r_N(K)$ takes a different value depending on the choice of the initial phases around $K \in (1.6, 1.8)$. The inset in (c) shows the graph of $r_N^{(backward)}(K) - r_N^{(forward)}(K)$.

3.A   Bayesian Scaling Analysis

We briefly review the Bayesian scaling analysis [Har11; Har15], a statistical method for estimating the values such as β, $\bar{\nu}$, and K_c in Eq. (3.9). We write these values as $\theta_p = (\beta, \bar{\nu}, K_c)$. We assume that the scaling function F in Eq. (3.9) obeys a Gaussian process

$$F \sim \mathcal{GP}(m, k_{\theta_h}), \tag{3.13}$$

with mean function $m(\cdot)$ and covariance kernel $k_{\theta_h}(\cdot, \cdot)$. Here θ_h denotes the hyperparameters of covariance kernel. We also set $m = 0$ for simplicity. In the following, we also use the notation $\theta = (\theta_h, \theta_p)$. For the data $\{r_{N_i}(K_i)\}_{i=1}^{M}$, the rescaled data $X_{\theta_p, i} = (K_i - K_c)N_i^{1/\bar{\nu}}$ and $Y_{\theta_p, i} = r_{N_i}(K_i)N_i^{\beta/\bar{\nu}}$ must collapse on the scaling function as $Y_{\theta_p, i} = F(X_{\theta_p, i})$. Since F is a Gaussian process, Y_{θ_p} obeys a M-dimensional Gaussian distribution, and the probability of Y for the parameter
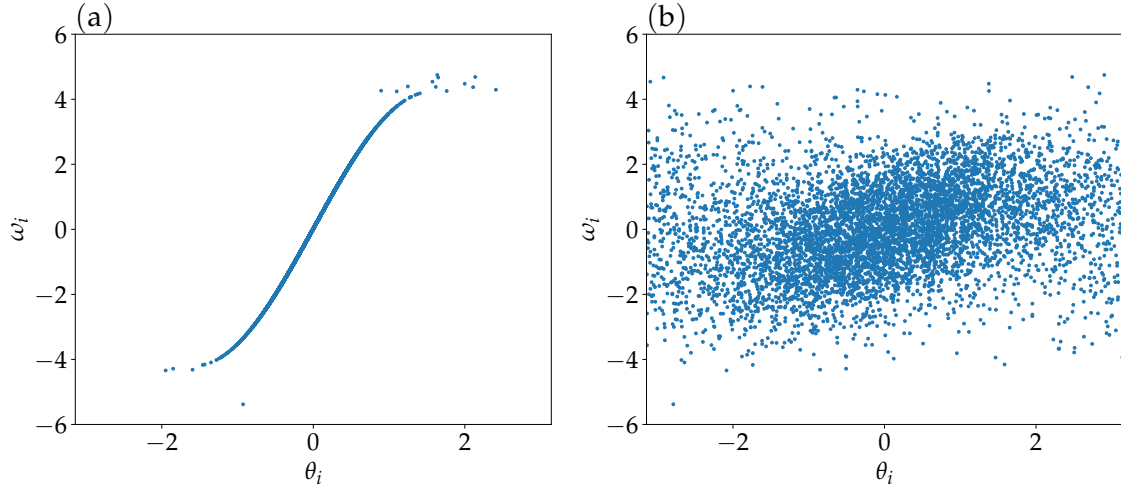
Figure 3.7: Snap shots of oscillators on the (θ_i, ω_i) plane at $t = 500$. (a) The
all-to-all network. (b) A small-world network. The system size $N = 6400$. The
coupling constant $K = 4.5$. $(a, n) = (0, 1)$.

$\boldsymbol{\theta}$ is

$$p(Y \mid \boldsymbol{\theta}) = \mathcal{N}(Y_{\theta_p} \mid \mathbf{0}, K_{\boldsymbol{\theta}})$$

$$= \frac{1}{(2\pi)^{N/2}[\det K_{\boldsymbol{\theta}}]^{1/2}} \exp\left[-\frac{1}{2}Y_{\theta_p}^{\mathsf{T}} K_{\boldsymbol{\theta}}^{-1} Y_{\theta_p}\right]. \tag{3.14}$$

Here, $[K_{\boldsymbol{\theta}}] = k_{\theta_h}(X_{\theta_p, i}, X_{\theta_p, j})$ is $M \times M$ dimensional matrix. By assuming that the
prior distribution of $\boldsymbol{\theta}$ is uniform, we have

$$p(\boldsymbol{\theta} \mid Y) \propto p(Y \mid \boldsymbol{\theta}), \tag{3.15}$$

from Bayes' theorem. The most probable parameters $\boldsymbol{\theta}$ are, therefore, estimated
by finding the minimum of likelihood function given by

$$L_{\boldsymbol{\theta}} = \log(\det K_{\boldsymbol{\theta}}) + Y_{\theta_p}^{\mathsf{T}} K_{\boldsymbol{\theta}}^{-1} Y_{\theta_p}, \tag{3.16}$$

which is obtained by taking log and discarding constants in Eq. (3.14). The gra-
dient of $L_{\boldsymbol{\theta}}$ for an element $\theta \in \boldsymbol{\theta}$ is given by

$$\frac{\partial L_{\boldsymbol{\theta}}}{\partial \theta} = \mathrm{tr}\left[K_{\boldsymbol{\theta}}^{-1} \frac{\partial K_{\boldsymbol{\theta}}}{\partial \theta}\right] - (K_{\boldsymbol{\theta}}^{-1} Y_{\theta_p})^{\mathsf{T}} \frac{\partial K_{\boldsymbol{\theta}}}{\partial \theta}(K_{\boldsymbol{\theta}}^{-1} Y_{\theta_p})$$
$$+ 2Y_{\theta_p}^{\mathsf{T}} K_{\boldsymbol{\theta}}^{-1} \frac{\partial Y_{\theta_p}}{\partial \theta}, \tag{3.17}$$

and using this gradient, the gradient method gives us the most probable param-
eters $\boldsymbol{\theta}$.

In this paper, we consider a kernel based on a radial basis function (RBF) ker-
nel

$$k_{\theta_h}(x, y) = \theta_1 \exp\left[-\frac{(x-y)^2}{\theta_2}\right] + \theta_3 \delta(x, y), \tag{3.18}$$

which is parameterized by $\theta_h = (\theta_1, \theta_2, \theta_3)$ with $\theta_{1,2,3} > 0$, and $\delta(x, y) = 1$ when $x = y$, otherwise $\delta(x, y) = 0$. Here, θ_3 denotes the data fidelity. Roughly speaking, a sample path of Gaussian process associated with a RBF kernel are known to be an infinitely differentiable function; see [Kan+18, Corollary 4.13] for a rigorous statement. Therefore, the Bayesian scaling analysis only assumes the smoothness of a scaling function, and it does not need an explicit form. See the reference [Har11; Har15] for more detailed discussions.

References

[Aih+14] Ikkyu Aihara, Takeshi Mizumoto, Takuma Otsuka, Hiromitsu Awano, Kohei Nagira, Hiroshi G. Okuno, and Kazuyuki Aihara. "Spatio-Temporal Dynamics in Collective Frog Choruses Examined by Mathematical Modeling and Field Observations". In: *Scientific Reports* 4.1 (Jan. 2014), p. 3891. DOI: 10.1038/srep03891. URL: https://doi.org/10.1038/srep03891.

[BB68] John Buck and Elisabeth Buck. "Mechanism of Rhythmic Synchronous Flashing of Fireflies". In: *Science* 159.3821 (1968), pp. 1319–1327. ISSN: 0036-8075. DOI: 10.1126/science.159.3821.1319. URL: https://science.sciencemag.org/content/159/3821/1319.

[BJP82] R Botet, R Jullien, and P Pfeuty. "Size scaling for infinitely coordinated systems". In: *Physical Review Letters* 49.7 (1982), p. 478.

[BU07] Lasko Basnarkov and Viktor Urumov. "Phase transitions in the Kuramoto model". In: *Physical Review E* 76.5 (2007), p. 057201.

[CDJ17] Tommaso Coletta, Robin Delabays, and Philippe Jacquod. "Finite-size scaling in the Kuramoto model". In: *Physical Review E* 95.4 (2017), p. 042207.

[Chi15] Hayato Chiba. "A proof of the Kuramoto conjecture for a bifurcation structure of the infinite-dimensional Kuramoto model". In: *Ergodic Theory and Dynamical Systems* 35.3 (2015), pp. 762–834.

[CMM18] Hayato Chiba, Georgi S Medvedev, and Matthew S Mizuhara. "Bifurcations in the Kuramoto model on graphs". In: *Chaos: An Interdisciplinary Journal of Nonlinear Science* 28.7 (2018), p. 073109.

[CN11] Hayato Chiba and Isao Nishikawa. "Center manifold reduction for large populations of globally coupled phase oscillators". In: *Chaos: An Interdisciplinary Journal of Nonlinear Science* 21.4 (2011), p. 043103.

[Cra95] John David Crawford. "Scaling and singularities in the entrainment of globally coupled oscillators". In: *Physical review letters* 74.21 (1995), p. 4341.

[DA18] JD Da Fonseca and CV Abud. "The Kuramoto model revisited". In: *Journal of Statistical Mechanics: Theory and Experiment* 2018.10 (2018), p. 103204.

[Dai15] Hiroaki Daido. "Susceptibility of large populations of coupled oscillators". In: *Physical Review E* 91.1 (2015), p. 012925.

[Dai88]   Hiroaki Daido. "Lower critical dimension for populations of oscilla-
           tors with randomly distributed frequencies: a renormalization-group
           analysis". In: *Physical review letters* 61.2 (1988), p. 231.

[Dai90]   Hiroaki Daido. "Intrinsic fluctuations and a phase transition in a class
           of large populations of interacting oscillators". In: *Journal of Statistical
           Physics* 60.5 (1990), pp. 753–800.

[Dai94]   Hiroaki Daido. "Generic scaling at the onset of macroscopic mutual
           entrainment in limit-cycle oscillators with uniform all-to-all coupling".
           In: *Physical review letters* 73.5 (1994), p. 760.

[DGM08]   S. N. Dorogovtsev, A. V. Goltsev, and J. F. F. Mendes. "Critical phe-
           nomena in complex networks". In: *Reviews of Modern Physics* 80.4
           (Oct. 2008), pp. 1275–1335. DOI: 10.1103/revmodphys.80.1275. URL:
           https://doi.org/10.1103/revmodphys.80.1275.

[Har11]   Kenji Harada. "Bayesian inference in the scaling analysis of critical
           phenomena". In: *Physical Review E* 84.5 (2011), p. 056704.

[Har15]   Kenji Harada. "Kernel method for corrections to scaling". In: *Physical
           Review E* 92.1 (2015), p. 012106.

[Has10]   Martin Hasenbusch. "Finite size scaling study of lattice models in the
           three-dimensional Ising universality class". In: *Physical Review B* 82.17
           (2010), p. 174433.

[HCK02]   Hyunsuk Hong, Moo-Young Choi, and Beom Jun Kim. "Synchro-
           nization on small-world networks". In: *Physical Review E* 65.2 (2002),
           p. 026139.

[Hon+07]   Hyunsuk Hong, Hugues Chaté, Hyunggyu Park, and Lei-Han Tang.
           "Entrainment transition in populations of random frequency oscilla-
           tors". In: *Physical review letters* 99.18 (2007), p. 184101.

[Hon+15]   Hyunsuk Hong, Hugues Chaté, Lei-Han Tang, and Hyunggyu Park.
           "Finite-size scaling, dynamic fluctuations, and hyperscaling relation
           in the Kuramoto model". In: *Physical Review E* 92.2 (2015), p. 022122.

[JKÓ19]   Róbert Juhász, Jeffrey Kelling, and Géza Ódor. "Critical dynamics of
           the Kuramoto model on sparse random networks". In: *Journal of Sta-
           tistical Mechanics: Theory and Experiment* 2019.5 (2019), p. 053403.

[Kan+18]   Motonobu Kanagawa, Philipp Hennig, Dino Sejdinovic, and Bharath
           K Sriperumbudur. "Gaussian processes and kernel methods: A re-
           view on connections and equivalences". In: *arXiv preprint arXiv:1807.02582*
           (2018).

[KN19]   Yoshiki Kuramoto and Hiroya Nakao. "On the concept of dynamical
           reduction: the case of coupled oscillators". In: *Philosophical Transac-
           tions of the Royal Society A* 377.2160 (2019), p. 20190041.

[KP13]   Maxim Komarov and Arkady Pikovsky. "Multiplicity of singular syn-
           chronous states in the Kuramoto model of coupled oscillators". In:
           Physical review letters 111.20 (2013), p. 204101.

[KP14]   M Komarov and A Pikovsky. "The Kuramoto model of coupled oscillators with a bi-harmonic coupling function". In: *Physica D: Nonlinear Phenomena* 289 (2014), pp. 18–31.

[Kur75]   Yoshiki Kuramoto. "Self-entrainment of a population of coupled nonlinear oscillators". In: *International Symposium on Mathematical Problems in Theoretical Physics*. Springer-Verlag, 1975, pp. 420–422. DOI: 10.1007/bfb0013365. URL: https://doi.org/10.1007/bfb0013365.

[Lov12]   László Lovász. *Large networks and graph limits*. Vol. 60. American Mathematical Soc., 2012.

[Med14]   Georgi S Medvedev. "Small-world networks of Kuramoto oscillators". In: *Physica D: Nonlinear Phenomena* 266 (2014), pp. 13–22.

[Pan02]   James Pantaleone. "Synchronization of metronomes". In: *American Journal of Physics* 70.10 (2002), pp. 992–1000. DOI: 10.1119/1.1501118. URL: https://doi.org/10.1119/1.1501118.

[Paz05]   Diego Pazó. "Thermodynamic limit of the first-order phase transition in the Kuramoto model". In: *Physical Review E* 72.4 (2005), p. 046211.

[PDD18]   Bastian Pietras, Nicolás Deschle, and Andreas Daffertshofer. "First-order phase transitions in the Kuramoto model with compact bimodal frequency distributions". In: *Physical Review E* 98.6 (2018), p. 062219.

[PR15]   Arkady Pikovsky and Michael Rosenblum. "Dynamics of globally coupled oscillators: Progress and perspectives". In: *Chaos: An Interdisciplinary Journal of Nonlinear Science* 25.9 (2015), p. 097616.

[PV02]   Andrea Pelissetto and Ettore Vicari. "Critical phenomena and renormalization-group theory". In: *Physics Reports* 368.6 (2002), pp. 549–727.

[Sak88]   Hidetsugu Sakaguchi. "Cooperative phenomena in coupled oscillator systems under external fields". In: *Progress of theoretical physics* 79.1 (1988), pp. 39–46.

[Smi35]   Hugh M. Smith. "SYNCHRONOUS FLASHING OF FIREFLIES". In: *Science* 82.2120 (1935), pp. 151–152. ISSN: 0036-8075. DOI: 10.1126/science.82.2120.151. URL: https://science.sciencemag.org/content/82/2120/151.

[SSK87]   Hidetsugu Sakaguchi, Shigeru Shinomoto, and Yoshiki Kuramoto. "Local and grobal self-entrainments in oscillator lattices". In: *Progress of Theoretical Physics* 77.5 (1987), pp. 1005–1010.

[Str00]   Steven H. Strogatz. "From Kuramoto to Crawford: exploring the onset of synchronization in populations of coupled oscillators". In: *Physica D: Nonlinear Phenomena* 143.1-4 (Sept. 2000), pp. 1–20. DOI: 10.1016/s0167-2789(00)00094-4. URL: https://doi.org/10.1016/s0167-2789(00)00094-4.

[Win67]   Arthur T. Winfree. "Biological rhythms and the behavior of populations of coupled oscillators". In: *Journal of Theoretical Biology* 16.1 (1967), pp. 15–42. ISSN: 0022-5193. DOI: https://doi.org/10.1016/0022-5193(67)90051-3. URL: https://www.sciencedirect.com/science/article/pii/0022519367900513.

[WS98]   Duncan J Watts and Steven H Strogatz. "Collective dynamics of 'small-world' networks". In: *nature* 393.6684 (1998), pp. 440–442.

[YHY20]   Ryosuke Yoneda, Kenji Harada, and Yoshiyuki Y. Yamaguchi. "Critical exponents in coupled phase-oscillator models on small-world networks". In: *Physical Review E* 102.6 (Dec. 2020). DOI: 10.1103/physreve. 102.062212. URL: https://doi.org/10.1103/physreve.102.062212.

Table 3.1: Critical exponents $\beta, \bar{v}$ and the critical point K_c of (3.1) depending on the coupling function $f_a(\theta) = \sin\theta + a\sin 2\theta$ and the natural frequency distribution $g_n(\omega)$ in (3.2), for $a = 0$ and -0.2 and $n = 1, 2, 3,$ and ∞. For each pair of (a, n), we use $N_{\min} = 1600, 3200, 6400$, and execute the Bayesian scaling analysis [Har11] to find the best parameters fitting (3.9). We extrapolate the critical values to $N_{\min} = \infty$ by using the least square method, and they are listed in the line of $N_{\min} = \infty$. Here, we show the confidence intervals for the last digit of the estimated values in parentheses; for example, $2.13(3) = 2.13 \pm 0.03$.

$f_a(\theta)$	$g_n(\omega)$	$N_{\min}$	K_c	β	$\bar{v}$
$a = 0$	$n = 1$	1600	2.13(3)	0.33(4)	2.61(7)
		3200	2.07(1)	0.42(3)	2.53(5)
		6400	2.05(1)	0.47(3)	2.45(4)
		∞	**2.02(2)**	**0.51(4)**	**2.40(6)**
	$n = 2$	1600	1.85(1)	0.27(2)	2.67(5)
		3200	1.78(1)	0.37(2)	2.53(3)
		6400	1.755(9)	0.44(2)	2.50(3)
		∞	**1.72(1)**	**0.49(2)**	**2.43(4)**
	$n = 3$	1600	1.80(1)	0.28(2)	2.62(4)
		3200	1.76(1)	0.33(2)	2.51(3)
		6400	1.723(8)	0.44(2)	2.51(3)
		∞	**1.69(1)**	**0.47(2)**	**2.46(4)**
	$n = \infty$	1600	1.83(1)	0.27(1)	2.50(4)
		3200	1.79(1)	0.36(2)	2.52(3)
		6400	1.780(8)	0.41(2)	2.46(3)
		∞	**1.76(1)**	**0.46(2)**	**2.46(4)**
$a = -0.2$	$n = 1$	1600	2.43(5)	0.38(8)	2.67(9)
		3200	2.35(2)	0.44(6)	2.58(7)
		6400	2.34(1)	0.45(4)	2.42(6)
		∞	**2.31(3)**	**0.48(6)**	**2.36(8)**
	$n = 2$	1600	2.09(3)	0.31(4)	2.87(7)
		3200	1.99(2)	0.41(4)	2.65(5)
		6400	1.96(1)	0.47(3)	2.52(4)
		∞	**1.91(2)**	**0.51(4)**	**2.41(6)**
	$n = 3$	1600	2.04(3)	0.27(5)	2.85(8)
		3200	1.96(2)	0.37(4)	2.65(5)
		6400	1.91(1)	0.49(3)	2.59(4)
		∞	**1.86(2)**	**0.55(4)**	**2.50(6)**
	$n = \infty$	1600	2.08(3)	0.25(4)	2.76(6)
		3200	2.00(1)	0.38(4)	2.69(5)
		6400	1.97(1)	0.43(3)	2.54(4)
		∞	**1.94(2)**	**0.49(4)**	**2.49(6)**

CHAPTER 4

THE LOWER BOUND OF THE NETWORK CONNECTIVITY GUARANTEEING IN-PHASE SYNCHRONIZATION

This chapter is constructed based on the published paper [YTT21].

4.1 Introduction

Synchronization appears in various natural and artificial phenomena and has attracted much attention in various fields. Examples of the phenomena include swinging metronomes [Pan02], flashing fireflies [Smi35; BB68], singing frogs in chorus [Aih+14], and firing of neurons [CAY03; Win67; Lu+16]. The coupled phase-oscillators are the widely used model of synchronization [Kur75]. Previous studies have revealed conditions to ensure oscillators converge to the in-phase synchronization [Str00; OA08; Chi13; FA18; DGM08]. However, the relationship between network structure and the tendency of synchronization has not been fully understood yet.

One of the most important questions is how synchronization depends on connectivity, or connection density, of the network [WS94; WSG06; Tay12; CM15; LXB19; TSS20; LS20]. The connectivity μ of a network having N nodes has been defined as the minimum degree of the nodes divided by $N - 1$, the total number of other nodes. In 2012, Taylor considered networks of coupled phase-oscillators whose natural frequencies are identical and the connection among them has unit strength if it exists. For the networks, he showed that the in-phase synchronization is the only stable state if μ of a network is greater than 0.9395[Tay12], regardless of the structure of the network. This surprising result has attracted much attention and been refined by recent studies[LXB19; LS20]. Now it is proven that networks always synchronize if μ is greater than 0.7889[LS20]. Therefore, by defining the critical connectivity μ_c as the minimum connectivity of the networks to ensure globally stable in-phase synchronization, we can say that the best

41

known upper bound of μ_c is 0.7889 while the exact value of μ_c is not yet known.

Besides the upper bound, many studies has also revealed the lower bound of μ_c[WSG06; CM15; TSS20]. In particular, Townsend *et al.* have provided a circulant network whose connectivity is less than $0.6828\cdots$ and has a stable state other than the in-phase synchronization[TSS20], which means that the best known lower bound of μ_c is $0.6828\cdots$.

Previous studies, however, have used heuristic approaches rather than systematic ones to find dense networks in which competing attractors coexist with in-phase synchronization, which might have overlooked denser networks. To solve the problem, in this chapter, we map the search problem to an optimization problem, namely, an integer programming problem. Following the previous study[TSS20], we consider the circulant networks. Owing to the symmetry of the networks, we can analytically derive linear eigenvalues of the states, which enables us to formulate the optimization problem. The formulation allows us to systematically analyze a class of stable states called twisted states, which provides us an improvement on the best known lower bound from $0.6828\cdots$ to $0.6838\cdots$.

This chapter is organized as follows. In Section 4.2, we introduce a model of coupled identical phase-oscillators and define the network connectivity μ. In Section 4.3, we consider the twisted states of the circulant networks to derive the linear eigenvalues of the states analytically. In Section 4.4, we formulate the problem to find the densest network in which at least one twisted state is stable as an integer programming problem. We also provide a theorem yielding the rigorous solution of the optimization problem. The proof of the theorem is given in Section 4.5. In Section 4.6, we provide the maximum connectivity circulant network that has a stable twisted state, which allows us to update the lower bound of μ_c. In Section 4.7, we numerically validate the results. Section 4.8 gives conclusions and discussions.

4.2 Preliminaries

4.2.1 Coupled identical phase-oscillators

Identical N phase-oscillators coupled with each other on a network with undirected and unit-strength interactions are defined as

$$\frac{\mathrm{d}\theta_i}{\mathrm{d}t} = \sum_{j=1}^{N} a_{ij} \sin(\theta_j - \theta_i), \tag{4.1}$$

for $i \in [N]$, where $[N] = \{1, 2, \ldots, N\}$. Here, $\theta_i \in [0, 2\pi) \simeq \mathbb{S}^1$ is the phase of the i-th oscillator and a_{ij} is the (i, j)th-element of the $N \times N$ adjacency matrix A of the network. Since the network is undirected and unweighted, the matrix A is symmetric $a_{ij} = a_{ji} \in \{0, 1\}$. We also set $a_{ii} = 0$ for all $i \in [N]$ to avoid self-connection.

Note that coupled phase-oscillators have generally been defined as

$$\frac{\mathrm{d}\theta_i}{\mathrm{d}t} = \omega_i + \sum_{j=1}^{N} a_{ij} \sin(\theta_j - \theta_i), \tag{4.2}$$

for $i \in [N]$ and referred as Kuramoto model, where ω_i is the natural frequency of the i-th oscillator[Kur75]. Assuming that the natural frequencies are identical, $\omega_i = \bar{\omega}$, and rotating the whole system by $\bar{\omega}t$ recovers Eq. (4.1).

4.2.2 Equilibrium points and their linear stability

Let us denote an equilibrium point of (4.1) as $\boldsymbol{\theta}^* = (\theta_1^*, \ldots, \theta_N^*)^\top$. Then, $\boldsymbol{\theta}^*$ satisfies

$$\sum_{j=1}^{N} a_{ij} \sin(\theta_j^* - \theta_i^*) = 0 \tag{4.3}$$

for $i \in [N]$. Note that if $\boldsymbol{\theta}^*$ is an equilibrium point, $\boldsymbol{\theta}^* + c = (\theta_1^* + c, \ldots, \theta_N^* + c)^\top$ is also an equilibrium point of Eq. (4.1) for any $c \in \mathbb{S}^1$ due to its rotational symmetry.

The linear stability of the equilibrium point $\boldsymbol{\theta}^*$ is determined by eigenvalues of the Jacobian matrix $J_{\boldsymbol{\theta}^*}$ whose coefficient is

$$[J_{\boldsymbol{\theta}^*}]_{i,j} = \begin{cases} a_{ij} \cos(\theta_j^* - \theta_i^*) & i \neq j \\ -\sum_{k=1}^{N} a_{ik} \cos(\theta_k^* - \theta_i^*) & i = j \end{cases}. \tag{4.4}$$

All eigenvalues of the matrix are real because of its reflection symmetry, and one of them is always equal to zero due to the rotational symmetry $\boldsymbol{\theta}^* + c$. Thus, $\boldsymbol{\theta}^*$ is linearly stable if all other $N - 1$ eigenvalues are negative, and it is linearly unstable if at least one of them is positive. If more than one eigenvalue is equal to zero, one needs higher-order evaluation to realize the stability analysis. In this chapter, however, we only consider the linear stability of equilibrium states.

The model (4.1) always has a trivial in-phase state, in which $\theta_i = 0$ for all $i \in [N]$. Because $\boldsymbol{v}^\top J_0 \boldsymbol{v} = -\sum_{i>j} a_{ij}(v_i - v_j)^2 < 0$ for any $\boldsymbol{v} = (v_1, \ldots, v_N)^\top \in \mathbb{R}^N$ unless $\boldsymbol{v} = k\mathbf{1}$ with $k \in \mathbb{R}$, the in-phase state is always stable regardless of network structure.

4.2.3 Critical connectivity μ_c

The *connectivity* μ of a network consisting of N nodes is defined as the minimum degree of the network divided by $N - 1$, the maximum possible degree of the network. The devisor is $N - 1$ rather than N because the self-connection is not allowed. Because the degree of i-th oscillator is equal to the sum of the i-th row of the adjacency matrix A, the connectivity is given as

$$\mu = \frac{\min_{i \in [N]} \sum_{j \in [N]} a_{ij}}{N - 1}. \tag{4.5}$$

The connectivity value is equal to one for the all-to-all network, while it is equal to zero for disconnected networks.

The *critical connectivity* is defined as follows:

Definition 4.1 (Critical connectivity μ_c[TSS20])**.** *The critical connectivity μ_c is the smallest value of μ such that any network of N identical phase oscillators of unit connections is globally synchronizing if $\mu \geq \mu_c$; otherwise, for any $\mu < \mu_c$, at least one network having some other attractor besides the in-phase state exists.*

The best known bound of μ_c so far is

$$0.6828 \cdots \leq \mu_c \leq 0.7889. \tag{4.6}$$

4.3 Circulant networks

Following a previous study[TSS20], we focus on circulant networks. The circulant network is defined as a network whose adjacency matrix is a circulant matrix of the following form,

$$
\begin{aligned}
A = \left(a_{ij} \right)_{1 \leq i,j \leq N} &= \left(x_{j-i} \right)_{1 \leq i,j \leq N} \\
&= \begin{pmatrix}
x_0 & x_1 & \cdots & x_{N-2} & x_{N-1} \\
x_{N-1} & x_0 & x_1 & & x_{N-2} \\
\vdots & x_{N-1} & x_0 & \ddots & \vdots \\
x_2 & & \ddots & \ddots & x_1 \\
x_1 & x_2 & \cdots & x_{N-1} & x_0
\end{pmatrix},
\end{aligned}
\tag{4.7}
$$

where $x_k = x_{k \bmod N}$ for any $k \in \mathbb{Z}$, and $x_0 = 0$ because self-connection is not allowed now. Because $x_i \in \{0,1\}$ and $x_i = x_{N-i}$ for $i \in [N-1]$ for the undirected and unweighted networks, the structure of a circulant network is specified by the choice of $x_1, \ldots, x_{\lfloor N/2 \rfloor}$ to be 0 or 1, which has $2^{\lfloor N/2 \rfloor}$ possible combinations. The connectivity of the circulant network is given as

$$\mu = \frac{\sum_{i \in [N-1]} x_i}{N-1}, \tag{4.8}$$

because all nodes of the network share the same degree.

Townsend *et al.* have proven that

$$\boldsymbol{\theta}_p^* = \left(0, \frac{2\pi p}{N}, \ldots, \frac{2\pi p(N-1)}{N} \right)^\top \tag{4.9}$$

is an equilibrium state of the model (4.1) on any circular networks for any $0 \leq p \leq \lfloor N/2 \rfloor$. Below, we refer to the state $\boldsymbol{\theta}_p^*$ as the *p-twisted state*. The zero-twisted state $\boldsymbol{\theta}_0^*$ is the in-phase state.

Equation (4.4) gives the Jacobian matrix of the *p*-twisted state $\boldsymbol{\theta}_p^*$ as

$$
\left[J_{\boldsymbol{\theta}_p^*} \right]_{i,j} = \begin{cases}
x_{j-i} \cos \left(\dfrac{2\pi p(j-i)}{N} \right) & i \neq j \\
-\displaystyle\sum_{k=1}^{N} x_{k-i} \cos \left(\dfrac{2\pi p(k-i)}{N} \right) & i = j
\end{cases}.
\tag{4.10}
$$

The elements of $J_{\boldsymbol{\theta}_p^*}$ depend only on the difference of the indices, thus setting

$$
y_k = \begin{cases}
x_k \cos \left(\dfrac{2\pi pk}{N} \right) & k \in [N-1] \\
-\displaystyle\sum_{l=1}^{N-1} x_l \cos \left(\dfrac{2\pi pl}{N} \right) & k = 0
\end{cases},
\tag{4.11}
$$

enables us to simplify the (i, j)-th element of the Jacobian matrix to $\left[J_{\theta_p^*}\right]_{i,j} = y_{j-i}$. Since $x_{N-k} = x_k$ implies $y_{N-k} = y_k$, $J_{\theta_p^*}$ is again a symmetric circulant matrix. Using this property, we can derive its eigenvalues as

$$
\begin{aligned}
\lambda_k &= \sum_{l=0}^{N-1} y_l \cos\left(\frac{2\pi kl}{N}\right) \\
&= \sum_{l=1}^{N-1} x_l \cos\left(\frac{2\pi pl}{N}\right)\left[-1 + \cos\left(\frac{2\pi kl}{N}\right)\right]
\end{aligned}
\tag{4.12}
$$

for $k \in [N-1]$. The eigenvalue λ_0 is always equal to zero as we have mentioned.

4.4 Integer programming

Consider a search problem aiming to find the densest network having a stable state besides the in-phase one. By restricting ourselves to the twisted states of the circulant networks, we can map the search problem to an optimization problem. The objective of the optimization is to maximize the connectivity μ (4.8) by varying x_i under the condition that the eigenvalues λ_k in (4.12) should be negative for all $k \in [N-1]$.

Because x_i must be an integer, the optimization problem is expressed as a canonical form of the integer programming [CCZ14]:

Problem 4.1. *For $N \geq 2$ and $1 \leq p \leq \lfloor N/2 \rfloor$,*

$$
\begin{aligned}
\textit{maximize} \quad & \mu = \frac{1}{N-1}\mathbf{1}^\top x, \\
\textit{subject to} \quad & x \in \{0, 1\}^{N-1}, \\
& L^{(N,p)}x < 0, \\
& C^{(N)}x = 0.
\end{aligned}
\tag{4.13}
$$

Here we defined the matrices $L^{(N,p)} \in \mathbb{R}^{(N-1)\times(N-1)}$ and $C^{(N)} \in \mathbb{R}^{(N-1)\times(N-1)}$ such that their (k, l)-th elements are

$$
\left[L^{(N,p)}\right]_{k,l} = \cos\left(\frac{2\pi pl}{N}\right)\left[-1 + \cos\left(\frac{2\pi kl}{N}\right)\right],
\tag{4.14}
$$

and

$$
\left[C^{(N)}\right]_{k,l} = \delta_{k,l} - \delta_{k,N-l}.
\tag{4.15}
$$

Because the k-th eigenvalue satisfies $\lambda_k = \left[L^{(N,p)}x\right]_k$, the constraint $L^{(N,p)}x < 0$ means that the p-twisted state of the N-body network is linearly stable. The condition $C^{(N)}x = 0$ represents the constraint that the networks need be undirected, $x_k = x_{N-k}$ for $k \in [N-1]$. Intuitively, the optimization problem means that one should set as many x_ls as possible to 1 while satisfying constraint conditions $L^{(N,p)}x < 0$ and $C^{(N)}x = 0$.
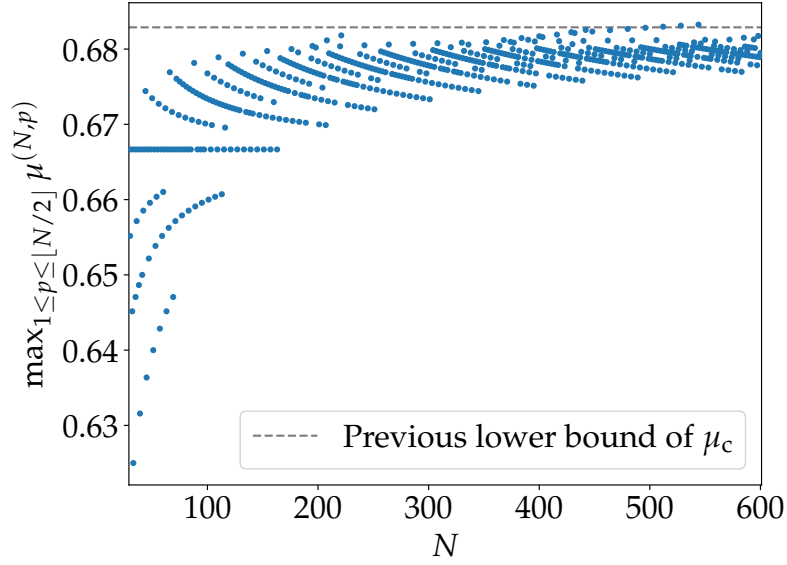
Figure 4.1: Numerical solutions $\max_{1 \le p \le \lfloor N/2 \rfloor} \mu^{(N,p)}$ of the integer programming Problem 4.1 as a function of N for $30 \le N \le 600$. The gray dashed line shows the best known lower bound of μ_c, $0.6828 \cdots$ [TSS20]. The maximum connectivity exceeds the known lower bound at $N = 512$ and 544.

The conversion of the search problem into the integer programming problem enables us to systematically survey the maximum connectivity. Let $\mu^{(N,p)}$ be the solution, i.e., the maximum μ, of the integer programming problem of N and p. Figure 4.1 shows numerical solutions of $\mu^{(N,p)}$ for $30 \le N \le 600$. We used a solver Cbc[For+20] that can be called through the library PuLP in Python and JuMP[DHL17] in Julia[Bez+17]. (Our codes are available on GitHub [1].) While further numerical computation beyond $N = 600$ is intractable due to the explosion of the solution space, the search up to $N = 600$ has already provided the $\mu^{(N,p)}$ that exceeds the best known lower bound at $N = 512$ and 544.

Integer programming problems are generally NP-hard [CCZ14]. However, for the specific problem, Problem 4.1, we can obtain analytical solutions of $\mu^{(N,p)}$ for any given values of (N, p). The following theorem states the result in general.

Theorem 4.1 (Maximum connectivity $\mu^{(N,p)}$). *For $N \ge 2$ and $1 \le p \le \lfloor N/2 \rfloor$, we set $m = \gcd(N, p)$ and $\widetilde{N} = N/m$.*

1. *For $\widetilde{N} \le 4$, Problem 4.1 does not have any feasible solutions.*

2. *For $\widetilde{N} \ge 5$, let s_k be*

$$s_k = \sum_{l=1}^{k} \cos\left(\frac{2\pi l}{\widetilde{N}}\right)\left[-1 + \cos\left(\frac{2\pi l}{\widetilde{N}}\right)\right], \tag{4.16}$$

and k_c be the minimum value of k such that $s_k \ge 0$. Then, the maximum connectivity $\mu^{(N,p)}$ is given as

$$\mu^{(N,p)} = \frac{m(2k_c - 1) - 3 - 2\lfloor ms_{k_c-1}/(s_{k_c} - s_{k_c-1})\rfloor}{N - 1}. \tag{4.17}$$

[1] https://github.com/yonesuke/DenseSync

46

Note that one can easily find k_c because s_k is a one-dimensional function of k. The proof of Theorem 4.1 is in the next section. We have observed a perfect agreement between the analytical prediction and the numerical solutions up to $N = 600$ (results not shown).

4.5 Proof

This section gives the proof of Theorem 4.1. Define a set of indices

$$S^{(N,p)} = \left\{ l \in [N-1] \ \middle| \ \left\{ \frac{pl}{N} \right\} \in \left[0, \frac{1}{4} \right] \cup \left[\frac{3}{4}, 1 \right] \right\}, \qquad (4.18)$$

where $\{\alpha\}$ is the fractional part of α. The (k,l)-th element of $L^{(N,p)}$ satisfies $\left[L^{(N,p)} \right]_{k,l} \leq 0$ for $l \in S^{(N,p)}$ because $\cos(2\pi pl/N) \geq 0$, whereas $\left[L^{(N,p)} \right]_{k,l} > 0$ for $l \in [N-1] \backslash S^{(N,p)}$ (please also see Fig. 4.2). Then, using the identity for $a \in \mathbb{Z}$

$$\sum_{l=1}^{N-1} \cos \frac{2\pi al}{N} = \begin{cases} -1 & a \not\equiv 0 \bmod N \\ N-1 & a \equiv 0 \bmod N \end{cases}, \qquad (4.19)$$

one can show that, for $k \neq p, N-p$ and $x \neq \mathbf{1}$,

$$\left[L^{(N,p)} x \right]_k \qquad (4.20)$$

$$< \sum_{l \in S^{(N,p)}} \left[L^{(N,p)} \right]_{k,l} + \sum_{l \in [N-1] \backslash S^{(N,p)}} \left[L^{(N,p)} \right]_{k,l} = \sum_{l=1}^{N-1} \left[L^{(N,p)} \right]_{k,l} \qquad (4.21)$$

$$= - \sum_{l=1}^{N-1} \cos \left(\frac{2\pi pl}{N} \right) + \frac{1}{2} \sum_{l=1}^{N-1} \cos \left(\frac{2\pi(p+k)l}{N} \right) + \frac{1}{2} \sum_{l=1}^{N-1} \cos \left(\frac{2\pi(p-k)l}{N} \right) \qquad (4.22)$$

$$= 0, \qquad (4.23)$$

which reduces the constraint of the optimization problem to

$$\left[L^{(N,p)} x \right]_p = \sum_{l=1}^{N-1} x_l \left[- \cos \left(\frac{2\pi pl}{N} \right) + \cos^2 \left(\frac{2\pi pl}{N} \right) \right] < 0, \qquad (4.24)$$

because $\left[L^{(N,p)} x \right]_p = \left[L^{(N,p)} x \right]_{N-p}$. Therefore, introducing $b^{(N,p)} = \left(b_1^{(N,p)}, \ldots, b_{N-1}^{(N,p)} \right)^\top$ where $b_l^{(N,p)} = - \cos \left(\frac{2\pi pl}{N} \right) + \cos^2 \left(\frac{2\pi pl}{N} \right)$, we can reduce Problem 4.1 to the equivalent problem,

Problem 4.2 (Equivalent representation of Problem 4.1). *For $N \geq 2$ and $1 \leq p \leq \lfloor N/2 \rfloor$,*

$$\begin{aligned} maximize \quad & \mu = \frac{1}{N-1} \mathbf{1}^\top x, \\ subject \ to \quad & x \in \{0,1\}^{N-1}, \\ & b^{(N,p)\top} x < 0, \\ & C^{(N)} x = \mathbf{0}. \end{aligned} \qquad (4.25)$$

We can easily confirm that Problem 4.2 has no feasible solutions when $\widetilde{N} \leq 4$ because $b_l^{(N,p)} \geq 0$ in these cases. Note that one can always set $x_l = 1$ for $l \in S^{(N,p)}$ because $\left[L^{(N,p)}\right]_{k,l} \leq 0$. (Remember that the objective of the optimization problem is to set as many x_ls as possible to 1 with satisfying the constraints.) One can, therefore, focus only on how many additional x_l of $l \in [N-1] \backslash S^{(N,p)}$ can be 1 with satisfying the constraint condition $b^{(N,p)\top} x < 0$ and $C^{(N)} x = 0$. In the following subsections, assuming that $\widetilde{N} \geq 5$, we solve Problem 4.2 by dividing the problem into four cases: $p = 1$; $p/m = 1$; $p/m \neq 1$ and $m = 1$; $p/m \neq 1$ and $m \neq 1$.

4.5.1 $p = 1$

Denote the cumulative sum of $b_l^{(N,p)}$ as

$$s_k = \sum_{l=1}^{k} b_l^{(N,p)}. \tag{4.26}$$

Because the function $-\cos\theta + \cos^2\theta$ (see solid line of Fig. 4.2 as an example) is symmetric around $\theta = \pi$ and monotonically increases from zero for $\theta \in [\pi/2, \pi]$, s_k takes its minimum negative value at $l = \lfloor N/4 \rfloor$, i.e., when $2\pi pl/N$ is just below $\pi/2$, and monotonically increases up to $l = \lfloor N/2 \rfloor$. Therefore, in order to set as many x_k to 1 as possible while keeping the condition $b^{(N,p)\top} x < 0$, one can set $x_k = 1$ for $k = 1, \ldots, k_c - 1$, and $N - k_c + 1, \ldots, N - 1$ due to the symmetry constraint $C^{(N)} x = 0$, where k_c is the smallest value of k such that $s_k \geq 0$. Other x_ks of $k \in \{k_c, \ldots, N - k_c\}$ must be zero. Thus, the maximum number of x_k that can be 1 is $2(k_c - 1)$, which means that the maximum connectivity is

$$\mu^{(N,1)} = \frac{\sum_{k \in [N-1]} x_k^*}{N - 1} = \frac{2(k_c - 1)}{N - 1}. \tag{4.27}$$

This expression agrees with Eq. (4.17) for the case of $p = 1$ because $\lfloor s_{k_c-1}/(s_{k_c} - s_{k_c-1}) \rfloor = -1$. Figure 4.2 shows $b_l^{(60,1)}$ as a function of $2\pi pl/N$, as an example. Because $s_{19} = -0.6972 \cdots < 0$ while $s_{20} = 0.0527 \cdots \geq 0$, $k_c = 20$, which provides $\mu^{(60,1)} = \frac{2 \cdot 19}{60-1} = 0.6440 \cdots$.

4.5.2 $p = m$

Define an integer $\widetilde{N} = N/m$ (remember that $m = \gcd(N, p)$) and divide the index domain $[N-1]$ of x_ls into $m + 1$ disjoints subsets; $[N-1] = I + I_1 + \cdots + I_m$, where $I = \{\widetilde{N}, 2\widetilde{N}, \ldots, (m-1)\widetilde{N}\}$ and $I_n = \{(n-1)\widetilde{N} + 1, \ldots, n\widetilde{N} - 1\}$. Because the function $-\cos\theta + \cos^2\theta$ is 2π-periodic (see solid line of Fig. 4.3 as an example), $b^{(N,p)} = b^{(\widetilde{N},1)}$ on each I_n. Figure 4.3 shows the case of $(N, m) = (180, 3)$ as an example. Thus, following discussion of the previous subsection, one can set $2(k_c - 1)$ x_ls to 1 on each I_n with keeping $b^{(N,p)\top} x < 0$ (blue filled circles in Fig. 4.3). One can also set all x_l to 1 for $l \in I$ because $\left[b^{(N,p)}\right]_l = 0$ on the subsets (red filled diamonds in Fig. 4.3).

Figure 4.2: $b_l^{(N,p)}$ as a function of $2\pi pl/N$ for $l \in [N-1]$ when $(N,p) = (60,1)$. The solid gray line is $-\cos\theta + \cos^2\theta$ for $\theta \in [0,2\pi]$. As $k_c = 20$ for $(N,p) = (60,1)$, x_k can be 1 for $k = 1, 2, \ldots, 19, 41, 42, \ldots, 59$ (filled circles) whereas other x_ks should be zero (empty circles). Note that both ends, $2\pi pl/N = 0, 2\pi$, are out of the domain.

So far, the value of $\boldsymbol{b}^{(N,p)\top}\boldsymbol{x}$ is equal to $2ms_{k_c-1}$ that is still negative. This implies that the possibility of additional x_ls being 1 still remains. The lowest value of $\left[b^{(N,p)}\right]_l$ in remaining, i.e. indices for which x_l has not set to 1 yet, is $b_{k_c}^{(\tilde{N},1)}$ that equals $s_{k_c} - s_{k_c-1}$. There are $2m$ such ls in the domain due to periodicity and the symmetry of $\left[b^{(N,p)}\right]_l$ (green empty and filled squares in Fig. 4.3). To set as many additional x_ls to 1 as possible, one should use these ls. Therefore, one can set a maximum of

$$2\left(\left\lceil\frac{-2ms_{k_c-1}}{2(s_{k_c} - s_{k_c-1})} - 1\right\rceil\right) \tag{4.28}$$

additional x_ls to 1 (pink filled circles in Fig. 4.3). The factor 2 being at the front and in the divisor of Eq. (4.28) appears because one has to simultaneously set x_l and x_{N-l} to 1 to keep the symmetry condition $C^{(N)}\boldsymbol{x} = \boldsymbol{0}$. Note that, as far as one keeps the numbers and conditions, one can choose any combination of ls from the $2m$ ls.

Putting the above results together, we obtain that

$$\mu^{(N,p)} = \frac{2m(k_c - 1) + m - 1 - 2\left(\left\lfloor\frac{ms_{k_c-1}}{s_{k_c} - s_{k_c-1}}\right\rfloor + 1\right)}{N - 1}, \tag{4.29}$$

which agrees with Eq. (4.17) of the theorem. Here we use the identity $\lceil\alpha\rceil = -\lfloor-\alpha\rfloor$ to derive the above result.
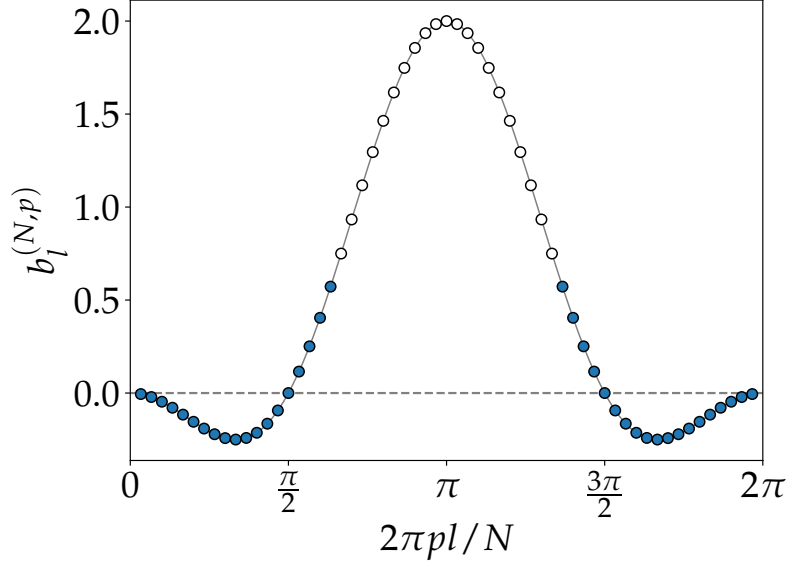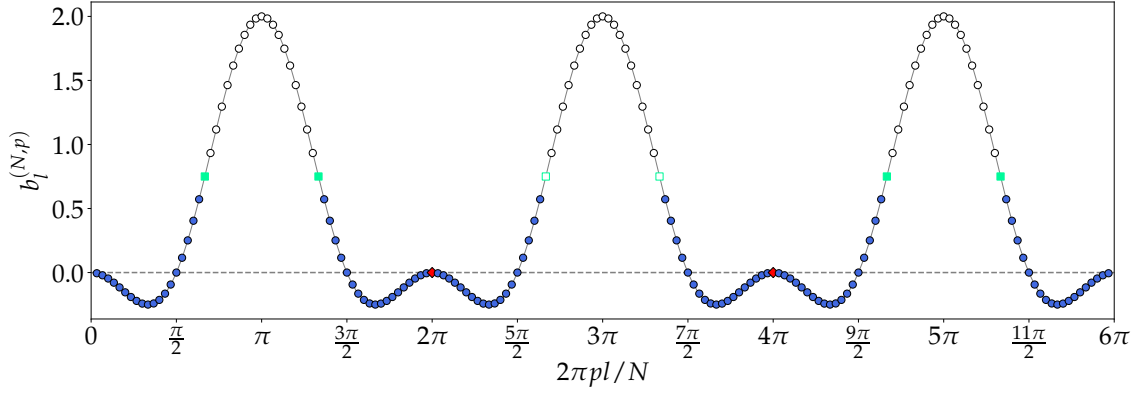
Figure 4.3: $b_l^{(N,p)}$ as a function of $2\pi pl/N$ for $l \in [N-1]$ when $(N,p) = (180,3)$. The solid gray line is $-\cos\theta + \cos^2\theta$ for $\theta \in [0,6\pi]$. $2(k_c - 1)$ x_ls on each $I_n, n = 1,2,\ldots,m$ (blue filled circles) and $m-1$ x_ls on I (red filled diamonds) can be 1. Additionally, $2\left(\lceil (-ms_{k_c-1})/(s_{k_c} - s_{k_c-1}) - 1 \rceil\right)$ (green filled squares) of $2m$ x_ls (green empty and filled squares) can be 1. Note that both ends, $2\pi pl/N = 0, 6\pi$, are out of the domain.

4.5.3 $p \neq m, m = 1$

Because $m = \gcd(N,p) = 1$, we have

$$\{1,2,\ldots,N-1\} = \{p,2p,\ldots,(N-1)p\} \pmod{N}, \tag{4.30}$$

which means that $\left\{\left[b^{(N,p)}\right]_l\right\}$ is equal to $\left\{\left[b^{(N,1)}\right]_l\right\}$ as a set. Thus, we obtain $\mu^{(N,p)} = \mu^{(N,1)}$, and are able to reduce this case to the case of subsection 4.5.1.

4.5.4 $p \neq m, m \neq 1$

Using the same argument as before, one can see that $\left\{\left[b^{(N,p)}\right]_l\right\} = \left\{\left[b^{(m\widetilde{N},m)}\right]_l\right\}$ as a set, which results in $\mu^{(N,p)} = \mu^{(m\widetilde{N},m)}$. Thus, this case is reduced to the case of subsection 4.5.2.

Putting all cases of subsections 4.5.1–4.5.4 together, we arrive Theorem 4.1.

4.6 The supremum of $\mu^{(N,p)}$

In this section, we derive the supremum $\overline{\mu}$ of $\mu^{(N,p)}$ defined as

$$\overline{\mu} := \sup\left\{\mu^{(N,p)} \,\middle|\, 1 \leq p \leq \lfloor N/2 \rfloor, N \geq 2\right\}, \tag{4.31}$$

which leads to improvement of the lower bound of the critical connectivity μ_c.

From the proof of Theorem 4.1, we have that

$$\overline{\mu} = \sup\left\{\mu^{(m\widetilde{N},m)} \,\middle|\, m \geq 1, \widetilde{N} \geq 5\right\}. \tag{4.32}$$
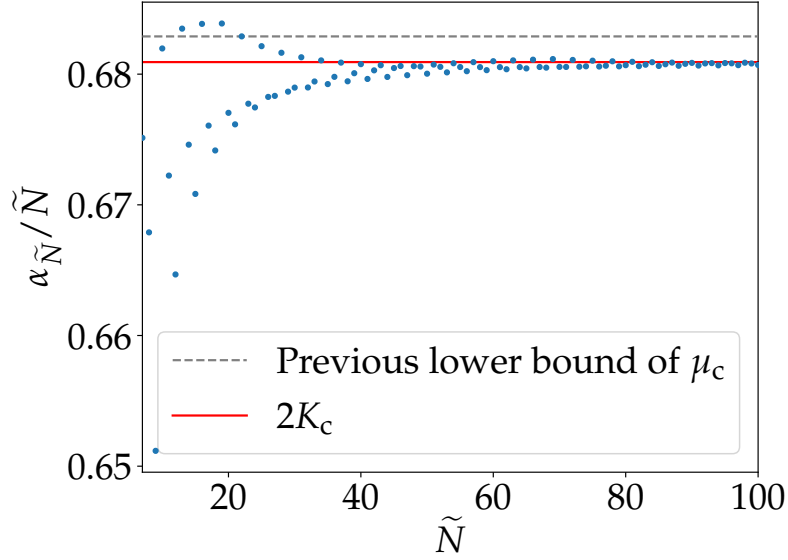
Figure 4.4: $\alpha_{\widetilde{N}}/\widetilde{N}$ for $5 \leq \widetilde{N} \leq 100$ (blue circles). The gray dashed line is the best known lower bound of the critical connectivity μ_{c}. The solid red line represents $2K_{\mathrm{c}}$.

Then, because

$$\frac{\alpha_{\widetilde{N}}m - 3}{\widetilde{N}m - 1} \leq \mu^{(m\widetilde{N},m)} \leq \frac{\alpha_{\widetilde{N}}m - 2}{\widetilde{N}m - 1}, \tag{4.33}$$

where

$$\alpha_{\widetilde{N}} = 2k_{\mathrm{c}} - 1 - 2\frac{s_{k_{\mathrm{c}}-1}}{s_{k_{\mathrm{c}}} - s_{k_{\mathrm{c}}-1}}, \tag{4.34}$$

we have

$$\mu^{(m\widetilde{N},m)} \leq \lim_{m\to\infty} \mu^{(m\widetilde{N},m)} = \frac{\alpha_{\widetilde{N}}}{\widetilde{N}} \tag{4.35}$$

for $m \geq 1, \widetilde{N} \geq 5$ by the squeeze theorem. Here we used

$$\frac{\alpha_{\widetilde{N}}m - 2}{\widetilde{N}m - 1} \leq \lim_{m\to\infty} \frac{\alpha_{\widetilde{N}}m - 2}{\widetilde{N}m - 1} = \frac{\alpha_{\widetilde{N}}}{\widetilde{N}} \tag{4.36}$$

that follows from $k_{\mathrm{c}} \leq N/2$ and $-1 \leq s_{k_{\mathrm{c}}-1}/(s_{k_{\mathrm{c}}} - s_{k_{\mathrm{c}}-1}) < 0$. Then there holds,

$$\bar{\mu} = \sup\left\{ \frac{\alpha_{\widetilde{N}}}{\widetilde{N}} \;\middle|\; \widetilde{N} \geq 5 \right\}. \tag{4.37}$$

Figure 4.4 shows $\alpha_{\widetilde{N}}/\widetilde{N}$ for $5 \leq \widetilde{N} \leq 100$.

Now let us derive the maximum of $\alpha_{\widetilde{N}}/\widetilde{N}$. We first obtain the inequality

$$\frac{\alpha_{\widetilde{N}}}{\widetilde{N}} \leq 2K_{\mathrm{c}} + \frac{2}{\widetilde{N}} + \frac{4\pi}{3\widetilde{N}^2} \tag{4.38}$$

from

$$\frac{k_c}{\widetilde{N}} \le K_c + \frac{1}{2\widetilde{N}} + \frac{2\pi}{3\widetilde{N}^2}, \tag{4.39}$$

where

$$2K_c := \lim_{\widetilde{N}\to\infty} \frac{\alpha_{\widetilde{N}}}{\widetilde{N}} = 2 \lim_{\widetilde{N}\to\infty} \frac{k_c}{\widetilde{N}} = 2 \cdot 0.34046 \cdots . \tag{4.40}$$

The proof of Eq. (4.38) and the derivation of the value of K_c are given in Appendix 4.A. Then, from the above inequality, we have $\alpha_{\widetilde{N}}/\widetilde{N} \le 0.683$ for $\widetilde{N} \ge 1001$.

For $\widetilde{N} \le 1000$, as Fig. 4.4 shows, some $\alpha_{\widetilde{N}}/\widetilde{N}$ exceed 0.683. Calculating these values, we can find that the maximum is given by $\widetilde{N} = 19$. Combining this with the result of the previous paragraph leads to the theorem, which sets a new lower bound of the critical connectivity exceeding the previous one:

Theorem 4.2 (Supremum value of $\mu^{(N,p)}$)**.**

$$\bar{\mu} = \frac{11}{19} - \frac{2}{19} \frac{\sum_{l=1}^{5}\left[-\cos\left(\frac{2\pi l}{19}\right) + \cos^2\left(\frac{2\pi l}{19}\right)\right]}{-\cos\left(\frac{12\pi}{19}\right) + \cos^2\left(\frac{12\pi}{19}\right)} \tag{4.41}$$

$$= 0.683875 \cdots . \tag{4.42}$$

The above discussion shows that the densest circulant network having a competing stable state besides the in-phase synchronization is given at $m \to \infty$ when $(N, p) = (19m, m)$. In other words, when we increase network connectivity, the network that most persistently keeps a stable twisted state is the infinitary large network of $19m$ nodes ($m \to \infty$), and the most persistent twisted state is the m-twisted state. We summarize an explicit construction of the adjacency matrix of the dense $19m$-node circulant network as Algorithm 4.1. We also show the optimal networks for $(N, p) = (19m, m)$ with $m = 1, 2, 3, 4$ in Fig. 4.5. As the limit of $m \to \infty$, the output of the algorithm converges to the adjacency matrix of the densest circulant network that delivers the new bound $\bar{\mu}$ along with the stable m-twisted state. Whether the series of the $19m$-node network has some specific topological features remains an open question.

4.7 Numerical Simulations

To validate Theorem 4.1, we numerically integrate the model (4.1) for $(N, p) = (1900, 100)$, as an example, using the fourth-order Runge–Kutta algorithm with a time step of $\delta t = 10^{-3}$. Thus $m = \gcd(N, p) = 100$, $\widetilde{N} = 19$, and the maximum connectivity of the network is

$$\mu^{(1900,100)} = \frac{1297}{1899} = 0.682991 \cdots , \tag{4.43}$$

which is greater than the previously reported value of the lower bound.

Algorithm 4.1 An explicit construction of the adjacency matrix of the dense circulant network having the stable m-twisted state. Here, $x[i]$ is the i-th element of x, $A[i,j]$ is the (i,j)-th element of A, and $b_l = -\cos(2\pi l/19) + \cos^2(2\pi l/19)$.

Require: m
1: $x \in \{0,1\}^{19m} \leftarrow \mathbf{0}$
2: $A \in \{0,1\}^{19m \times 19m}$ (Adjacency matrix)
3: ExtraAllowance $\leftarrow 2 \left\lceil -m \sum_{l=1}^{5} b_l / b_6 - 1 \right\rceil$
4: $c \leftarrow 0$
5: **for** $k \leftarrow 0$ to $m - 1$ **do**
6:     **for** $i \leftarrow 1$ to 5 **do**
7:         $x[19k + i], x[19(k + 1) - i] \leftarrow 1$
8:     **end for**
9:     **if** $k \geq 1$ **then**
10:         $x[19k] \leftarrow 1$
11:     **end if**
12: **end for**
13: **for** $k \leftarrow 0$ to $m - 1$ **do**
14:     $x[19k + 6], x[19(m - k) - 6] \leftarrow 1$
15:     $c \leftarrow c + 2$
16:     **if** $c >$ ExtraAllowance **then**
17:         break
18:     **end if**
19:     $x[19k + 13], x[19(m - k) - 13] \leftarrow 1$
20:     $c \leftarrow c + 2$
21:     **if** $c >$ ExtraAllowance **then**
22:         break
23:     **end if**
24: **end for**
25: **for** $i, j \leftarrow 1$ to $19m$ **do**
26:     $A[i, j] \leftarrow x[i - j \bmod 19m]$
27: **end for**
28: **return** A (Resulting adjacency matrix)
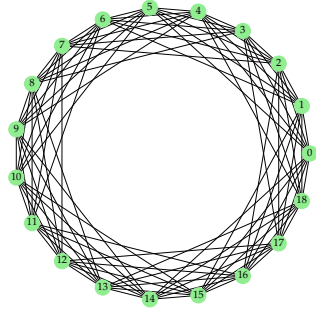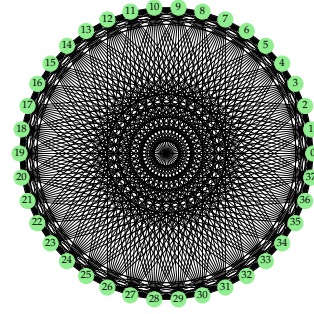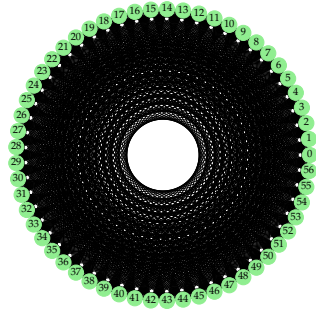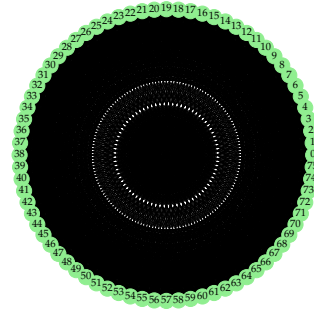
Figure 4.5: Optimal networks for $(N, p) = (19m, m)$ with $m = 1, 2, 3, 4$.

We set initial phases as $\boldsymbol{\theta}(0) = \boldsymbol{\theta}_p^* + \bar{\boldsymbol{\varepsilon}}$ to see the stability of the p-twisted state $\boldsymbol{\theta}_p^*$, where $\boldsymbol{\theta}(t) = (\theta_1(t), \ldots, \theta_N(t))^\top$ and $\bar{\boldsymbol{\varepsilon}}$ is a small initial perturbation. Remember that the p-twisted state is the most stable twisted state now because $p = m$. The initial perturbation $\bar{\boldsymbol{\varepsilon}}$ is prepared as follows: We first draw an N-dimensional Gaussian random variable $\boldsymbol{\varepsilon} = (\varepsilon_1, \ldots, \varepsilon_N)^\top$ with $\varepsilon_i \sim \mathcal{N}(0, \sigma^2/N)$ and $\sigma = 0.1\pi$ and then set $\bar{\boldsymbol{\varepsilon}} = \boldsymbol{\varepsilon} - \varepsilon_0$, where $\varepsilon_0 = (\sum_{i=1}^N \varepsilon_i)/N$, to ensure $\sum_{i=1}^N \bar{\varepsilon}_i = 0$, which is indispensable for the stability analysis because without the condition $\boldsymbol{\theta}(t)$ never converges to $\boldsymbol{\theta}_p^*$ due to the rotational symmetry of the model.

Figure 4.6 shows the results of the numerical simulation for realizations of the initial perturbation. To measure the distance between $\boldsymbol{\theta}(t)$ and $\boldsymbol{\theta}_p^*$ on the 2π-periodic space, we defined a quasinorm

$$\|\boldsymbol{\varphi}\| = \sqrt{\sum_{i=1}^N \mathrm{d}(\varphi_i)^2}, \tag{4.44}$$

$$\mathrm{d}(\varphi) = \begin{cases} \varphi \bmod 2\pi & 0 \le (\varphi \bmod 2\pi) < \pi \\ 2\pi - (\varphi \bmod 2\pi) & \pi \le (\varphi \bmod 2\pi) < 2\pi \end{cases}. \tag{4.45}$$

We see that the distance $\|\boldsymbol{\theta}(t) - \boldsymbol{\theta}_p^*\|$ monotonically decreases to zero regardless of the initial conditions, revealing that the p-twisted state, besides the trivial in-phase state, is stable on the dense network whose connectivity exceeds the previous lower bound.

The inset of Fig. 4.6 shows the developments of $\log\|\boldsymbol{\theta}(t) - \boldsymbol{\theta}_p^*\|$. As indicated by our analysis, the distance exponentially decreases to zero with the exponent
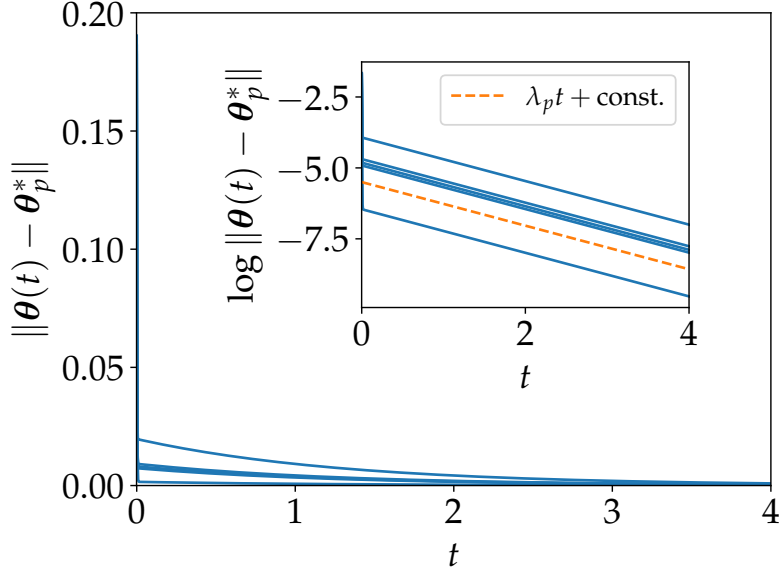
Figure 4.6: Temporal developments of $\|\boldsymbol{\theta}(t) - \boldsymbol{\theta}_p^*\|$ for five different initial conditions. The inset shows the semi-log plot of them. The orange dashed line in the inset represents exponential decay with the exponent λ_p.

of $\lambda_p = \left[L^{(N,p)}\boldsymbol{x}^*\right]_p$, where $\boldsymbol{x}^*$ is the binary vector specified in Sec. 4.5 to achieve the maximum connectivity of the network.

4.8 Summary and Discussions

In this chapter, we searched for the densest networks of identical phase oscillators that have at least one attractor besides the trivial in-phase state. Focusing on the twisted states of the circulant networks, we replaced the search problem with an optimization problem, an integer programming problem, which enables us to systematically study the stability of all twisted states on all possible circulant networks. The rigorous solution of the optimization problem provides us a new record of the network connectivity $0.6838\cdots$ such that a twisted state remains stable in a dense network, in other words, the record-breaking lower bound of the critical connectivity μ_c.

Many open questions remain about the critical connectivity. While this study revealed the stability of all twisted states of all circulant networks, it remains unclear whether circulant networks have other stable states besides the twisted states. It also remains unknown whether some dense networks not included in the circulant networks have stable states that break a record of the lower bound of the critical connectivity. One may be required stability analysis beyond the linear region to answer these questions. The problem of determining the upper bound of the critical connectivity also remains open as another essential subject. Because the network model of coupled identical phase oscillators can be written as a gradient system using a potential function, geometric approaches, utilizing the Morse theory[Mat02] for instance, may be helpful to approach the problem.

4.A Upper bound of k_c

In this appendix, we prove that

$$\frac{k_c}{\widetilde{N}} \leq K_c + \frac{1}{2\widetilde{N}} + \frac{2\pi}{3\widetilde{N}^2}, \tag{4.46}$$

where K_c is the limit of $k_c/\widetilde{N}$.

We first derive K_c. Setting $y = l/\widetilde{N}$ gives the continuum limit $\widetilde{N} \to \infty$ of $s_k/\widetilde{N}$ as

$$t(x) = \int_0^x b(y)\mathrm{d}y, \tag{4.47}$$

$$b(y) = -\cos 2\pi y + \cos^2 2\pi y. \tag{4.48}$$

Then K_c is given as the solution of the self-consistent equation;

$$8\pi t(K_c) = 4\pi K_c + \sin 4\pi K_c - 4\sin 2\pi K_c = 0. \tag{4.49}$$

Conventional search algorithms such as the binary search or the Newton–Raphson method give us an approximate value of K_c as $0.34046\cdots$.

To see the difference between K_c and $k_c/\widetilde{N}$, we calculate $s_k/\widetilde{N}$ as an equation deviated from $t(k/\widetilde{N})$. In the following, we restrict the range of k to $1/4 \leq k/\widetilde{N} \leq 1/2$ to focus on the value of $s_k/\widetilde{N}$ around $k = k_c$. From a trigonometric identity

$$\sum_{l=0}^{k} \cos l\theta = \frac{\sin(k\theta)}{2\tan(\theta/2)} + \cos^2\left(\frac{k\theta}{2}\right), \tag{4.50}$$

we rewrite $s_k/\widetilde{N}$ as

$$\frac{s_k}{\widetilde{N}} = \frac{1}{2}\frac{k}{\widetilde{N}} - \frac{1}{2\pi}\frac{\pi/\widetilde{N}}{\tan[\pi/\widetilde{N}]}\sin\left(2\pi\frac{k}{\widetilde{N}}\right) \tag{4.51}$$

$$+ \frac{1}{8\pi}\frac{2\pi/\widetilde{N}}{\tan[2\pi/\widetilde{N}]}\sin\left(4\pi\frac{k}{\widetilde{N}}\right) \tag{4.52}$$

$$+ \frac{1}{2\widetilde{N}}b\left(\frac{k}{\widetilde{N}}\right). \tag{4.53}$$

Using an inequality

$$\tan x \geq x + \frac{x^3}{3} \quad x \geq 0, \tag{4.54}$$

we have

$$\frac{s_k}{\widetilde{N}} > \frac{1}{2}\frac{k}{\widetilde{N}} - \frac{1}{2\pi}\sin\left(2\pi\frac{k}{\widetilde{N}}\right) + \frac{1}{8\pi}\sin\left(4\pi\frac{k}{\widetilde{N}}\right) \tag{4.55}$$

$$+ \frac{1}{2\widetilde{N}}b\left(\frac{k}{\widetilde{N}}\right) - \frac{\pi}{3N^2} + \frac{5\pi^3}{18N^4} \tag{4.56}$$

$$> t\left(\frac{k}{\widetilde{N}}\right) + \frac{1}{2\widetilde{N}}b\left(\frac{k}{\widetilde{N}}\right) - \frac{\pi}{3N^2}. \tag{4.57}$$

Assume that $k \geq \widetilde{N}K_c - 1/2 + 2\pi/(3\widetilde{N})$. Then, from the mean value theorem and the monotonicity of $b(x)$, we have

$$t(K_c) - t\left(K_c - \frac{1}{2\widetilde{N}} + \frac{2\pi}{3\widetilde{N}^2}\right) < \left(\frac{1}{2\widetilde{N}} - \frac{2\pi}{3\widetilde{N}^2}\right)b(K_c). \tag{4.58}$$

Since $t(K_c) = 0$ and $b(x) \leq 2$,

$$t\left(K_c - \frac{1}{2\widetilde{N}} + \frac{2\pi}{3\widetilde{N}^2}\right) > -\frac{1}{2\widetilde{N}}b(K_c) + \frac{4\pi}{3\widetilde{N}^2}. \tag{4.59}$$

Hence we have

$$\frac{s_k}{\widetilde{N}} > -\frac{1}{2\widetilde{N}}b(K_c) + \frac{4\pi}{3\widetilde{N}^2} + \frac{1}{2\widetilde{N}}b\left(\frac{k}{\widetilde{N}}\right) - \frac{\pi}{3N^2} \tag{4.60}$$

$$> -\frac{1}{2\widetilde{N}}\left[b(K_c) - b\left(K_c - \frac{1}{2\widetilde{N}} + \frac{2\pi}{3\widetilde{N}^2}\right)\right] + \frac{\pi}{\widetilde{N}^2}. \tag{4.61}$$

Using the mean value theorem again gives

$$b(K_c) - b\left(K_c - \frac{1}{2\widetilde{N}} + \frac{2\pi}{3\widetilde{N}^2}\right) = \left(\frac{1}{2\widetilde{N}} - \frac{2\pi}{3\widetilde{N}^2}\right)b'(x), \tag{4.62}$$

for some $x \in (K_c - 1/2\widetilde{N} + 2\pi/(3\widetilde{N}^2), K_c)$. Since $b'(x)$ is less than 4π, we obtain an evaluation of $s_k/\widetilde{N}$ as

$$\frac{s_k}{\widetilde{N}} > -\frac{2\pi}{\widetilde{N}}\left(\frac{1}{2\widetilde{N}} - \frac{2\pi}{3\widetilde{N}^2}\right) + \frac{\pi}{\widetilde{N}^2} = \frac{4\pi^2}{3\widetilde{N}^3} > 0, \tag{4.63}$$

meaning that $s_k > 0$ as long as $k \geq \widetilde{N}K_c - 1/2 + 2\pi/(3\widetilde{N})$. From this, the desired evaluation holds:

$$k_c \leq \left\lceil \widetilde{N}K_c - \frac{1}{2} + \frac{2\pi}{3\widetilde{N}} \right\rceil \leq \widetilde{N}K_c + \frac{1}{2} + \frac{2\pi}{3\widetilde{N}}, \tag{4.64}$$

Figure 4.7 shows $k_c/\widetilde{N}$ together with the derived bound.

References

[Aih+14] Ikkyu Aihara, Takeshi Mizumoto, Takuma Otsuka, Hiromitsu Awano, Kohei Nagira, Hiroshi G. Okuno, and Kazuyuki Aihara. "Spatio-Temporal Dynamics in Collective Frog Choruses Examined by Mathematical Modeling and Field Observations". In: *Scientific Reports* 4.1 (Jan. 2014), p. 3891. DOI: 10.1038/srep03891. URL: https://doi.org/10.1038/srep03891.

[BB68] John Buck and Elisabeth Buck. "Mechanism of Rhythmic Synchronous Flashing of Fireflies". In: *Science* 159.3821 (1968), pp. 1319–1327. ISSN: 0036-8075. DOI: 10.1126/science.159.3821.1319. URL: https://science.sciencemag.org/content/159/3821/1319.
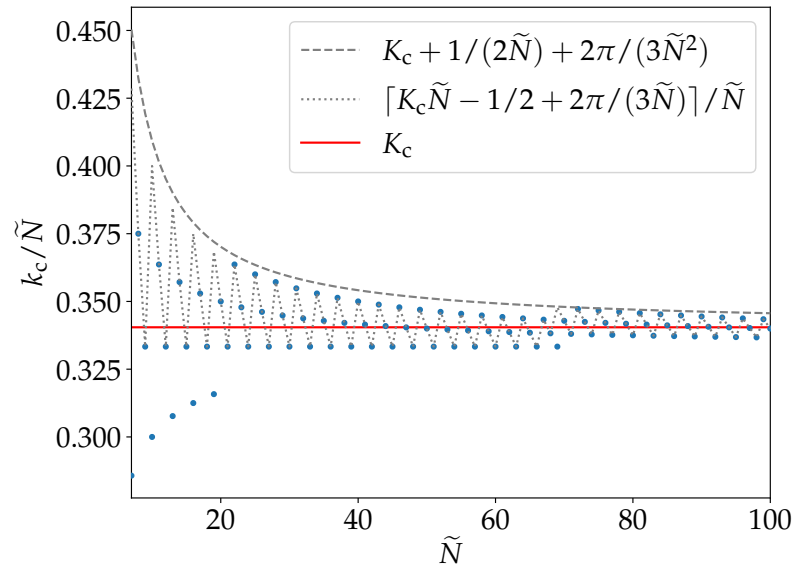
Figure 4.7: $k_c/\widetilde{N}$ for $7 \leq \widetilde{N} \leq 100$ together with the bound of $k_c/\widetilde{N}$ obtained in (4.64). We see that $k_c/\widetilde{N}$ gets close to K_c as $\widetilde{N} \to \infty$.

[Bez+17]   Jeff Bezanson, Alan Edelman, Stefan Karpinski, and Viral B Shah. "Julia: A fresh approach to numerical computing". In: *SIAM Review* 59.1 (2017), pp. 65–98. DOI: 10.1137/141000671.

[CAY03]   Rosa Cossart, Dmitriy Aronov, and Rafael Yuste. "Attractor dynamics of network UP states in the neocortex". In: *Nature* 423.6937 (May 2003), pp. 283–288. DOI: 10.1038/nature01614. URL: https://doi.org/10.1038/nature01614.

[CCZ14]   Michele Conforti, Gérard Cornuéjols, and Giacomo Zambelli. *Integer Programming*. Springer International Publishing, 2014. DOI: 10.1007/978-3-319-11008-0. URL: https://doi.org/10.1007/978-3-319-11008-0.

[Chi13]   Hayato Chiba. "A proof of the Kuramoto conjecture for a bifurcation structure of the infinite-dimensional Kuramoto model". In: *Ergodic Theory and Dynamical Systems* 35.3 (Oct. 2013), pp. 762–834. DOI: 10.1017/etds.2013.68. URL: https://doi.org/10.1017/etds.2013.68.

[CM15]   Eduardo A. Canale and Pablo Monzón. "Exotic equilibria of Harary graphs and a new minimum degree lower bound for synchronization". In: *Chaos: An Interdisciplinary Journal of Nonlinear Science* 25.2 (2015), p. 023106. DOI: 10.1063/1.4907952. URL: https://doi.org/10.1063/1.4907952.

[DGM08]   S. N. Dorogovtsev, A. V. Goltsev, and J. F. F. Mendes. "Critical phenomena in complex networks". In: *Reviews of Modern Physics* 80.4 (Oct. 2008), pp. 1275–1335. DOI: 10.1103/revmodphys.80.1275. URL: https://doi.org/10.1103/revmodphys.80.1275.

[DHL17]   Iain Dunning, Joey Huchette, and Miles Lubin. "JuMP: A Modeling Language for Mathematical Optimization". In: *SIAM Review* 59.2 (2017), pp. 295–320. DOI: 10.1137/15M1020575.

[FA18]   J D da Fonseca and C V Abud. "The Kuramoto model revisited". In: *Journal of Statistical Mechanics: Theory and Experiment* 2018.10 (Oct. 2018), p. 103204. DOI: 10.1088/1742-5468/aadb05. URL: https://doi.org/10.1088/1742-5468/aadb05.

[For+20]   John Forrest, Ted Ralphs, Stefan Vigerske, LouHafer, Bjarni Kristjansson, jpfasano, EdwinStraver, Miles Lubin, Haroldo Gambini Santos, rlougee, and Matthew Saltzman. *coin-or/Cbc: Version 2.10.5*. 2020. DOI: 10.5281/ZENODO.3700700. URL: https://zenodo.org/record/3700700.

[Kur75]   Yoshiki Kuramoto. "Self-entrainment of a population of coupled nonlinear oscillators". In: *International Symposium on Mathematical Problems in Theoretical Physics*. Springer-Verlag, 1975, pp. 420–422. DOI: 10.1007/bfb0013365. URL: https://doi.org/10.1007/bfb0013365.

[LS20]   Jianfeng Lu and Stefan Steinerberger. "Synchronization of Kuramoto oscillators in dense networks". In: *Nonlinearity* 33.11 (Oct. 2020), pp. 5905–5918. DOI: 10.1088/1361-6544/ab9baa. URL: https://doi.org/10.1088/1361-6544/ab9baa.

[Lu+16]   Zhixin Lu, Kevin Klein-Cardeña, Steven Lee, Thomas M. Antonsen, Michelle Girvan, and Edward Ott. "Resynchronization of circadian oscillators and the east-west asymmetry of jet-lag". In: *Chaos: An Interdisciplinary Journal of Nonlinear Science* 26.9 (Sept. 2016), p. 094811. DOI: 10.1063/1.4954275. URL: https://doi.org/10.1063/1.4954275.

[LXB19]   Shuyang Ling, Ruitu Xu, and Afonso S. Bandeira. "On the Landscape of Synchronization Networks: A Perspective from Nonconvex Optimization". In: *SIAM Journal on Optimization* 29.3 (Jan. 2019), pp. 1879–1907. DOI: 10.1137/18m1217644. URL: https://doi.org/10.1137/18m1217644.

[Mat02]   Yukio Matsumoto. *An Introduction to Morse Theory*. Vol. 208. American Mathematical Soc., 2002. URL: https://bookstore.ams.org/mmono-208/.

[OA08]   Edward Ott and Thomas M. Antonsen. "Low dimensional behavior of large systems of globally coupled oscillators". In: *Chaos: An Interdisciplinary Journal of Nonlinear Science* 18.3 (Sept. 2008), p. 037113. DOI: 10.1063/1.2930766. URL: https://doi.org/10.1063/1.2930766.

[Pan02]   James Pantaleone. "Synchronization of metronomes". In: *American Journal of Physics* 70.10 (2002), pp. 992–1000. DOI: 10.1119/1.1501118. URL: https://doi.org/10.1119/1.1501118.

[Smi35]   Hugh M. Smith. "SYNCHRONOUS FLASHING OF FIREFLIES". In: *Science* 82.2120 (1935), pp. 151–152. ISSN: 0036-8075. DOI: 10.1126/science.82.2120.151. URL: https://science.sciencemag.org/content/82/2120/151.

[Str00]   Steven H. Strogatz. "From Kuramoto to Crawford: exploring the on-
          set of synchronization in populations of coupled oscillators". In: *Phys-
          ica D: Nonlinear Phenomena* 143.1-4 (Sept. 2000), pp. 1–20. DOI: 10 .
          1016/s0167-2789(00)00094-4. URL: https://doi.org/10.1016/
          s0167-2789(00)00094-4.

[Tay12]   Richard Taylor. "There is no non-zero stable fixed point for dense net-
          works in the homogeneous Kuramoto model". In: *Journal of Physics A:
          Mathematical and Theoretical* 45.5 (Jan. 2012), p. 055102. DOI: 10.1088/
          1751-8113/45/5/055102. URL: https://doi.org/10.1088/1751-
          8113/45/5/055102.

[TSS20]   Alex Townsend, Michael Stillman, and Steven H. Strogatz. "Dense
          networks that do not synchronize and sparse ones that do". In: *Chaos:
          An Interdisciplinary Journal of Nonlinear Science* 30.8 (2020), p. 083142.
          DOI: 10 . 1063 / 5 . 0018322. URL: https : / / doi . org / 10 . 1063 / 5 .
          0018322.

[Win67]   Arthur T. Winfree. "Biological rhythms and the behavior of popu-
          lations of coupled oscillators". In: *Journal of Theoretical Biology* 16.1
          (1967), pp. 15–42. ISSN: 0022-5193. DOI: https://doi.org/10.1016/
          0022-5193(67)90051-3. URL: https://www.sciencedirect.com/
          science/article/pii/0022519367900513.

[WS94]   Shinya Watanabe and Steven H. Strogatz. "Constants of motion for
          superconducting Josephson arrays". In: *Physica D: Nonlinear Phenom-
          ena* 74.3 (1994), pp. 197–253. ISSN: 0167-2789. DOI: https://doi.org/
          10.1016/0167-2789(94)90196-1. URL: http://www.sciencedirect.
          com/science/article/pii/0167278994901961.

[WSG06]   Daniel A. Wiley, Steven H. Strogatz, and Michelle Girvan. "The size
          of the sync basin". In: *Chaos: An Interdisciplinary Journal of Nonlinear
          Science* 16.1 (2006), p. 015103. DOI: 10.1063/1.2165594. URL: https:
          //doi.org/10.1063/1.2165594.

[YTT21]   Ryosuke Yoneda, Tsuyoshi Tatsukawa, and Jun-nosuke Teramae. "The
          lower bound of the network connectivity guaranteeing in-phase syn-
          chronization". In: *Chaos: An Interdisciplinary Journal of Nonlinear Sci-
          ence* 31.6 (June 2021), p. 063124. DOI: 10.1063/5.0054271. URL: https:
          //doi.org/10.1063/5.0054271.

CHAPTER 5

GAUSSIAN PROCESS REGRESSION APPROACH TO ESTIMATING PHASE DYNAMICS FROM RHYTHMIC DATA

This chapter is constructed based on the published paper [Yon+22].

5.1 Introduction

The coupled phase-oscillator model is a mathematical model that describes the dynamics of a system of coupled oscillators. It is commonly used in the study of synchronization phenomena [Str03], such as the coordinated behavior of neurons in the brain [CAY03; Win67; Lu+16] or the synchronized flashing of fireflies [Smi35; BB68]. The model consists of a set of oscillators, each with its own phase, which are coupled through various forms of interactions, such as direct coupling or global coupling. The dynamics of the system are governed by a set of coupled differential equations, which can be analyzed to study the emergence of collective behavior and the effects of different coupling mechanisms on the oscillators' synchronization [KM11]. This model has been widely applied in various fields, including physics [WW88] and biology [Lu+16], to gain insight into the mechanisms underlying synchronization in complex systems.

The estimation of equations describing rhythmic phenomena from data is a crucial step in understanding the underlying mechanisms of these phenomena. Revealing the equation of a rhythmic phenomenon can provide valuable insights into the behavior of the system and its properties. Many studies have been conducted to estimate the parameters of oscillator systems from data using methods such as Fourier series expansion. This approach has been widely applied in the study of rhythmic phenomena and has yielded important results in fields such as neuroscience and engineering.

The Bayesian linear regression formulation has been successfully applied to estimate the coefficients of the Fourier series, which is commonly used to repre-

sent the coupling function in oscillator systems [OA14]. However, the order of the
Fourier series, which determines the accuracy of the approximation, is typically
arbitrary and subject to the limitations of the evidence approximation. Further-
more, the finite order approximation of the Fourier series may introduce oscilla-
tory errors known as the Gibbs phenomenon, which can affect the accuracy of the
estimates.

One potential solution to the limitations of the Bayesian linear regression ap-
proach is to use Gaussian process regression, which offers greater flexibility in
estimating the coupling function of the phase oscillator. Gaussian process regres-
sion is a non-parametric regression method that allows for the flexible modeling
of complex functions through the use of a kernel function [RW06]. This kernel
function can be designed to capture the smoothness, periodicity, and additive na-
ture of the coupling function, enabling us to estimate the underlying dynamics of
the phase oscillator system accurately [Kan+18]. In this chapter, we will introduce
the concept of Gaussian process regression and demonstrate its effectiveness in
estimating the coupling function of the phase oscillator.

This chapter is organized as follows. In Sec. 5.3, we propose a method for ex-
tracting the coupling functions of oscillator systems from data exhibiting rhyth-
mic phenomena using Gaussian process regression. This allows for more flexible
estimation than Bayesian linear regression. The proposed method is applied to
equation 1 and equation 2 in the next Section 5.4. Finally, we conclude this chap-
ter and give some remarks in Sec. 5.5.

5.2   Problem setting

In this chapter, we consider the general coupled limit-cycle oscillator models and
predict the coupling functions of their reduced coupled phase-oscillator models
from the phase data. General coupled phase-oscillator models consist of N oscil-
lators with their phase θ_i, and is governed by the following ODE,

$$\frac{d\theta_i}{dt} = \Gamma_i(\theta_1 - \theta_i, \ldots, \theta_N - \theta_i), \tag{5.1}$$

for $i = 1, \ldots, N$. The domain of a ith coupling function Γ_i is $N-1$ dimensional
torus $\mathbb{T}^{N-1}$, and each entry is the phase difference with another oscillator. There-
fore, our problem is to predict the coupling function $\Gamma_i \colon \mathbb{T}^{N-1} \to \mathbb{R}$ from data
$\mathcal{D} = \{(x_j, y_j)\}_{j=1}^{n_{\text{data}}}$ with $x_j \in \mathbb{T}^{N-1}$ and $y_j \in \mathbb{R}$ for $j = 1, 2, \ldots, n_{\text{data}}$.

5.3   Methodology: Gaussian process

In this chapter, we use the Gaussian process for regression and predict the cou-
pling function. We briefly address the procedure of the Gaussian process regres-
sion followed by the definition of Gaussian process.

5.3.1   Gaussian process

Gaussian process is a type of stochastic processes, and it is defined as follows:

Definition 5.1 (Gaussian process). *A stochastic process $\{X_t\}_{t\in T}$ is said to be a **Gaussian process** if for any finite slices of index set T, say $(t_1,\ldots,t_k)$,*

$$(X_{t_1}, X_{t_2}, \ldots, X_{t_k}) \tag{5.2}$$

becomes a k-dimensional Gaussian random variable.

In many cases the index set T is infinite one, hence a sample of Gaussian process can be seen as a function. When $f\colon \mathcal{X} \to \mathbb{R}$ is a Gaussian process, we define functions $m\colon \mathcal{X} \to \mathbb{R}, k\colon \mathcal{X} \times \mathcal{X} \to \mathbb{R}$ by calculating

$$m(x) = \mathbb{E}[f(x)], \tag{5.3}$$
$$k(x,\tilde{x}) = \mathbb{E}[(f(x) - m(x))(f(\tilde{x}) - m(\tilde{x}))], \tag{5.4}$$

for any $x, \tilde{x} \in \mathcal{X}$. We refer to the function m as a **mean function** and to the function k as a **covariance function**. It is known that Gaussian process is completely characterized by the functions m and k. In the following, we define the Gaussian process by determining m and k, and we write a Gaussian process variable (function) f as

$$f \sim \mathcal{GP}(m,k). \tag{5.5}$$

Let's say a function f be a Gaussian process with $f \sim \mathcal{GP}(m,k)$. For finite points $X = (x_1,\ldots,x_n)^\top$,

$$\boldsymbol{f} = f(X) := (f(x_1),\ldots,f(x_n))^\top \tag{5.6}$$

obeys a n-dimensional Gaussian distribution with a mean m_X and a covariance matrix k_{XX}, which read

$$m_X = m(X) := (m(x_1), m(x_2),\ldots,m(x_n))^\top, \tag{5.7}$$

$$k_{XX} = k(X,X) := \begin{pmatrix} k(x_1,x_1) & k(x_1,x_2) & \cdots & k(x_1,x_n) \\ k(x_2,x_1) & k(x_2,x_2) & \cdots & k(x_2,x_n) \\ \vdots & \vdots & \ddots & \vdots \\ k(x_n,x_1) & k(x_n,x_2) & \cdots & k(x_n,x_n) \end{pmatrix}. \tag{5.8}$$

This is a direct consequence of the definition and its characterization of Gaussian process. Sampling functions of Gaussian process is done by sampling Gaussian distribution random variables with $\mathcal{N}(m_X, k_{XX})$, and the procedure is summarized in Algorithm 5.1. We also plot samples of Gaussian process in Fig. 5.1 using this algorithm.

5.3.2 Gaussian process regression

Gaussian process regression is a non-parametric regression method that allows for the flexible modeling of complex functions. It is a Bayesian approach that uses a prior distribution over functions, which is updated based on the observed data to obtain a posterior distribution. The smoothness, periodicity, and additive nature of the function can be controlled through the use of a kernel function, which defines the covariance between different points in the function space.

Algorithm 5.1 A function sampling Gaussian process `GP_SAMPLE`

Input: sampling points $X = (x_1, \dots, x_n)$
Input: Gaussian process $\mathcal{GP}(m, k)$ $\quad \triangleright$ mean function $m(\cdot)$, covariance function $k(\cdot, \cdot)$
Output: values of a sample of function from $\mathcal{GP}(m, k)$ of X
$\quad$ **function** GP_SAMPLE$(X, \mathcal{GP}(m, k))$
$\qquad$ calculate mean array $m_X \leftarrow m(X) = (m(x_1, \dots, m(x_n)))^\top$
$\qquad$ calculate covariance matrix $k_{XX} \leftarrow [k_{XX}]_{i,j} = (k(x_i, x_j))_{i,j}$
$\qquad$ calculate Cholesky decomposition matrix $L \leftarrow$ `cholesky`(k_{XX})
$\qquad$ generate N samples from the standard normal distribution $z \leftarrow$ `randn`(n)
$\qquad$ calculate affine transformation $f \leftarrow m_X + Lz$ $\qquad \triangleright f \sim \mathcal{N}(m_X, k_{XX})$
$\qquad$ **return** f
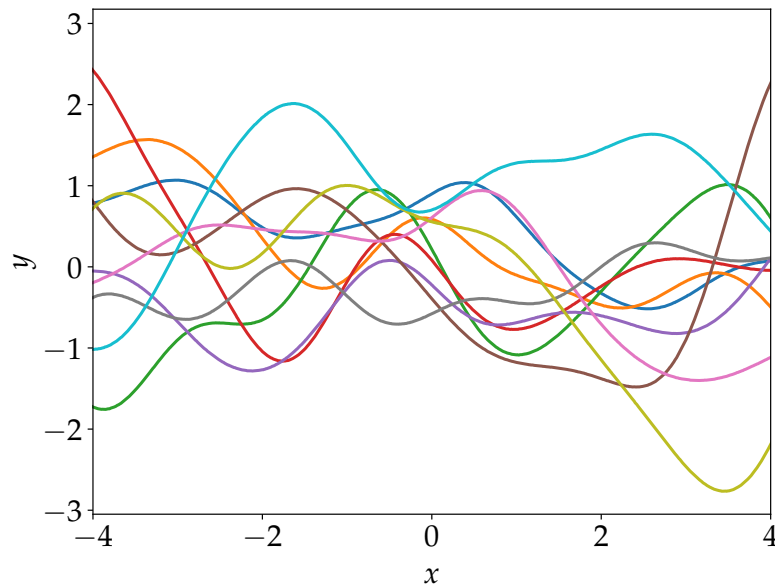$\quad$ **end function**

Figure 5.1: Gaussian process sample paths. The mean function is $m(x) = 0$ and the covariance function is $k(x, \tilde{x}) = \exp[-(x - \tilde{x})^2/2]$.

One of the main merits of Gaussian process regression is its ability to provide uncertainty estimates for the regression parameters, which can be useful in situations where the data are noisy or sparse. It also allows for the modeling of complex functions without requiring the specification of a fixed functional form, which can be difficult to determine in many cases. Additionally, the use of a kernel function allows for the incorporation of prior knowledge about the function, such as its smoothness or periodicity, which can improve the accuracy of the estimates.

Let's say we have a data $\mathcal{D} = \{(\boldsymbol{x}_j, y_j)\}_{j=1}^{n_{\text{data}}} \subset \mathcal{X} \times \mathbb{R}$ with n_{data} number of data and a function $f: \mathcal{X} \to \mathbb{R}$, such that

$$y_i = f(\boldsymbol{x}_i) + \xi_i, \tag{5.9}$$

for $i = 1, \ldots, n_{\text{data}}$, where ξ_i is a random variable of $\mathcal{N}(0, \sigma^2)$ that represents a "noise" in the output. Our task is to predict the unknown function f from the data $\mathcal{D}$ using the Gaussian process.

We start by assuming that the unknown regression function f is drawn from a given Gaussian process prior,

$$f \sim \mathcal{GP}(m, k), \tag{5.10}$$

where $m: \mathcal{X} \to \mathbb{R}$ is the mean function and $k: \mathcal{X} \times \mathcal{X} \to \mathbb{R}$ is the covariance function. The covariance function k should be chosen so that they reflect one's prior knowledge or belief about the regression function f, and we will discuss this in the next subsection. In many cases, the mean function m is set to a constant zero function for simplicity.

The posterior distribution of f is calculated analytically by linear algebra, and is again a Gaussian process. The distribution is given by the following closed form:

$$f \mid \mathcal{D} \sim \mathcal{GP}(\overline{m}, \overline{k}), \tag{5.11}$$

where the posterior mean function $\overline{m}$ and the posterior covariance function $\overline{k}$ are

$$\overline{m}(\boldsymbol{x}) = m(\boldsymbol{x}) + k_{\boldsymbol{x}X}(k_{XX} + \sigma^2 I_{n_{\text{data}}})^{-1}(\boldsymbol{y} - m_X), \tag{5.12}$$

$$\overline{k}(\boldsymbol{x}, \boldsymbol{x}') = k(\boldsymbol{x}, \boldsymbol{x}') - k_{\boldsymbol{x}X}(k_{XX} + \sigma^2 I_{n_{\text{data}}})^{-1}k_{X\boldsymbol{x}'}. \tag{5.13}$$

where $k_{XX} \in \mathbb{R}^{n_{\text{data}} \times n_{\text{data}}}$ denotes the matrix with elements $[k_{XX}]_{ij} = k(\boldsymbol{x}_i, \boldsymbol{x}_j)$, $k_{X\boldsymbol{x}} = k_{\boldsymbol{x}X}^{\top} = (k(\boldsymbol{x}_1, \boldsymbol{x}), \ldots, k(\boldsymbol{x}_{n_{\text{data}}}, \boldsymbol{x}))^{\top}$, $m_X = (m(\boldsymbol{x}_1), \ldots, m(\boldsymbol{x}_{n_{\text{data}}}))^{\top}$, and $\boldsymbol{y} = (y_1, \ldots, y_{n_{\text{data}}})^{\top}$. We demonstrate the Gaussian process regression in Fig. 5.2. We see that the posterior mean function $\overline{m}$ is a good approximation of the true function.

Gaussian process regression has the advantage that all calculations can be done in a closed form using only matrix operations. However, as the number of data n_{data} increases, inverse matrix calculations for $n_{\text{data}} \times n_{\text{data}}$ matrices are required, and the amount of memory and computation is enormous. Many sparse approximations have been proposed to overcome the computational complexity of Gaussian process regression. We give two examples of sparse approximations. One is the sparse Gaussian process regression [HFL13], which uses a subset of data as inducing variables. Other is the sparse variational Gaussian process
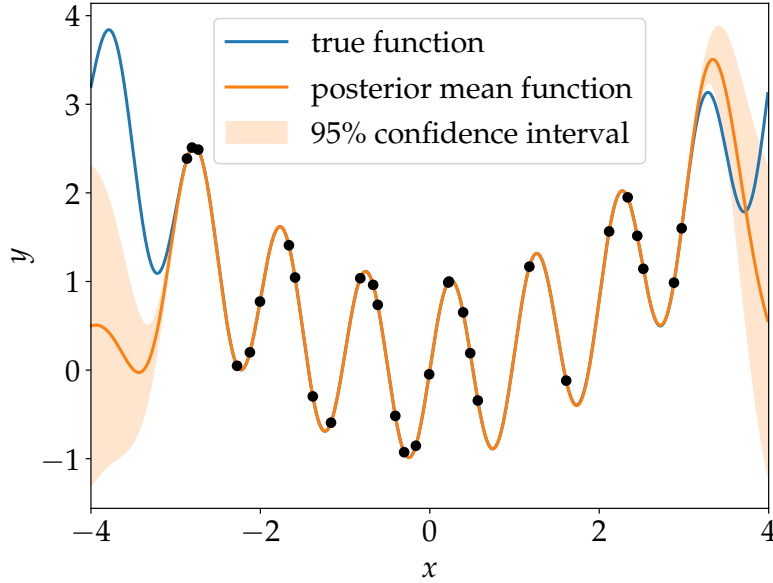
Figure 5.2: Demonstration of Gaussian process regression. Black points denotes the data $\mathcal{D} = \{(x_i, y_i)\}_{i=1}^{30}$. The true function is $x \mapsto \sin(2\pi x) + x^2/5$. The prior mean function is $m(x) = 0$ and the prior covariance function is $k(x, \tilde{x}) = \exp[-(x - \tilde{x})^2/(2\sigma^2)]$ with $\sigma = 0.5$.

(SVGP) regression [Tit09], which uses a variational distribution to approximate the posterior distribution of f. Computation cost comparison is summarized in Table 5.1. In the following, we use the SVGP regression as our model.

Table 5.1: Computation cost comparison of Gaussian process regression. n denotes the total number of data, m denotes the number of inducing variables, and b denotes the minibatch size. Sparse GP denotes the sparse Gaussian process regression [HFL13], and SVGP denotes the sparse variational Gaussian process regression [Tit09].

	GP	sparse GP	SVGP
Inference cost	$\mathcal{O}(n^3)$	$\mathcal{O}(nm^2)$	$\mathcal{O}(bm^2 + m^3)$
Memory cost	$\mathcal{O}(n^2)$	$\mathcal{O}(nm)$	$\mathcal{O}(bm + m^2)$

5.3.3 Choice of a covariance function

A covariance function is a crucial ingredient in a Gaussian process predictor, as it encodes our assumptions about the function which we wish to learn. For example, the radius basis function (RBF) is known to generate a C^∞ function with probability one. Matérn covariance function is known to generate a finite-time differentiable function with probability one. See [Kan+18] for a detailed discussion. In this chapter, the coupling function which we wish to learn has a domain of torus $\mathcal{X} = \mathbb{T}^{N-1}$. When $N = 2$, the domain is $\mathcal{X} = \mathbb{T}^1 = \mathbb{S}^1$ and the coupling function is a simple periodic function. By assuming that the function is smooth, we can set the covariance function as

$$k(x, x') = \theta_0 \exp(\theta_1 \cos(x - x')), \tag{5.14}$$

which is often called a *periodic kernel*. Here, θ_0 and θ_1 are positive hyperparameters. θ_0 determines the *amplitude* of the covariance function, and θ_1 can be said as an *inverse lengthscale*, which specifies the width of the covariance function. Therefore θ_1 determines the smoothness of the coupling function, and it is important to choose an appropriate value of θ_1. In many cases, the hyperparameters are to set by maximizing the marginal likelihood, and we will see this in the next subsection. We demonstrate the heatmaping of the covariance function and the corresponding samples of Gaussian process in Fig. 5.3.

When $N \geq 3$, the domain is defined on the product space $\mathcal{X} = \mathbb{S}^1 \times \cdots \times \mathbb{S}^1$, and the coupling function is expected to be periodic and smooth with respect to each entry of the domain. We can construct the covariance function from (5.14) by tensor product as follows:

$$k(\boldsymbol{x}, \boldsymbol{x}') = \theta_0 \exp \left(\sum_{i=1}^{N-1} \theta_1^{(j)} \cos(x_j - x_j') \right), \qquad (5.15)$$

where $\theta_0, \theta_1^{(j)}$ are positive hyperparameters.

Some systems can further be reduced to coupled phase-oscillator models in the following ODE form called an *additive model*:

$$\Gamma_i(\theta_1 - \theta_i, \ldots, \theta_N - \theta_i) = \omega_i + \sum_{j \neq i} \Gamma_{ij}(\theta_j - \theta_i), \qquad (5.16)$$

which is a linear combination of functions of one variable [DNR11; RW06]. In this case, we can construct a covariance function which generates the additive model shown in (5.16). By assuming that each coupling function Γ_{ij} is the periodic function of the phase difference and is smooth, the covariance function of Γ_i will have the form of a direct sum of periodic kernels, which reads

$$k(\boldsymbol{x}, \boldsymbol{x}') = \sum_{j=1}^{N-1} \theta_0^{(j)} \exp \left(\theta_1^{(j)} \cos(x_j - x_j') \right), \qquad (5.17)$$

where $\theta_0^{(j)}, \theta_1^{(j)}$ are positive hyperparameters.

5.3.4 Optimization

In the Gaussian process regression described so far, hyperparameters remain in the kernel $\theta_{0,1}$ and the noise strength σ. For brevity of notation, we will write these parameters as $\boldsymbol{\theta}$.

To estimate $\boldsymbol{\theta}$, we consider the *maximum likelihood estimation*, which makes inferences about the population that is most likely to have generated the data $\mathcal{D}$. The (marginal) log-likelihood for parameters $\boldsymbol{\theta}$ is

$$\mathcal{L}(\boldsymbol{\theta}) = \log p(\boldsymbol{y} \mid X, \boldsymbol{\theta}) = -\frac{1}{2} \boldsymbol{y}^\top K_{\boldsymbol{\theta}} \boldsymbol{y} - \frac{1}{2} \log \det K_{\boldsymbol{\theta}} - \frac{n_{\text{data}}}{2} \log 2\pi, \qquad (5.18)$$

where $K_{\boldsymbol{\theta}} = k_{XX} + \sigma^2 I_{n_{\text{data}}}$ is the covariance matrix for the noisy data $\mathcal{D}$. The most probable parameters $\boldsymbol{\theta}$ are, therefore, estimated by finding the maximum of the log-likelihood function $\mathcal{L}(\boldsymbol{\theta})$.
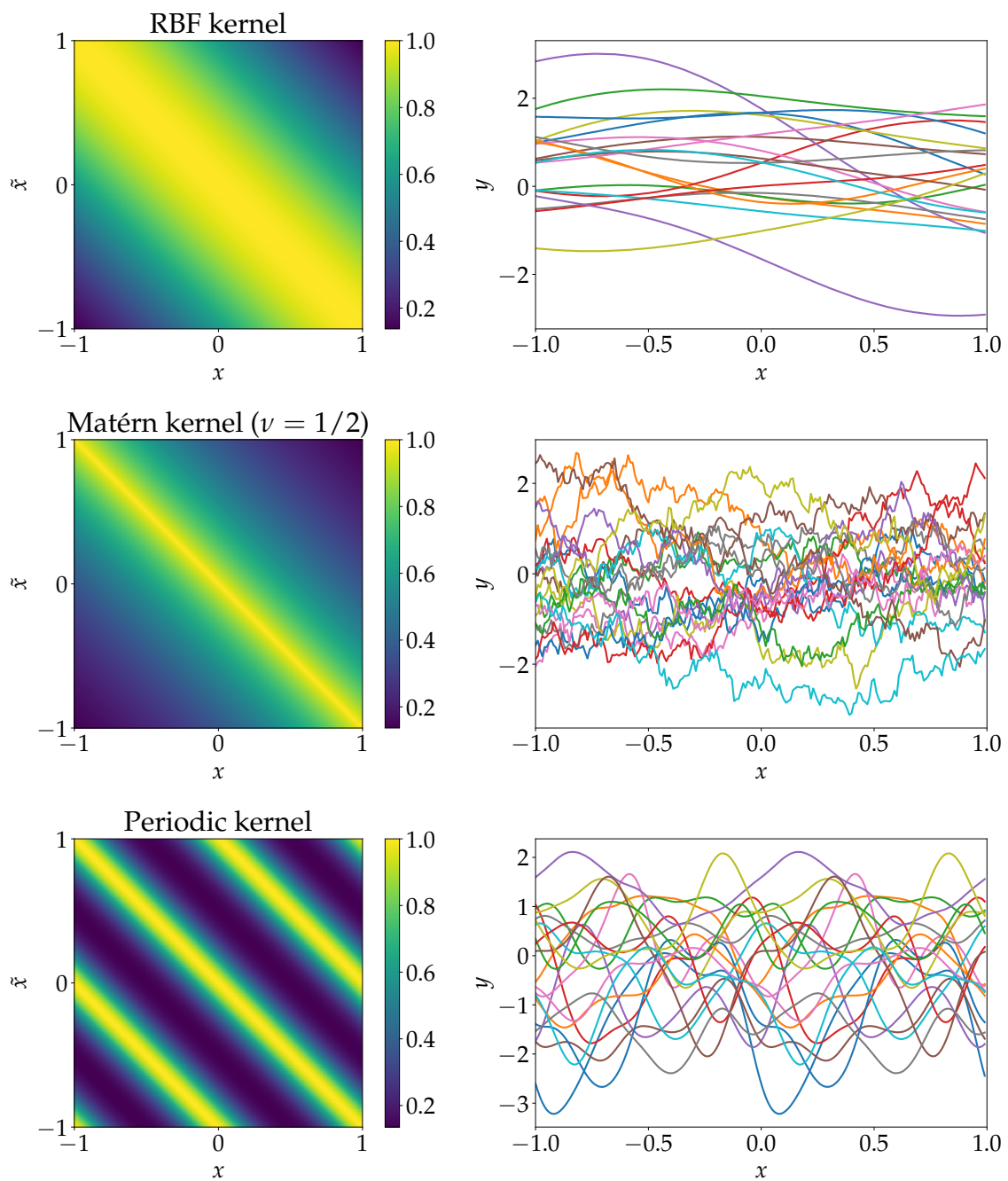
Figure 5.3: (left) Heatmaps of the RBF kernel, Matérn kernel ($\nu = 1/2$), and periodic kernel. (right) Samples of Gaussian process with the RBF kernel, Matérn kernel ($\nu = 1/2$), and periodic kernel.

The problem of finding the point that maximizes the marginal likelihood while changing hyperparameters is formulated as an optimization problem. In this chapter, we use the gradient descent method is to find the maximum point of the marginal likelihood. The hyperparameters θ is updated using the gradient with the following manner:

$$\theta^{(t+1)} \leftarrow \theta^{(t)} + \alpha \frac{\partial \mathcal{L}}{\partial \theta}(\theta^{(t)}), \tag{5.19}$$

where α denotes the learning rate.

Stochastic gradient decent (SGD) method, regarded as a stochastic approximation of gradient descent optimization methods, is another way of optimization. In the SGD method, the gradient is determined by different minibatches at each step, and parameter updating proceeds accordingly. The greatest benefit is that it requires less computation time to converge than the gradient method, which uses all data at each step. It is also thought to be less likely to be trapped in local solutions, thanks to stochastic fluctuations in the gradient direction for each minibatch.

5.4 Numerical Simulations

5.4.1 Coupled Van der Pol oscillators

Next, we consider the Van der Pol equation, which is a mathematical model that describes the nonlinear dynamics of a damped oscillator [Pol26]. It is commonly used in the study of oscillator systems, such as those found in electrical circuits and mechanical systems. The equation takes the form:

$$\dot{x} = y, \tag{5.20}$$
$$\dot{y} = \varepsilon(1 - x^2)y - x, \tag{5.21}$$

where x and y are the position and velocity of the oscillator, respectively, and ε is a constant that determine the damping and frequency of the oscillation. The equation exhibits a wide range of behavior, including limit cycles, bifurcations, and chaos, depending on the values of ε.

In this subsection, we connect two Van der Pol oscillators in the following manner:

$$\dot{x}_1 = y_1 + K(x_2 - x_1) + \xi_{x_1}(t), \tag{5.22}$$
$$\dot{y}_1 = \varepsilon_1(1 - x_1^2)y_1 - x_1 + Kx_2^2 y_2 + \xi_{y_1}(t), \tag{5.23}$$
$$\dot{x}_2 = y_2 - Kx_1^2 y_1 + \xi_{x_2}(t), \tag{5.24}$$
$$\dot{y}_2 = \varepsilon_2(1 - x_2^2)y_2 - x_2 + Kx_1 y_1^2 + \xi_{y_2}(t), \tag{5.25}$$

where $\xi_\alpha(t)$ are Gaussian white noises with $\langle \xi_\alpha(s)\xi_\beta(t) \rangle = \sigma^2 \delta_{\alpha,\beta}\delta(s-t)$ for $\alpha, \beta \in \{x_1, y_1, x_2, y_2\}$. Parameter values are $\varepsilon_1 = 0.3, \varepsilon_2 = 0.7, K = 0.01, \sigma = 0.03$.

We first obtain the oscillators' orbit by numerically integrating the equations using Euler–Maruyama method. We use the position values $x_{1,2}$ as observables of the Van der Pol oscillators. These values are different from the phase representation, and we need to transform to phases. In this chapter, we use the Hilbert

transformation, which transform the real valued function $u(t)$ to another real valued $\mathcal{H}[u](t)$, and calculate the argument of complex $u(t) + i\mathcal{H}[u](t)$ as the phase function of time t. However, this method has the problem that the phase does not vary monotonically when there is no interaction or noise. Therefore, we transform the phase using the method proposed by Kralemann as the following:

$$\phi[\theta](t) = 2\pi \int_0^\theta f(\theta)\mathrm{d}\theta, \tag{5.26}$$

where $f(\theta)$ denotes the probability distribution of time series θ [KPR11; Kra+08; Kra+07]. After these procedures, we obtain the time series of phases in the following form:

$$\begin{bmatrix} \theta_1(t_1) & \theta_1(t_2) & \cdots & \theta_1(t_k) \\ \theta_2(t_1) & \theta_2(t_2) & \cdots & \theta_2(t_k) \end{bmatrix}. \tag{5.27}$$

Since our goal is to do the regression for coupling functions, we create input-output data from the phase time series $\mathcal{D}$ for each dimension. For the firs oscillator, we set the data $\mathcal{D} = \{(x_i, y_i)\}_{i=1}^{n_{\text{data}}}$ with

$$x_i = \theta_2(t_i) - \theta_1(t_i), \quad y_i = \frac{\theta_1(t_{i+1}) - \theta_1(t_i)}{t_{i+1} - t_i}, \tag{5.28}$$

where y_i is approximation of time differentiation of θ_1 at time t_i using the finite time difference. For simplicity, x_i, y_i are used here as variables, which are different from the variables in the original Van der Pol equations.

Now we have the input-output data $\mathcal{D}$ for the coupling funtion, we conduct the Gaussian process regression. We especially use the stochastic variational Gaussian process regression for lighter computation cost compared to the original Gaussian process regression approach. Since total number of oscillators are two, the input dimension of the coupling function is one, and the covariance fucntion for the Gaussian process regression should take the form:

$$k(x, \tilde{x}) = \theta_0 \exp[\theta_1 \cos(x - \tilde{x})], \tag{5.29}$$

for $x, \tilde{x} \in \mathbb{S}^1$. Parameters $\theta_{0,1} > 0$ are optimized by Adam optimizer in the stochastic variational Gaussian process regression learning process [Tit09; KB14]. The result is shown in Fig. 5.4, comparing with the true coupling function and the The Gaussian process regression approach successfully obtains the coupling function.

We also give a situation where the previous method, using the Fourier series expansions, fails to estimate the coupling function while the Gaussian process regression approach succeeds in Fig. 5.5. We estimate the coupling function of the Van der Pol oscillators for the second oscillator with the same parameters as the previous example. The Fourier series expansion approach fails to choose the appropriate number of degrees through the evidence approximations. On the other hand, the Gaussian process regression approach is non-parametric, hence it can focus only on the estimation of the coupling function without worrying about the number of degrees.
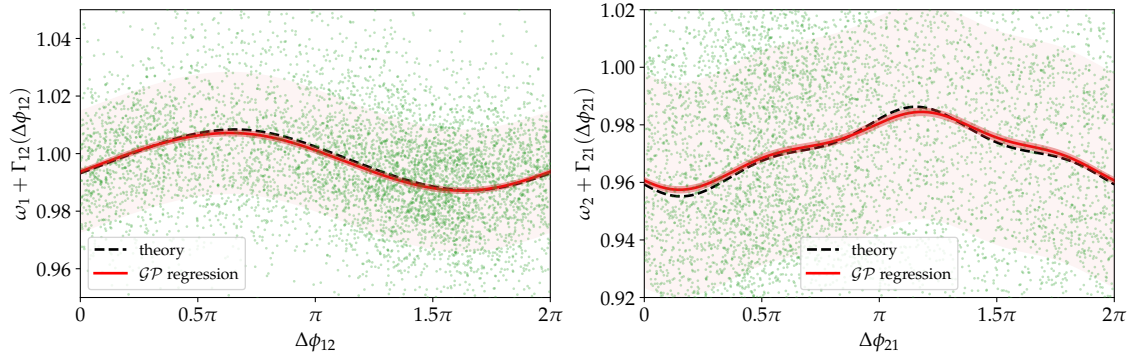
Figure 5.4: Estimation of the coupling functions of the Van der Pol oscillators. The Gaussian process approach is compared to the theory plot, which is obtained by the phase reduction theory. Green dots are the data points used for the Gaussian process regression. Dark red bars are the standard deviation of the Gaussian process regression with respect to the estimated function, and pale red bars are the standard deviation of the Gaussian process regression with respect to the data points.
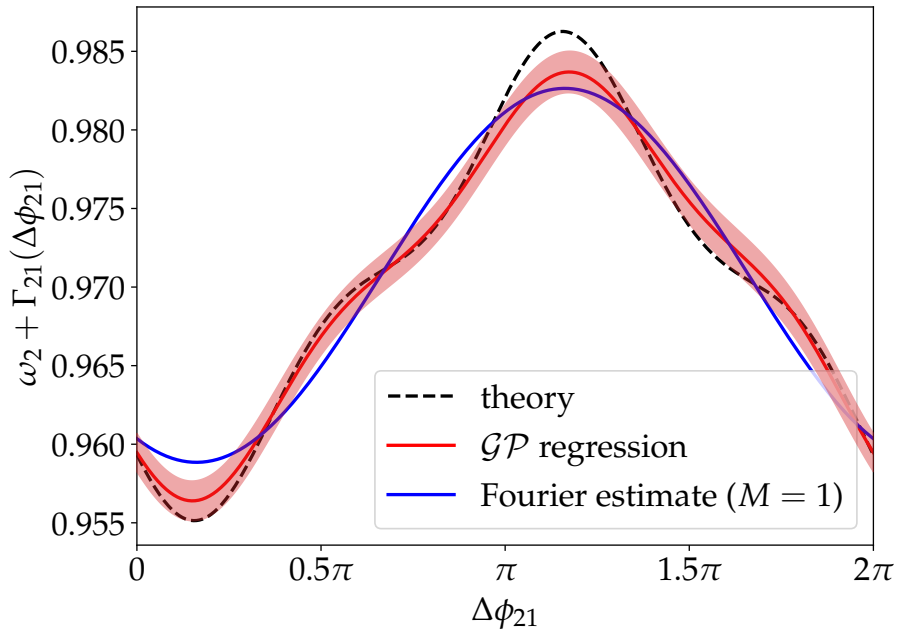

Figure 5.5: Comparison of the Fourier series and the Gaussian process regression.

5.4.2 Spiking Neural Network oscillators

We next estimate the network of seven neuron oscillators. The network consists of five excitatory neurons, which is modeled by Hodgkin–Huxley model [HH52], and two inhibitory neurons, which is modeled by fast spiking neuron model [Eri+99]. Details of these models are summarized in Appendix 5.A. See the upper left network plot in Fig. 5.6. We observe the time series by numerically solving the equations of spiking neurons (which is shown in Appendix 5.A), and use the membrane voltages $V_i(t)$ for the regression. Time series of the membrane voltages are shown in the upper right of Fig. 5.6. We apply the same procedures as done in Sec. 5.4.1 and get the phase time series, which takes the following form:

$$
\begin{bmatrix}
\theta_1(t_1) & \theta_1(t_2) & \cdots & \theta_1(t_k) \\
\theta_2(t_1) & \theta_2(t_2) & \cdots & \theta_2(t_k) \\
\vdots & \vdots & & \vdots \\
\theta_7(t_1) & \theta_7(t_2) & \cdots & \theta_7(t_k)
\end{bmatrix}.
\tag{5.30}
$$

For the first oscillator, we set the data $\mathcal{D} = \{(x_i, y_i)\}_{i=1}^{n_{\text{data}}}$ with

$$
x_i =
\begin{bmatrix}
\theta_2(t_i) - \theta_1(t_i) \\
\theta_3(t_i) - \theta_1(t_i) \\
\vdots \\
\theta_7(t_i) - \theta_1(t_i)
\end{bmatrix}
\in \mathbb{T}^6, \quad
y_i = \frac{\theta_1(t_{i+1}) - \theta_1(t_i)}{t_{i+1} - t_i}.
\tag{5.31}
$$

Since the input space in $\mathbb{T}^6$, the covariance function for the Gaussian process regression is

$$
k(x, \tilde{x}) = \sum_{j=1}^{6} \theta_0^{(j)} \exp(\theta_1^{(j)} \cos(x_i - \tilde{x}_i)),
\tag{5.32}
$$

for $x, \tilde{x} \in \mathbb{T}^6$. For this input-output data, we employ the stochastic variational Gaussian process regression and estimate the first oscillator's coupling function. We simultaneously estimate the coupling functions for other oscillators. See the lower graphs of Fig. 5.6 for the estimation result compared to the theoretical coupling functions obtained by the phase reduction approach. We confirm that the coupling functions between each oscillators are qualitatively consistent with the results from Gaussian process regression and the theoretical results.

5.5 Summary and Discussions

In this chapter, we focus on the real data that represent rhythmic phenomena, and from them, we consider estimating the coupling function that is modeled as a phase oscillator system. A method for estimating the coupling function using Gaussian process regression is proposed. By designing the kernel function flexibly, the regression can be performed without going through a finite order approximation by Fourier series. We confirmed that this works well in the case of Van der Pol equations. We also confirmed that the coupling function can be
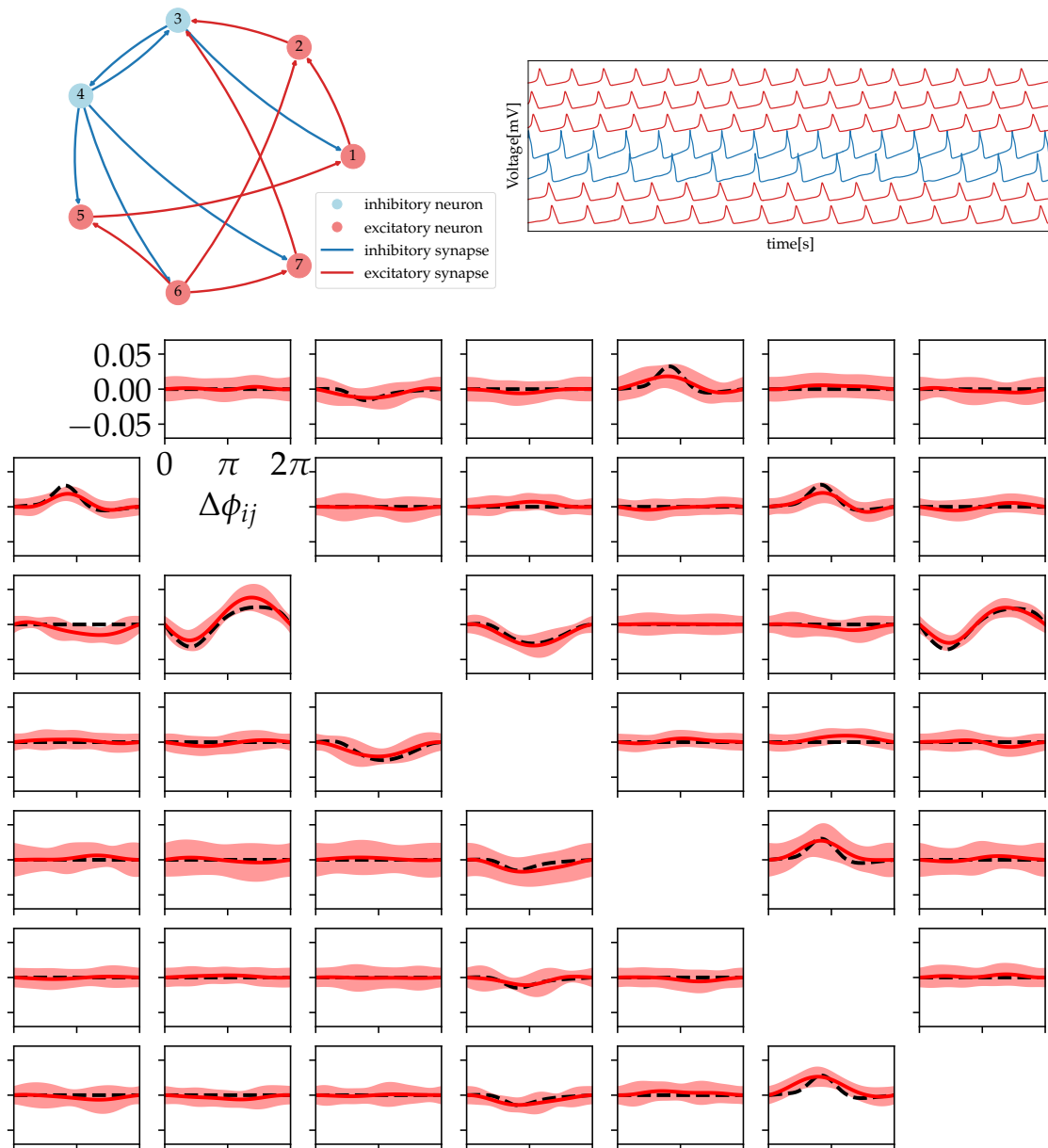
Figure 5.6: (Upper left) Network of spiking neurons coupled with inhibitory and excitatory neurons. (Upper right) Time series of the voltage of each neuron. (lower) Theoretically derived coupling function between each neuron (black dotted line) and the coupling function estimated from the data using Gaussian process regression (red solid line). Red bars are the standard deviation of the Gaussian process regression with respect to the estimated functions. Note that for comparison each coupling function Γ_{ij} is translated to take 0 at $\Delta\phi_{ij} = 0$.

successfully estimated qualitatively for as many as seven many-body systems of
coupled spiking neurons.

Finally, we comment on the proposed method using Gaussian process regression. The main idea was to reduce the data to a regression problem about a vector field of differential equations of phase. However, the possibility arises that the data used in the regression may contain systematic errors because it involves an approximation of the derivative in terms of differences due to finite time. To overcome this problem, a new idea has recently been proposed to calculate the parameter derivatives of time series data obtained from parameterized vector fields using the accompanying equations [Che+18; Li+20]. We leave the application of the adjoint equation to the estimation of coupling functions as a future work.

5.A Nueron models

The Hodgkin–Huxley model reads the following:

$$C\dot{V} = G_{\text{Na}}m^3h(E_{\text{Na}} - V) + G_{\text{K}}n^4(E_{\text{K}} - V) + G_{\text{L}}(E_{\text{L}} - V) + I_{\text{input}} + \xi_V, \quad (5.33)$$
$$\dot{m} = \alpha_m(V)(1 - m) - \beta_m(V)m + \xi_m, \quad (5.34)$$
$$\dot{h} = \alpha_h(V)(1 - h) - \beta_h(V)m + \xi_h, \quad (5.35)$$
$$\dot{n} = \alpha_n(V)(1 - n) - \beta_n(V)n + \xi_n, \quad (5.36)$$

with the parameter values $C = 1, G_{\text{Na}} = 120, G_{\text{K}} = 36, G_{\text{L}} = 0.3, E_{\text{Na}} = 50, E_{\text{K}} = -77, E_{\text{L}} = -54.4$. The auxiliary functions $\alpha_{m,h,n}, \beta_{m,h,n}$ are

$$\alpha_m(V) = \frac{0.1(V + 40)}{1 - \exp[(-V - 40)/10]}, \quad \beta_m(V) = 4\exp\frac{-V - 65}{18}, \quad (5.37)$$

$$\alpha_h(V) = 0.07\exp\frac{-V - 65}{20}, \quad \beta_h(V) = \frac{1}{1 + \exp[(-V - 35)/10]}, \quad (5.38)$$

$$\alpha_n(V) = \frac{0.01(V + 55)}{1 - \exp[(-V - 55)/10]}, \quad \beta_n(V) = 0.125\exp\frac{-V - 65}{80}. \quad (5.39)$$

The model of fast-spiking neurons reads the following:

$$C\dot{V} = G_{\text{Na}}m^3h(E_{\text{Na}} - V) + G_{\text{K}}n^2(E_{\text{K}} - V) + G_{\text{L}}(E_{\text{L}} - V) + I_{\text{input}} + \xi_V, \quad (5.40)$$
$$\dot{m} = \alpha_m(V)(1 - m) - \beta_m(V)m + \xi_m, \quad (5.41)$$
$$\dot{h} = \alpha_h(V)(1 - h) - \beta_h(V)m + \xi_h, \quad (5.42)$$
$$\dot{n} = \alpha_n(V)(1 - n) - \beta_n(V)n + \xi_n, \quad (5.43)$$

with the parameter values $C = 1, G_{\text{Na}} = 112, G_{\text{K}} = 224, G_{\text{L}} = 0.1, E_{\text{Na}} = 55, E_{\text{K}} = -97, E_{\text{L}} = -70.0$. The auxiliary functions $\alpha_{m,h,n}, \beta_{m,h,n}$ are

$$\alpha_m(V) = \frac{40(V - 75)}{1 - \exp[(75 - V)/13.5]}, \quad \beta_m(V) = 1.2262\exp\frac{-V}{42.248}, \quad (5.44)$$

$$\alpha_h(V) = 0.0035\exp\frac{-V}{24.186}, \quad \beta_h(V) = \frac{0.017(-51.25 - V)}{\exp[(-51.25 - V)/5.2] - 1}, \quad (5.45)$$

$$\alpha_n(V) = \frac{V - 95}{1 - \exp[(95 - V)/11.8]}, \quad \beta_n(V) = 0.025\exp\frac{-V}{22.222}. \quad (5.46)$$

The input current for each cell, denoted by i, is the combination of the bias current and the current flowing through the synapses. It can be expressed mathematically as: $I_{\text{input},i} = I_{\text{bias},i} + \sum_{j \in \text{pre}_i} I_{\text{syn},ij}$. The symbol "pre" represents the set of cells that have a synaptic connection with cell i. In this case, the bias current for cell 1 is 30, for cell 2 is 32 and so on, with the values being $30, 32, 6, 6.5, 34, 36, 38$ respectively for cells 1 through 7.

The current flowing through the synapses, $I_{\text{syn},ij}$, is modeled using the kinetic synapse model [DMS94], where it is represented as

$$I_{\text{syn},ij} = G_{ij} r_{ij}(t)[V_i(t) - E_{ij}]. \tag{5.47}$$

The fraction of bound receptor proteins is represented by r_{ij}, and its dynamics are described by the following equation:

$$\frac{dr_{ij}}{dt} = \alpha_{ij} T_{ij}(1 - r_{ij}) - \beta_{ij} r_{ij}, \tag{5.48}$$

where T_{ij} is the concentration of neurotransmitters, which is set to 1 when a spike is emitted by the presynaptic cell and resets to 0 after 1 millisecond. The constants α_{ij} and β_{ij} govern the kinetics of r_{ij}, while E_{ij} is the reversal potential and G_{ij} is the synaptic conductance. The values used for excitatory and inhibitory synapses are $(\alpha_{ij}, \beta_{ij}, E_{ij}, G_{ij}) = (1.1, 0.67, 0, 0.5)$ and $(9.8, 0.2, -75, 0.4)$ respectively. Additionally, a weak, independent noise function $\xi_{x,i}$ is added to the membrane voltage V_i and channel variables m_i, h_i and n_i. The noise follows a Gaussian white noise distribution, with $\langle \xi_{x,i}(t) \rangle = 0$ and $\langle \xi_{x,i}(t) \xi_{y,j}(s) \rangle = \sigma_x^2 \delta_{xy} \delta_{ij} \delta(t - s)$, where x,y = V, m, h, n, and i and j are the cell indices. The noise strengths used are $\sigma_V = 0.5$ and $\sigma_m = \sigma_h = \sigma_n = 5 \times 10^{-6}$.

5.B Sparse Gaussian process

Here, we show the algorithm of the sparse Gaussian process (SGP) regression in Algorithm 5.2.

References

[BB68]   John Buck and Elisabeth Buck. "Mechanism of Rhythmic Synchronous Flashing of Fireflies". In: *Science* 159.3821 (1968), pp. 1319–1327. ISSN: 0036-8075. DOI: 10.1126/science.159.3821.1319. URL: https://science.sciencemag.org/content/159/3821/1319.

[CAY03]   Rosa Cossart, Dmitriy Aronov, and Rafael Yuste. "Attractor dynamics of network UP states in the neocortex". In: *Nature* 423.6937 (May 2003), pp. 283–288. DOI: 10.1038/nature01614. URL: https://doi.org/10.1038/nature01614.

[Che+18] Ricky TQ Chen, Yulia Rubanova, Jesse Bettencourt, and David K Duvenaud. "Neural ordinary differential equations". In: *Advances in neural information processing systems* 31 (2018).

Algorithm 5.2 Sparse Gaussian process regression `GP_SPARSE_REGRESSION`

Input: training data X, y $\triangleright$ `X[i]` $= x_i, y$`[i]` $= y_i$
Input: test input data x^*
Input: prior Gaussian process $\mathcal{GP}(0, k)$ $\triangleright$ covariance function $k(\cdot, \cdot)$
Input: variance of noise σ^2
Input: inducing points Z $\triangleright$ `Z[i]` $= z_i$
Output: Gaussian distributions of values at x^*
   function `GP_SPARSE_REGRESSION`$(X, y, x^*, \mathcal{GP}(0, k), \sigma^2, Z)$
      calculate matrix $K_{XX} \leftarrow (K_{XX})_{i,j} = (k(x_i, x_j))_{i,j}$
      calculate matrix $K_{XZ} \leftarrow (K_{XZ})_{i,j} = (k(x_i, z_j))_{i,j}$
      calculate matrix $K_{ZZ} \leftarrow (K_{ZZ})_{i,j} = (k(z_i, z_j))_{i,j}$
      calculate array $k_{Zx^*} \leftarrow (K_{Zx^*})_i = (k(z_i, x^*))_i$
      calculate value $k_{x^*x^*} \leftarrow k(x^*, x^*)$
      calculate matrix $\Lambda \leftarrow \text{diag}(K_{XX} - K_{XZ}K_{ZZ}^{-1}K_{XZ}^{\top})$ $\triangleright$ Λ is a diagonal matrix
      calculate matrix $Q_{ZZ} \leftarrow K_{ZZ} + K_{XZ}^{\top}(\Lambda + \sigma^2 I)^{-1}K_{XZ}$
      calculate array $\hat{u} \leftarrow K_{ZZ}Q_{ZZ}^{-1}K_{XZ}^{\top}(\Lambda + \sigma^2 I)^{-1}y$
      calculate mean $m_{\text{sparse}} \leftarrow k_{Zx^*}^{\top}K_{ZZ}^{-1}\hat{u}$
      calculate variance $v_{\text{sparse}} \leftarrow k_{x^*x^*} - k_{Zx^*}^{\top}(K_{ZZ}^{-1} - Q_{ZZ}^{-1})k_{Zx^*} + \sigma^2$
      return $\mathcal{N}(m_{\text{sparse}}, v_{\text{sparse}})$
   end function

[DMS94]   A. Destexhe, Z. F. Mainen, and T. J. Sejnowski. "An Efficient Method for Computing Synaptic Conductances Based on a Kinetic Model of Receptor Binding". In: *Neural Computation* 6.1 (Jan. 1994), pp. 14–18. DOI: `10.1162/neco.1994.6.1.14`. URL: `https://doi.org/10.1162/neco.1994.6.1.14`.

[DNR11]   David K Duvenaud, Hannes Nickisch, and Carl Rasmussen. "Additive gaussian processes". In: *Advances in neural information processing systems* 24 (2011).

[Eri+99]   Alev Erisir, D Lau, Bernardo Rudy, and Christopher S Leonard. "Function of specific K+ channels in sustained high-frequency firing of fast-spiking neocortical interneurons". In: *Journal of neurophysiology* 82.5 (1999), pp. 2476–2489.

[HFL13]   James Hensman, Nicolo Fusi, and Neil D Lawrence. "Gaussian processes for big data". In: *arXiv preprint arXiv:1309.6835* (2013).

[HH52]   Allan L Hodgkin and Andrew F Huxley. "Currents carried by sodium and potassium ions through the membrane of the giant axon of Loligo". In: *The Journal of physiology* 116.4 (1952), p. 449.

[Kan+18]   Motonobu Kanagawa, Philipp Hennig, Dino Sejdinovic, and Bharath K Sriperumbudur. "Gaussian processes and kernel methods: A review on connections and equivalences". In: *arXiv preprint arXiv:1807.02582* (2018).

[KB14]   Diederik P Kingma and Jimmy Ba. "Adam: A method for stochastic optimization". In: *arXiv preprint arXiv:1412.6980* (2014).

[KM11]   Hiroshi Kori and Yoshihisa Morita. *Dynamical System Approach to Biological Rhythms*. Kyoritshu Shuppan, 2011.

[KPR11]   Björn Kralemann, Arkady Pikovsky, and Michael Rosenblum. "Reconstructing phase dynamics of oscillator networks". In: *Chaos: An Interdisciplinary Journal of Nonlinear Science* 21.2 (2011), p. 025104.

[Kra+07] Björn Kralemann, Laura Cimponeriu, Michael Rosenblum, Arkady Pikovsky, and Ralf Mrowka. "Uncovering interaction of coupled oscillators from data". In: *Physical Review E* 76.5 (2007), p. 055201.

[Kra+08] Björn Kralemann, Laura Cimponeriu, Michael Rosenblum, Arkady Pikovsky, and Ralf Mrowka. "Phase dynamics of coupled oscillators reconstructed from data". In: *Physical Review E* 77.6 (2008), p. 066205.

[Li+20]   Xuechen Li, Ting-Kam Leonard Wong, Ricky TQ Chen, and David Duvenaud. "Scalable gradients for stochastic differential equations". In: *International Conference on Artificial Intelligence and Statistics*. PMLR. 2020, pp. 3870–3882.

[Lu+16]   Zhixin Lu, Kevin Klein-Cardeña, Steven Lee, Thomas M. Antonsen, Michelle Girvan, and Edward Ott. "Resynchronization of circadian oscillators and the east-west asymmetry of jet-lag". In: *Chaos: An Interdisciplinary Journal of Nonlinear Science* 26.9 (Sept. 2016), p. 094811. DOI: 10.1063/1.4954275. URL: https://doi.org/10.1063/1.4954275.

[OA14]   Kaiichiro Ota and Toshio Aoyagi. *Direct extraction of phase dynamics from fluctuating rhythmic data based on a Bayesian approach*. 2014. DOI: 10.48550/ARXIV.1405.4126. URL: https://arxiv.org/abs/1405.4126.

[Pol26]   Balth van der Pol. "On relaxation-oscillations". In: *Philosophical Magazine* 2 (1926), pp. 978–992.

[RW06]   Carl Edward Rasmussen and Christopher K. I. Williams. *Gaussian Processes for Machine Learning*. The MIT Press, 2006. URL: http://gaussianprocess.org/gpml/.

[Smi35]   Hugh M. Smith. "SYNCHRONOUS FLASHING OF FIREFLIES". In: *Science* 82.2120 (1935), pp. 151–152. ISSN: 0036-8075. DOI: 10.1126/science.82.2120.151. URL: https://science.sciencemag.org/content/82/2120/151.

[Str03]   Steven H. Strogatz. *Sync: The Emerging Science of Spontaneous Order*. Penguin, 2003.

[Tit09]   Michalis Titsias. "Variational learning of inducing variables in sparse Gaussian processes". In: *Artificial intelligence and statistics*. PMLR. 2009, pp. 567–574.

[Win67]   Arthur T. Winfree. "Biological rhythms and the behavior of popu-
lations of coupled oscillators". In: *Journal of Theoretical Biology* 16.1
(1967), pp. 15–42. ISSN: 0022-5193. DOI: https://doi.org/10.1016/
0022-5193(67)90051-3. URL: https://www.sciencedirect.com/
science/article/pii/0022519367900513.

[WW88]   SS Wang and Herbert G Winful. "Dynamics of phase-locked semicon-
ductor laser arrays". In: *Applied physics letters* 52.21 (1988), pp. 1774–
1776.

[Yon+22]   Ryosuke Yoneda, Haruma Furukawa, Daigo Fujiwara, and Toshio
Aoyagi. "Gaussian process regression approach to estimating phase
dynamics from rhythmic data". In: *preparation* (2022).

CHAPTER 6

CONCLUSION

The thesis is concluded in this chapter. We summarize the results and discuss some future works.

6.1 Summary of Our Study

In this thesis, we study the coupled phase-oscillator models from theoretical and experimental point of view. In Chapter 3, we calculate the critical exponent β of the coupled phase-oscillator models on small world networks using the finite-size scaling analysis. We set the coupling functions as $\Gamma(\theta) = \sin\theta + a\sin 2\theta$ and the natural frequency distributions as $g_n(\omega) = g_n(0) - C_n\omega^{2n} + \cdots$, and check (a, n)-dependence of β. The result suggests that the transition exponent $\beta = 1/2$ for $a < 0$, which differs from the critical exponent result of all-to-all network. We also see that for $a = 0.5 > 0$, the transition is discontinuous and the critical exponent is undefeined. In Chapter 4, we consider the Kuramoto model on networks with identical natural frequency, and discuss the relation of network connectivity and in-phase synchronization. Several researches have considered dense networks that have equilibrium other than the in-phase synchronization state. In this research, we obtain the densest circulant network that have stable "p-twisted states" by formulating integer programming problems. Chapter 5 is devoted to the experimental research on the coupled pahse-oscilator models. Estimating the underlying mathematical model from the real data has been the central problem in physics. For the rhythmic data it is theoretically known that the model is always reduced to the coupled phase-oscilator model, therefore there have been several studies on estimating the phase dynamics, including usind the Bayesian linear regression analysis. However, this analysis appropriates the coupling function to Fourier expansion series with finite degree, and sometimes the Gibbs phenomena have been encountered. We propose a method to estimeate the coupling function by the Gaussian process regression. The regression can be regarded as the optimization in the infinite dimensional periodic function space, therefore we have a theoretical guarantee that the optimized function is smooth. We have checked the validity by applying this method to the Van der Pol oscilators and spiking neurons.

79

6.2 Future works

We give two future works to end this thesis.

In Chapter 4, we considered the dense network that do not synchronize. After the paper [YTT21] was published, the lower bound of μ_c was improved from $0.6838\ldots$ to $11/16 = 0.6875$ by Canale [Can22]. Also, the upper bound was improved to $3/4 = 0.75$ by Kassabov *et al.* [KST21]. These results are summarized in Table 6.1. Further research is needed to find the exact value of μ_c. Especially for the lower bound, other "solvable networks" with "solvable stable states" are needed to be considered. We will tackle this problem in the future.

Table 6.1: List of recent research on network connectivity μ and its tendency to synchronization.

network that do not synchronize	network that always synchronize
$\mu \leq 0.6809\ldots$ (Wiley, 2006 [WSG06])	$\mu = 1$ (Watanabe, 1994 [WS94])
$\mu \leq 0.6818\ldots$ (Canale, 2015 [CM15])	$\mu \geq 0.9395\ldots$ (Taylor, 2012 [Tay12])
$\mu \leq 0.6828\ldots$ (Townsend, 2020 [TSS20])	$\mu \geq 0.7929\ldots$ (Ling, 2019 [LXB19])
$\mu \leq 0.6838\ldots$ (Yoneda, 2021 [YTT21])	$\mu \geq 0.7889\ldots$ (Lu, 2020 [LS20])
$\mu \leq 0.6875$ (Canale, 2022 [Can22])	$\mu \geq 0.75$ (Kassabov, 2021 [KST21])

For a future work regarding Chapter 5, In Chapter 5, we have shown that the coupling function can be estimated by the Gaussian process regression. We have approximated the phase differentiation $\frac{d\theta_i}{dt}$ by a finite difference, but this approximation is one of the sources of error. In order to reduce the error, the time step width must be reduced, but this requires an increase in the number of data, a situation that is not very favorable for Gaussian process regression. In the recent machine learning boom, a method called "neural ode/sde" was proposed to efficiently compute the gradient of a parameterized differential equation [Che+18; Li+20]. We briefly introduce the algorithm here. We consider the stochastic differential equation of the following form:

$$\mathrm{d}x = f(t, x; \theta)\mathrm{d}t + g(t, x; \theta)\mathrm{d}W_t, \tag{6.1}$$

where f is the drift function, g is the diffusion function, and W_t is the Wiener process. θ is the parameter of the drift and diffusion functions. The paper [Li+20] shows that the gradient of the loss function $\mathcal{L}$ with respect to the initial value $x(t_0)$ and parameters θ can be calculated by the adjoint equation of the stochastic differential equation, where the adjoint state is defined as $a(t) = \partial\mathcal{L}/\partial x(t)$. The algorithm of this calculation is shown in Algorithm 6.1. Preliminary numerical calculations have shown that the adjoint method is effective for estimating dynamical systems. We would like to use this method to estimate coupled phase-oscillator models from rhythmic data in the future.

References

[Can22]   Eduardo A Canale. "From weighted to unweighted graphs in Synchronizing Graph Theory". In: *arXiv preprint arXiv:2209.06362* (2022).

Algorithm 6.1 Algorithm for calculating the gradient of the loss function $\mathcal{L}$ with respect to initial value $x(t_0)$ and parameters θ using `sdeint` function [Li+20]. Here `sdeint` is a function that takes $(x(t_0), f, g, w, t_0, t_1)$ as an input and calculate the SDE $\mathrm{d}x = f\mathrm{d}t + g\mathrm{d}W_t$ with the Wiener process $w(t)$ and the initial value $x(t_0)$ from time t_0 to time t_1 and return the final value $x(t_1)$.

Input: Parameters θ, start time t_0, stop time t_1, final state $x(t_1)$, loss gradient $\partial\mathcal{L}/\partial x(t_1)$, drift $f(t, x; \theta)$, diffusion $g(t, x; \theta)$, Wiener process sample $w(t)$.

Output: $\partial\mathcal{L}/\partial x(t_0), \partial\mathcal{L}/\partial\theta$

> **function** $\overline{f}(t, [a(t), x(t), \cdot]; \theta)$ ▷ Augmented drift
> $v = f(-t, x(t); \theta)$
>   **return** $[a(t)\partial v/\partial x, -v, a(t)\partial v/\partial \theta]$
> **end function**
> **function** $\overline{g}(t, [a(t), x(t), \cdot]; \theta)$ ▷ Augmented diffusion
> $v = g(-t, x(t); \theta)$
>   **return** $[a(t)\partial v/\partial x, -v, a(t)\partial v/\partial \theta]$
> **end function**
> **function** $\overline{w}(t)$ ▷ Replicated noise
>   **return** $[-w(-t), -w(-t), -w(-t)]$
> **end function**
> Calculate

$$\begin{bmatrix} \partial\mathcal{L}/\partial x(t_0) \\ x(t_0) \\ \partial L/\partial \theta \end{bmatrix} = \texttt{sdeint}\left(\begin{bmatrix} \partial\mathcal{L}/\partial x(t_1) \\ x(t_1) \\ \mathbf{0}_{\#\theta} \end{bmatrix}, \overline{f}, \overline{g}, \overline{w}, -t_1, -t_0\right)$$

[Che+18]   Ricky TQ Chen, Yulia Rubanova, Jesse Bettencourt, and David K Duvenaud. "Neural ordinary differential equations". In: *Advances in neural information processing systems* 31 (2018).

[CM15]   Eduardo A. Canale and Pablo Monzón. "Exotic equilibria of Harary graphs and a new minimum degree lower bound for synchronization". In: *Chaos: An Interdisciplinary Journal of Nonlinear Science* 25.2 (2015), p. 023106. DOI: 10.1063/1.4907952. URL: https://doi.org/10.1063/1.4907952.

[KST21]   Martin Kassabov, Steven H Strogatz, and Alex Townsend. "Sufficiently dense Kuramoto networks are globally synchronizing". In: *Chaos: An Interdisciplinary Journal of Nonlinear Science* 31.7 (2021), p. 073135.

[Li+20]   Xuechen Li, Ting-Kam Leonard Wong, Ricky TQ Chen, and David Duvenaud. "Scalable gradients for stochastic differential equations". In: *International Conference on Artificial Intelligence and Statistics*. PMLR. 2020, pp. 3870–3882.

[LS20]   Jianfeng Lu and Stefan Steinerberger. "Synchronization of Kuramoto oscillators in dense networks". In: *Nonlinearity* 33.11 (Oct. 2020), pp. 5905–5918. DOI: 10.1088/1361-6544/ab9baa. URL: https://doi.org/10.1088/1361-6544/ab9baa.

[LXB19]   Shuyang Ling, Ruitu Xu, and Afonso S. Bandeira. "On the Landscape of Synchronization Networks: A Perspective from Nonconvex Optimization". In: *SIAM Journal on Optimization* 29.3 (Jan. 2019), pp. 1879–1907. DOI: 10.1137/18m1217644. URL: https://doi.org/10.1137/18m1217644.

[Tay12]   Richard Taylor. "There is no non-zero stable fixed point for dense networks in the homogeneous Kuramoto model". In: *Journal of Physics A: Mathematical and Theoretical* 45.5 (Jan. 2012), p. 055102. DOI: 10.1088/1751-8113/45/5/055102. URL: https://doi.org/10.1088/1751-8113/45/5/055102.

[TSS20]   Alex Townsend, Michael Stillman, and Steven H. Strogatz. "Dense networks that do not synchronize and sparse ones that do". In: *Chaos: An Interdisciplinary Journal of Nonlinear Science* 30.8 (2020), p. 083142. DOI: 10.1063/5.0018322. URL: https://doi.org/10.1063/5.0018322.

[WS94]   Shinya Watanabe and Steven H. Strogatz. "Constants of motion for superconducting Josephson arrays". In: *Physica D: Nonlinear Phenomena* 74.3 (1994), pp. 197–253. ISSN: 0167-2789. DOI: https://doi.org/10.1016/0167-2789(94)90196-1. URL: http://www.sciencedirect.com/science/article/pii/0167278994901961.

[WSG06]   Daniel A. Wiley, Steven H. Strogatz, and Michelle Girvan. "The size of the sync basin". In: *Chaos: An Interdisciplinary Journal of Nonlinear Science* 16.1 (2006), p. 015103. DOI: 10.1063/1.2165594. URL: https://doi.org/10.1063/1.2165594.

[YTT21]   Ryosuke Yoneda, Tsuyoshi Tatsukawa, and Jun-nosuke Teramae. "The lower bound of the network connectivity guaranteeing in-phase synchronization". In: *Chaos: An Interdisciplinary Journal of Nonlinear Science* 31.6 (June 2021), p. 063124. DOI: 10.1063/5.0054271. URL: https://doi.org/10.1063/5.0054271.

ACKNOWLEDGEMENT